SECURITY CLASSIFICATION OF THIS PAGE UNCLASSIFIED

DOCUMENTATION PAGE

Form Approved OMB No. 0704-0188

AD-A196 838

DTIC ELECTE JL 0 7 1988 D

1b. RESTRICTIVE MARKINGS: NONE	
2b. DECLASSIFICATION / DOWNGRADING SCHEDULE	3. DISTRIBUTION / AVAILABILITY OF REPORT: Unlimited
4. PERFORMING ORGANIZATION REPORT NUMBER(S): WRAIR/ONR 5/88	5. MONITORING ORGANIZATION REPORT NUMBER(S)
6a. NAME OF PERFORMING ORGANIZATION: Theodore C. Guo and Wendy W. Guo, The Catholic University of America	6b. OFFICE SYMBOL (If applicable)
7a. NAME OF MONITORING ORGANIZATION: Department of the Navy, Office of Naval Research	
6c. ADDRESS (City, State, and ZIP Code): Department of Physics, 620 Michigan Avenue, N.E., Washington, D.C. 20064	7b. ADDRESS (City, State, and ZIP Code): Program Manager Cellular Biosystems, Office of Naval Research, 800 North Quincy Street, Arlington, Virginia 22217-5000
8a. NAME OF FUNDING / SPONSORING ORGANIZATION: Walter Reed Army Institute of Research	8b. OFFICE SYMBOL (If applicable)
9. PROCUREMENT INSTRUMENT IDENTIFICATION NUMBER: N00014-85-K-0475, N00014-85-K-0475/P00002	
8c. ADDRESS (City, State, and ZIP Code): Building 40, Department of Microwave Research, Walter Reed Army Medical Center, Washington, D.C. 20307-5001	10. SOURCE OF FUNDING NUMBERS

PROGRAM ELEMENT NO.	PROJECT NO.	TASK NO.	WORK UNIT ACCESSION NO.
	NR 207-434/4-12-85 NR4414434---01/6-13-86 (1141CB)		

11. TITLE (Include Security Classification)

Transient Interaction of Electromagnetic Pulses in Dielectrics and Microwave Biophysics (Unclassified)

12. PERSONAL AUTHOR(S)

Dr. Theodore C. Guo and Dr. Wendy W. Guo

13a. TYPE OF REPORT	13b. TIME COVERED	14. DATE OF REPORT (Year, Month, Day)	15. PAGE COUNT
FINAL REPORT	FROM 6/1/85 TO 5/30/88	5/12/88	22 plus 63 pages in Appendices

16. SUPPLEMENTARY NOTATION

DISTRIBUTION STATEMENT A
Approved for public release;
Distribution Unlimited

17. COSATI CODES		
FIELD	GROUP	SUB-GROUP

18. SUBJECT TERMS (Continue on reverse if necessary and identify by block number)
Transient Dielectric Response, Microwave Pulse Effect, Microwave Acoustics, Microwave Electrostrictive Effect, Microwave Thermoacoustic Effect, Microwave Scattering, Microwave Dosimetry, Microwave Imaging.

19. ABSTRACT (Continue on reverse if necessary and identify by block number)

This research includes the following three subjects:

1. Pressure Waves Generated by Microwave Pulses: A thorough formulation on microwave thermoelastic and microwave electrostrictive effects is developed. It is shown that pressure waves may be generated via two physical mechanisms, one by thermoelastic process and another by electrostrictive force. On the thermoelastic process, pressure waves are generated by microwave pulses if there are thermal, mechanical, or electrical discontinuities in dielectrics. Therefore, pressure wave may be generated in a dielectric even when the microwave absorption is homogeneous, such as a small dielectric body. The theoretical results, confirmed by experimental measurements, show that an absorption of microwave energy by water at the rate of 6.5 kW/gram in a water-air interface produces a pressure wave with peak amplitude as high as 10% of the atmospheric pressure. This result does not include the electrostrictive effect, which may further enhance the pressure waves if microwave pulses have short rise time. For water or biological materials with high water content, a rise time of 1 nanosecond is the marginal modulation rate, beyond which the electrostrictive effect contributes more to the pressure waves than the thermoelastic effect.

(... Continued on reverse side)

20. DISTRIBUTION / AVAILABILITY OF ABSTRACT	21. ABSTRACT SECURITY CLASSIFICATION
☒ UNCLASSIFIED/UNLIMITED ☐ SAME AS RPT ☐ DTIC USERS	UNCLASSIFIED
22a. NAME OF RESPONSIBLE INDIVIDUAL: Col. Edward Elson	22b. TELEPHONE (Include Area Code): (202)576-3615, (301)427-5125 — 22c. OFFICE SYMBOL: WRAIR/Microwave Dept.

DD Form 1473, JUN 86 Previous editions are obsolete. SECURITY CLASSIFICATION OF THIS PAGE

TRANSIENT INTERACTION OF ELECTROMAGNETIC PULSES IN DIELECTRICS AND MICROWAVE BIOPHYSICS

by

Theodore C. Guo and Wendy W. Guo

Department of Physics
The Catholic University of America
Washington, D. C. 20064

FINAL REPORT

prepared for

Walter Reed Army Institute of Research
Department of Microwave Research

via

Office of Naval Research
Code 1141
800 N. Quincy Street

Contract No. N00014-85-K-0475
Contract Period: 6/1/85 - 5/30/88
Funded Period: 6/1/85 - 9/30/87

May 1988

TABLE OF CONTENTS

FINAL REPORT

on

TRANSIENT INTERACTION OF ELECTROMAGNETIC PULSES IN DIELECTRICS AND MICROWAVE BIOPHYSICS

by

Theodore C. Guo and Wendy W. Guo

The Catholic University of America
Washington, D. C. 20064

1. BACKGROUND

Due to recent progress in developing equipments that can generate short microwave and millimeter wave pulses, there has been an increasing proliferation of microwave pulse transmitters, some with short pulse width (0.1 microsecond) and extremely high intensity (100-1000 megawatts). Microwave pulse transmitters are used extensively by the military for communication and remote control; using microwave pulses as directive energy weaponry and as means of transporting energy has also been contemplated. Electromagnetic pulses (EMP) are also emitted in nuclear blasts and from EMP simulators. All this production of microwave pulses affects the operation of military personnel in non-combat environment as well as in battle fields. Therefore minimizing microwave damage is central to successful operations of all military units. Understanding basic interactions between microwave pulses and dielectric materials will contribute greatly to the protection of human subjects from microwave damage and to the development of preventive measure.

Until recently most analyses on microwave effects have been based on continuous wave approach. Recognizing the importance of basic understanding of the interactions between short radiation pulses and dielectric materials, and its potential application to radiation hazards and radiation treatment to biological materials, the Walter Reed Army Institute of Research (WRAIR) started a program at the Catholic University of America (CUA), beginning 6/1/85, to study the transient interaction of electromagnetic pulses in dielectrics and microwave biophysics. The program was administrated by the Office of Naval Research (ONR). Originally the program was intended for three years to end on 5/30/88. However, due to budget constraint, the third year funds was not provided and the program prematurely ended on 9/30/87. This document reports the program progress as of the end of funding and constitutes a final report of the program. The main body of the report provides a progress summary with technical details given in the appendices which are publication reprints.

2. PROGRAM OBJECTIVES

The long-term objectives of this program are as follows:

2.1. To understand the basic physics of interaction between microwave radiation pulses and dielectric materials, including biological systems.

2.2. To define and derive characteristic physical quantities relating to the absorption and energy conversion of short radiation pulses in dielectric materials, especially water dominated media, such as biological subjects, and to define biological hazard of microwave pulses.

2.3. To understand the basic interactions of microwave radiation pulses with biological subjects, and to understand the mechanisms of secondary interactions resulting from microwave pulses, to define and to quantify physical and biological parameters of these interactions with respect to dielectric properties and pulse parameters, such as carrier frequency, pulse width, and peak power.

2.4. To develop dosimetric techniques and hazard specification that are applicable for transient, near-field, and high-field regimes, and to develop applications of microwaves, including imagery and target organ analysis.

3. SCOPE OF WORK

The program consists of the following three subjects:

3.1. Transient Dielectric Relaxation and Absorption

This task is to study the interaction of microwave radiation pulses with dielectrics and biological systems, and the material response to ultra-short pulses in the transient regime.

3.2. Microwave to Acoustic Energy Conversion Induced by Microwave Pulses

This task is to study mechanisms through which pressure waves may be generated by microwave pulses, and to derive a relationship between microwave pulses and the generated pressure waves.

3.3. Microwave Scattering, Inverse Scattering, Dosimetry, and Imagery

This task is to develop non-invasive techniques for dosimetry of dielectric bodies under microwave exposure, and to develop algorithm for three-dimensional medical imaging using low-level microwaves.

4. PROJECT PROGRESS

During the first year of this project, research was performed on developing a non-invasive microwave dosimetry technique, and on continuing previous theoretical studies on transient dielectric interaction and microwave to acoustic energy conversion. As progress was being made in WRAIR on the installation of a high-power pulsed microwave generator, our effort in the second year was focused on developing theoretical basis to support forthcoming experiments in WRAIR on biological effects of transient and high power microwave damage. On the transient effects, we have developed a theoretical basis for experimental observation of temporal non-linearity in the transient regime, which may be measurable and applicable to the experimental setup being planned at WRAIR. On microwave acoustics, we incorporate electrostrictive effect in the pervious formulation, and established criteria to predict the dominant mechanism, thermoacoustic or electrostrictive, for generating pressure waves by microwave pulses.[1,2] On dosimetry, we have a major breakthrough on developing an algorithm for evaluating the vector fields both inside and outside a three-dimensional body of arbitrary geometry and dielectric profile.[3] We have also developed a formula for computing the vector fields inside the dielectric body from measurement of scattered fields in a limited region outside the body. Our success in developing the non-invasive dosimetry algorithm also led us

to discover a non-diffractional imagery technique, which may provide images with resolution limited only by signal-to-noise ratio, and not by wavelength of the probing microwave or by geometrical configuration of the receiving antenna.[4]

The effort of this program during the two funded years have resulted in publication of six papers.[1,2,3,4,5,6] The following gives a technical summary of the progress and status in each task of this program. Details of research results are given in the appendices, which are reprints of our publications.

4.1. Transient Dielectric Response

Theory of Transient Response

Our effort on this subject has been focused on developing theoretical basis to support forthcoming experiments in WRAIR on nonlinear biological effects of transient and high power microwave damage. The objective was to devise a theoretical scheme for experiments that are able to isolate the effects of short and high-intensity microwave pulses from low-intensity continuous waves (CW) on biological materials. One may directly analyze the materials and compare the damage between pulse-wave exposure and CW exposure. However, from the observation of the damage alone, it is not possible to conclude if the observed pulse or high-intensity effects are direct primary electromagnetic effects or indirect non-electromagnetic secondary effects that are induced by the microwave pulses. Therefore, instead of directly analyzing damage to biological materials, we studied the approach of analyzing the pulse propagation and the field strength of the microwave pulse.

Our previous theoretical studies have shown that, due to a *non-steady state* and irreversible process in the transient regime, dielectric relaxation cannot be parameterized by time-independent parameters, such as the damping coefficient in the transient regime. However, for experimental and practical purpose, macroscopic parameterization is desirable. Therefore we propose the following time-dependent model in the transient regime for the dielectric polarization current, J(t), which is the time-derivative of the dielectric polarization P(t):[7,8,9,10]

$$\tau(t)\cdot\frac{dJ}{dt} + J(t) = g\cdot\frac{dE}{dt} \tag{1}$$

$$\tau(t) = H(t)\tau_o[1 - \exp(-t/\tau_l)] \tag{2}$$

The model was conceived from the reasoning that the damping coefficient vanished initially and, as molecules approached an equilibrium or a steady state, it gradually increased to a final value, viz., Debye's steady-state value. The time it takes to reach the steady-state value is characterized by τ_l; the function H(t) is the Heavyside function which is zero for $t<0$, 1/2 for $t=0$, and 1 for $t>0$. With this model, it was found that the dielectric is nonlinear in the transient regime in a way that any frequency component of the the dielectric response may depend on the action of different frequencies. Thus, given an electric field as an action, then the dielectric polarization in the frequency regime, $P(\omega)$, depends on $E(\omega)$ in the following way:

$$P(\omega) = \int_{-\infty}^{\infty} \chi(\omega,\omega')E(\omega')\cdot d\omega' \tag{3}$$

where $\chi(\omega,\omega')$ is the dielectric susceptibility. In mathematical terms, dielectric susceptibility is not diagonal in the frequency regime. This means that, in the time regime, response at a certain time, t', caused by an action at an earlier time t, does not depend on the difference

t-t′ only. Therefore, linear superposition of action-response relationship is no longer valid. This is expected because, in the transient regime, the dielectric is in a non-steady state and undergoes irreversible processes. We also derived the function $\chi(\omega,\omega')$ from eqs. 1 and 2, and obtained:[7,8]

$$\chi(\omega,\omega') = \frac{g}{2\pi i}\frac{\tau_1}{\tau_o}\frac{\omega'}{\omega+i0}\frac{\Gamma(-i\omega\tau_1+\tau_1/\tau_o)\cdot\Gamma(-i\omega'\tau_1+1)}{\Gamma(-i\omega\tau_1+1)\cdot\Gamma(-i\omega'\tau_1+\tau_1/\tau_o)}\cdot\sum_{n=0}^{\infty}\frac{1}{(\omega'-\omega-in/\tau_1)(-i\omega'\tau_1+n+\tau_1/\tau_o)}$$

$$= \frac{g}{2\pi i}\frac{\tau_1}{\tau_o}\frac{\omega'}{(\omega+i0)(\omega'-\omega-i0)}\frac{\Gamma(-i\omega\tau_1+\tau_1/\tau_o)\cdot\Gamma(-i\omega'\tau_1+1)}{\Gamma(-i\omega\tau_1+1)\cdot\Gamma(-i\omega'\tau_1+\tau_1/\tau_o+1)}$$

$$\times {}_3F_2(i(\omega'-\omega)\tau_1, -i\omega'+\tau_1/\tau_o, 1;\ i(\omega'-\omega)\tau_1+1, -i\omega'\tau_1+\tau_1/\tau_o+1;\ 1)$$

where Γ is the gamma function and ${}_mF_n$ is the generalized hypergeometric function[11].

There are several experimental indications that electromagnetic pulses with pulse width of the order of nanoseconds or shorter may produce transient effects in biological materials. One of these experimental indications concerns the life-times of excited vibrational modes of DNA chains. Based on the line-widths of vibrational excitations by microwaves observed recently, the life-times are of the order of 120 nanoseconds.[12,13] The time it takes to reach an equilibrium state or steady state must be longer than these life-times. Another experimental evidence of transient phenomenon is the recent observation of time-dependency of dielectric susceptibility of an inorganic solid under high field.[14] The observation was derived from applying electric fields in the range of megavolts per centimeter to thin-film of amorphous aluminum oxide, Al_2O_3. It was found that the dielectric susceptibility depends on time for as long as hundred seconds. While the value of τ_o, which is the steady-state Debye's relaxation time, is known for most dielectrics, the exact values of τ_1 have never been measured. The above experimental observations indicate that non-steady state transient regime exists in dielectrics and it may last longer than the microwave pulse width. Availability of the values of τ_1 will provide much knowledge on dielectric response to high-intensity short microwave pulses. Therefore, our research was focused on devising some theoretical base for an experimental measurement of τ_1 for some materials, especially for solution of biological materials in liquid water. For dielectrics composed of large molecules, it is expected that τ_1 will be quite long comparing to pulse width of existing microwave pulse systems. From the observation of the excited vibrational modes of DNA chains,[12,13] it indicates that τ_1 must be of the order of 120 nanoseconds or longer. This suggests that transient non-steady state effect may play an important role in response of DNA solutions to nanosecond microwave pulses.

Experimental Proposal

The above result suggests that any transient effect or high field effect in dielectrics is expected to produce non-linear harmonic and anharmonic generation in the electromagnetic spectrum. Conventional non-linear analyses employ network analyzers to study the output spectrum from dielectric specimens which are exposed to a monochromatic wave; non-linearity is inferred if harmonic generations are observed in the output spectrum. This method cannot be applied to pulsed fields since the input contains a wide spectrum of frequencies. Therefore different method must be undertaken to analyze transient effects and high field pulse effects. To this end, we have found a macroscopic effect of the transient state model that is applicable to pulse inputs; the effect may also be measurable and applicable to an experimental setup that has been planned at WRAIR. To briefly summarize, our approach is to analyze the scattering matrix of a dielectric specimen under an incident pulsewave. The scattering matrix is

constructed from the measurements of input and output waves and analyzed in the frequency domain. Transient effects or high-field pulse effects are inferred if the scattering matrix have off-diagonal elements. This scattering matrix approach appears to be, in a very broad sense, similar to the inverse scattering approach that we have developed in microwave dosimetry and imagery. Indeed, all physical techniques which infer the characteristics of unknown objects by analyzing their action-response data are, in a broad sense, inverse scattering and imagery. The difference is in the physical characteristics that are being "imaged". In the scattering matrix approach described here, it is the temporal and spectral dielectric response that is "imaged", whereas in conventional imaging, the spatial distribution of some physical characteristics is imaged.

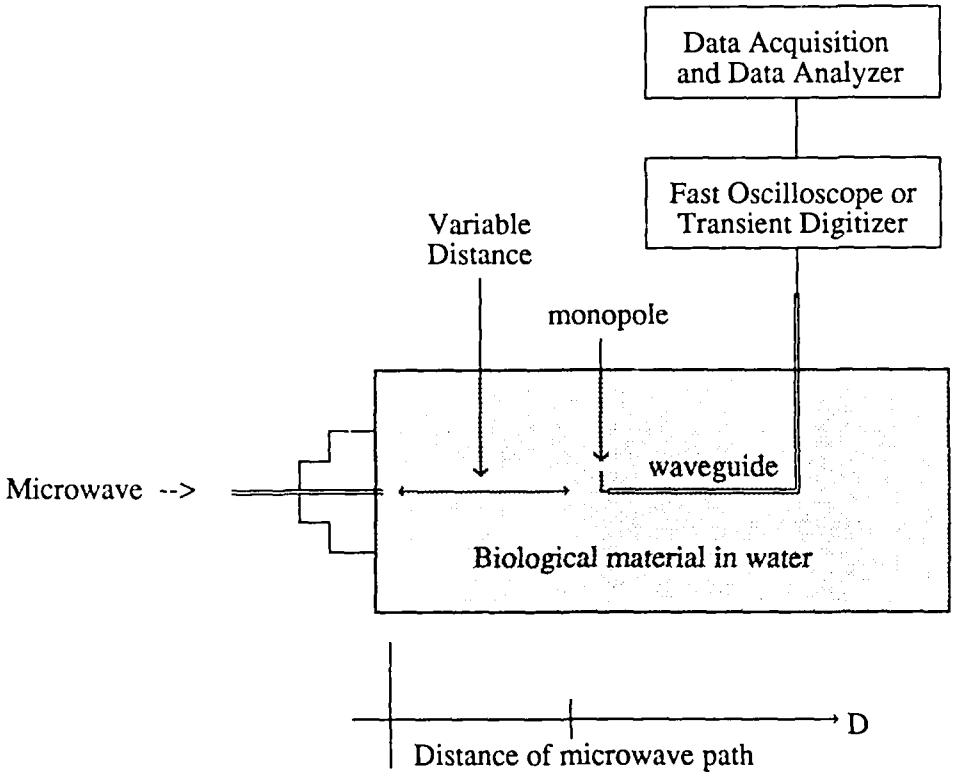

Figure 1. Sketch of experimental setup to measure the field strength along the path of a microwave pulse in a solution of a biological material in water.

To describe the scattering matrix approach in more detail, let us consider a one-dimensional propagation in an experimental setup as illustrated in Figure 1. Take two points along the propagation path of a microwave pulse, say x_1 and x_2. The material between these two points may be regarded as the specimen; the electric field of the microwave pulse at x_1 may be considered as an input field to this specimen, and that at x_2 may be considered as the output field from the specimen. Both the input field, denoted by $f^{(i)}$, and output field, denoted by $f^{(o)}$, are functions of time. By making time-resolved measurements of these two functions at a certain sampling rate, one obtains two column vectors in the time domain; these two vectors may be Fourier-transformed to the frequency space. We shall construct a scattering matrix from the measurements of a set of input fields and the corresponding set of

output fields. If there are total of N samples in the time-resolved measurements, then these two vectors are of N-dimensional. In order to construct the scattering matrix, one must then prepare N input fields and N output fields. So, measurements of the fields of N pulses must be made. Let $\{f_n^{(i)}\}$ and $\{f_n^{(o)}\}$, where n = 1, 2, ..., N, be the sets of output vectors and input vectors, respectively. From these two sets of fields, we may then construct the input matrix and output matrix as follows: Lining up the N input vectors, $f_n^{(i)}$, one by one as columns of a matrix, one obtains a square matrix $F^{(i)}$, which is the input matrix; similarly, lining up the N output vectors, $f_n^{(o)}$, one by one as columns of a matrix, one obtains the output matrix, $F^{(o)}$. It can then be proven that the scattering matrix is the product of these two matrices:

$$S = F^{(o)} \cdot [F^{(i)}]^{-1}. \tag{4}$$

The scattering matrix obtained this way has the property that

$$S f_n^{(i)} = f_n^{(o)} \quad (n = 1, ..., N). \tag{5}$$

It is remarked that the N microwave pulses must be linearly independent, viz., the input matrix, $F^{(i)}$, must be non-singular. In other words, the determinant of $F^{(i)}$ must not vanish. Instead of making measurements on N input pulses, one may alternatively use one single pulse, and make time resolved measurements at N+1 successive points of equal spacing along the path of the pulse. Thus, the pulse measured at, say x_i, is the output pulse of the previous layer of material and the input pulse of the next layer of material. Since the dielectric is assumed to be homogeneous, the layers of material between all successive pairs of points are identical. So, the pulses at x_1, x_2, ..., x_N are N input pulses to the specimen, and the pulses at x_2, x_3, ..., x_{N+1} are corresponding output pulses. Owing to dielectric dispersion and, perhaps, also transient or other non-linear effects, these N input pulses will be linearly independent, and may then be used to construct the input matrix.

Based on the transient state model that was discussed earlier (cf. eqs. 1-4), we have studied the properties of the scattering matrix S constructed from the field measurement data as described in the last paragraph. We found a distinct property which may be used to isolate transient effect from continuous wave (CW) effect. If there is any transient response in the biological material, or any dielectric material, between the two points x_1 and x_2, then the matrix S will not be diagonal in the frequency domain. Conversely, if there is no transient effect, then the scattering matrix must be diagonal in the frequency domain. Thus, this property may be used to isolate transient response from CW effect. This approach is applicable to the measurement setup planned at WRAIR. While we believe that the basic principle of this approach is sound, there is still a technical problem that needs further investigation. The problem concerns the finite sampling rate and finite time duration of measurement. Ideally, theory requires that infinitely many pulses be measured at both x_1 and x_2, and that measurements be made continuously in time. Finite sampling of measurement on finite number of pulses will then cause some "spreading" of the diagonal elements of the matrix S into off-diagonal part, thereby produce some mixing of the CW effect with transient effect. The effect of this spreading may be treated as a noise in the measurement data. The magnitude of this noise level remains to be investigated.

The effect of off-diagonal matrix elements in transient response is equivalent to harmonic generation in non-linear circuit theory. Therefore, the principle of the above approach also applies to high-field effect, however, there is a problem that needs separate consideration. Any high-field effect must give rise to a E^2 dependency in the output fields, therefore, some normalization method may also be needed on the output fields, as well as the input fields. The advantage of this method over conventional method of analyzing harmonic generation is that it is not limited to monochromatic input source; pulse input of arbitrary waveform may be employed.

4.2. Stress Waves and Pressure Waves Induced by Microwave Pulses

Acoustic waves generated by pulsed microwaves have been cited as a mechanism for microwave hearing.[15,16,17] More recently it has been demonstrated that acoustic waves are transduced in dielectric objects simulating the ocular lens when exposed to pulsed microwaves.[18] The effect has also been cited as the operant mechanism for cellular damage in studies of the murine ocular lens in vitro.[19] Three theories on the microwave auditory mechanism have been reviewed and compared by Lin,[20] viz., the radiation pressure theory, the electrostrictive theory, and the thermoacoustic theory. Among them it was found that only the thermoacoustic mechanism could produce elastic waves of magnitude large enough to explain the experimental observations. Comparing to the magnitude of acoustic pressure generated in typical biological tissues, the electrostrictive effect was found to be about two orders of magnitude smaller, while the radiation pressure three orders of magnitude smaller.[21]

Previous theories on microwave electrostrictive process and microwave thermoacoustic process are, however, based on a linear wave equation with a generating function derived from the microwave pulses. Pressure waves are thereby generated in a way similar to a forced harmonic oscillator. In the case of the thermoacoustic process, the generating function is derived from an inhomogeneous heating by the microwaves, whereas in the case of the electrostrictive process, it is derived from stress due to dielectric polarization.[22,23] This approach fails to consider the proper balance of the distribution of the absorbed microwave energy among the internal thermal energies and the bulk kinetic energy, and the effect of thermal or dielectric discontinuities at medium interface. Also neglected is the coupling between the thermoacoustic process and electrostrictive process, which may result from dependency of dielectric permittivity on various thermodynamical coefficients, such as mass density, temperature, and pressure; the transient effect of ultra-short electromagnetic pulses may further enhance the electrostrictive effect. We approached these problems by making a thorough formulation of the coupling of microwave pulses to pressure waves, with particular emphasis on material discontinuity and electromagnetic transient effect. Elastic wave equations were then derived for both thermoacoustic and electrostrictive effects, and some models of air-water system were used to make numerical computation and estimate the generated pressure waves in water. Contrary to previous theory that thermoacoustic pressure waves were generated mainly by inhomogeneous distribution of microwaves in dielectrics,[20] it was found that pressure waves are generated whenever there is a discontinuity in thermal or dielectric parameters in the medium. As to the ratio of electrostrictive effect to thermoacoustic effect, it depends on the rise time of the microwave pulse, being greater than one for rise time shorter than a nanosecond, and smaller than one for rise time longer than a nanosecond. This result is in contrary to previous estimate based on a simpler theory, which gave a ratio of the order of 10^{-2}, and independent of the rise time of microwave pulses.

The following paragraphs provide a summary of our results in thermoacoustic and electrostrictive effects. Details of the formulation are given in Appendices A, B, and F and other references cited therein.

Thermoacoustic Effect

Our approach to derive the coupling from microwave pulses to acoustic waves started from the basic laws of thermodynamics: the conservation of mass, the conservation of momentum, the conservation of energy, and the thermodynamic equation of state;the thermodynamic equation of state was represented by the following expression of internal energy in terms of some thermodynamical coefficients:

$$d_t U_I = [-C_p/(\rho\beta_p) + (1/\rho^2)p_{ij}\partial_j v_i/\nabla\cdot\mathbf{v}]d_t\rho + (C_v/\beta_p)(\kappa_T)_{ij}d_t p_{ij} \qquad (7)$$

which we derived from the first and second laws of thermodynamics.[24] In the above equation, ρ is the mass density, $\mathbf{v}$ is the bulk velocity, p_{ij} is the stress tensor, C_v and C_p are the specific heats (per unit mass) at constant volume and constant pressure, respectively, β_p is the isobaric thermal expansion coefficient, and $(\kappa_T)_{ij}$ is the isothermal compressibility tensor. By mutual substitution among equations representing these laws, one may obtain the wave equations for any of the thermodynamic quantities. The boundary conditions may be obtained by first transforming these equations to the Lagrangian specification (in which the boundary surface is stationary) and then integrating each term across a thin layer of the boundary interface.[6,24] If the strain tensor is isotropic, one obtains the following wave equation for the stress tensor, p_{ij}:

$$\partial_t[(\rho_o/\rho)^{1/3}(C_v/C_p)(\kappa_T)_{ij}\partial_t p_{ij}] - \partial_i[(\rho_o/\rho)^{1/3}(1/\rho)\partial_j p_{ij}] = \partial_t^2[(\rho_o/\rho)^{1/3}(\beta_p/C_p)P] \tag{8}$$

where C_v and C_p are the specific heats (per mass) at constant volume and constant pressure, respectively, β_p the isobaric thermal expansion coefficient, κ_T the isothermal compressibility, ρ the mass density, P the microwave specific absorption rate (SAR), and the subscript $_o$ signifies that the quantity is evaluated at its ambient equilibrium value.

To illustrate the implications of the wave equations and their respective boundary conditions, we consider a dielectric sphere of radius a surrounded by air at 1 atmospheric pressure. A square pulse of microwave of duration τ and amplitude P_o is incident upon the sphere. The sphere is assumed to be small so that the microwave absorption exhibits no spatial variation. In the linear approximation, the solutions of pressure waves in the frequency domain are then:

$$p_1(r,\omega) = -i\left(\frac{c^2\rho\beta_p}{C_p}\right)_1 \frac{P(\omega)}{\omega - i0} \cdot \left[\frac{j_o(k_1 r)}{j_o(k_1 a) - \tan\varphi \cdot \dfrac{h_o(k_2 a)}{h_o'(k_2 a)} \cdot j_o'(k_1 a)} - 1 \right] \tag{9}$$

and

$$p_2(r,\omega) = -i\left(\frac{c^2\rho\beta_p}{C_p}\right)_1 \frac{P(\omega)}{\omega - i0} \frac{h_o(k_2 r)}{h_o(k_2 a)} \cdot \left[\frac{j_o(k_1 a)}{j_o(k_1 a) - \tan\varphi \cdot \dfrac{h_o(k_2 a)}{h_o'(k_2 a)} \cdot j_o'(k_1 a)} - 1 \right] \tag{10}$$

where $j_n(x)$ and $h_n(x)$ are, respectively, the spherical Bessel and Hankel functions of the first kind of order n, the subscripts 1 and 2 label the dielectric and the air media, respectively, $c_{1,2} = [C_p/\rho C_v \kappa_T]^{1/2}$, $\tan\varphi = (\rho c)_2/(\rho c)_1$, and $P(\omega)$ is the Fourier transform of the square pulse SAR, which is given by:

$$P(\omega) = -(2\pi)^{1/2} P_o \frac{1 - e^{i\omega\tau}}{2\pi i \cdot (\omega - i0)} \tag{11}$$

Similar results may also be obtained for the bulk velocity at either side of the interface. The total acoustic energy coupled into the air may be obtained by calculating the work done by the dielectric on the air at the interface. To the first order, the result is:

$$E_{air} = 4\pi a^2 p_o \int_{-\infty}^{\infty} v_1(a,t)dt = 4\pi a^2 p_o (2\pi)^{1/2} \cdot v_1(a,\omega=0)$$

$$= (2\pi)^{1/2} \frac{4\pi a^3}{3} p_o \left[\frac{\beta_p}{C_p}\right]_1 \cdot P(\omega=0) \tag{12}$$

Since $E_{abs} = (2\pi)^{1/2}(4\pi a^3/3)\rho_l P(\omega=0)$ is the total microwave energy absorbed through the entire pulse, coupling efficiency of the absorbed microwave energy to the acoustic energy in the air is then:

$$\eta_{air} = \frac{E_{air}}{E_{abs}} = p_o[\frac{\beta_p}{\rho C_p}]_l \tag{13}$$

Take the dielectric to be water at 30 °C, so $\beta_p = 2.8\text{x}10^{-4}$ °C^{-1} and $C_p = 4.186\text{x}10^7$ erg/gm-°C. With the equilibrium pressure of the air, p_o, being 1 atm = $1.01\text{x}10^6$ dynes/cm^2, the coupling efficiency is then $\eta_{air} = 6.7\text{X}10^{-6}$ for a sphere of 1 cm diameter.

The minimum pressure amplitude generated in the water may be estimated by the fundamental harmonic in eq. 9. Taking an optimal pulse width of $\tau = \pi/\omega_o$, it gives a pressure amplitude of $(2a/\pi)(c\beta_p/C_p)_l P_o$. Using the values of β_p and C_p for 30 °C as cited above, a peak SAR of P_o = 15 kW/gm results in a pressure wave of amplitude equal to 0.1 bar in the water,[25] which is 10% of the initial equilibrium pressure. This fraction of variation in pressure will also result in at least equal fraction of error in the linear approximation. Similar calculation was also made for a one-dimensional air-water system.[24] It was found that, accounting for only the n = ±1 term, a peak SAR of 6.5 kW/gm results in a pressure wave of amplitude equal to 0.1 bar in the water;[26] if up to the first 11 terms are included, a peak SAR of 4.5 kW/gm suffices to generate pressure waves of such amplitude.

Electrostrictive Effect

We approached the problem of electrostrictive effect by including, in the equations of conservation of momentum and conservation of energy, the following electrostrictive tensor:[27]

$$\sigma_{ij} = \frac{E^2}{8\pi}[\varepsilon - \rho(\frac{\partial\varepsilon}{\partial\rho})_T]\delta_{ij} - \frac{\varepsilon}{4\pi}\cdot E_i E_j \tag{14}$$

The total stress on the dielectric is the sum of material stress and electrostrictive stress:

$$s_{ij} = p_{ij} + \sigma_{ij} \tag{15}$$

However, it is the material stress p_{ij} which is responsible for the material strain, and therefore accountable in the thermal internal energy. Indeed, in the presence of an electromagnetic field, the material stress automatically adjusts itself in reaction to the electrostrictive stress. Therefore, in deriving the equation of state which is represented by an expression of internal energy in terms of some thermodynamical coefficients (cf. eq. 7), only the material stress is included. Upon some isotropic assumption, we then derive the following wave equation for the total stress tensor:[1,2]

$$\partial_i\left(\frac{1}{\rho}\partial_j s_{ij}\right) - \partial_t\left(\frac{C_p}{\beta_p}+\frac{\sigma}{\rho}\right)^{-1}\cdot\left(\frac{C_v}{\beta\rho}(\kappa_T)_{ij}\,\partial_t s_{ij}\right)$$

$$= \left(\frac{C_p}{\beta_p}+\frac{\sigma}{\rho}\right)_o^{-1}\cdot\left[\rho_o\partial_t P + \left(\frac{\rho C_v}{\beta_p}(\kappa_T)_{ii}\right)_o\partial_t^2\sigma - \partial_t^2\left(\frac{\varepsilon|\mathbf{E}|^2}{8\pi}\right)\right] \tag{16}$$

where the subscript o signifies that the quantity is evaluated at its ambient equilibrium value, and σ is the isotropic electrostrictive pressure:

$$\sigma = -\left(\frac{|\mathbf{E}|^2}{16\pi} \left[\frac{\varepsilon}{3} - \rho\left(\frac{\partial \varepsilon}{\partial \rho}\right)_T \right] \right) \tag{17}$$

For an isotropic dielectric, $s_{ij} = -s\delta_{ij}$ and $(\kappa_T)_{ij} = \kappa_T/3$, so $\Sigma(\kappa_T)_{ii}$ (sum over i) is κ_T, the above wave equation is then further reduced to

$$\begin{aligned} \nabla^2 s - \left(\frac{C_p}{\beta_p} + \frac{\sigma}{\rho} \right)_o^{-1} \cdot \left(\frac{\rho C_v \kappa_T}{\beta_p} \right)_o \partial_t^2 s \\ = - \left(\frac{C_p}{\beta_p} + \frac{\sigma}{\rho} \right)_o^{-1} \cdot \left[\rho_o \partial_t P + \left(\frac{\rho C_v \kappa_T}{\beta_p} \right)_o \partial_t^2 \sigma - \partial_t^2 \left(\frac{\varepsilon |\mathbf{E}|^2}{8\pi} \right) \right] \end{aligned} \tag{18}$$

Equation 18 is a typical linear wave equation with the velocity $\tilde{c}$:

$$\tilde{u} = \left(1 + \frac{\sigma \beta_p}{\rho C_p} \right)_o^{1/2} \cdot \left(\frac{C_p}{\rho C_v \kappa_T} \right)_o^{1/2} = \left(1 + \frac{\sigma \beta_p}{\rho C_p} \right)_o^{1/2} \cdot u \tag{19}$$

where u denotes the acoustic velocity in the dielectrics in the absence of the electromagnetic waves. The electromagnetic waves change the acoustic velocity through the electrostrictive pressure σ. To estimate the magnitude of this correction, we consider water at room temperature as the dielectric, for which $\beta_p = 2.8\times10^{-4}$ °C^{-1}, $C_p = 4.186\times10^7$ erg/gm-°C, ρ = 1 gm/cm^3, and $\varepsilon = 80$. We also assume that the dielectric permittivity is linearly proportional to the mass density, so $(\partial\varepsilon/\partial\rho)_T = \varepsilon/\rho$, then eq. 17 gives $\sigma = (\varepsilon|\mathbf{E}|^2)/(24\pi)$. Assume a plane electromagnetic wave of intensity I = 1 kW/cm^2 (which is equivalent to an electric field of amplitude 2.9×10^4 volts/m), then its field magnitude is $|\mathbf{E}|^2 = 8\pi I/(c\sqrt{\varepsilon}) = 0.94$ erg/cm^3, where c is the speed of light in vacuum. Then σ = 1 dyne/cm^2, and the fractional change to the acoustic speed is $(\sigma\beta_p)/(\rho C_p) = 6.7\times10^{-12}$, which is insignificant. While the fractional change of acoustic speed is negligibly small for most dielectrics under currently available microwave sources, it may be appreciable for some dielectrics under lower frequency electromagnetic fields.

As illustrated at the end of the last paragraph, for most dielectrics and for microwave intensity up to gigawatts/cm^2, the term σ/ρ on both sides of eq. 18 may be neglected. Eq. 18 may then be rewritten as

$$\nabla^2 s - \frac{1}{u^2} \partial_t^2 s = - \frac{\beta_p}{C_p} \partial_t \left[\rho_o P + \left(\frac{\rho C_v \kappa_T}{\beta_p} \right)_o \partial_t \sigma - \partial_t \left(\frac{\varepsilon |\mathbf{E}|^2}{8\pi} \right) \right] \tag{20}$$

where $u = [\rho C_v \kappa_T / C_p]^{1/2}$ is the speed of sound in the dielectric in the absence of the electrostrictive force. The three terms inside the brackets on the right hand side are the generating forces of pressure waves. The first term represents the thermoelastic effect, the second term is the electrostrictive force, and the third term comes from the electromagnetic energy of dielectric polarization. The above equation will be our basis for comparing the relative strength of the three forces on microwave to pressure wave coupling. From the expression of these three forces in the above equation, one sees that time variation, namely,

transient effect, of the microwave pulses has an important effect on the electrostrictive force and on the polarization energy. Here we may make a preliminary estimation of the relative sizes of these three coupling forces. First we express them in terms of $|E|^2$. Let α be the attenuation coefficient of microwave intensity as defined by the equation $I(x) = I_o e^{-\alpha x}$. Then the first term is $\rho_o P = \alpha I = (\alpha c\sqrt{\varepsilon}/8\pi)|E|^2$. If the dielectric permittivity is linear in ρ, then $(\partial\varepsilon/\partial\rho)_T = \varepsilon/\rho$, so eq. 17 gives $\sigma = (\varepsilon|E|^2)/(24\pi)$ and the electrostrictive term gives $[(\rho\varepsilon C_v\kappa_T)/(24\pi\beta_p)]\partial_t|E|^2$. Denote by t_r the rise time of a microwave pulse, then $\partial_t|E|^2 \sim |E|^2/t_r$. Thus, the relative magnitudes of the electrostrictive and polarization terms with respect to the thermoelastic term are, respectively,

$$\frac{\text{Electrostrictive effect}}{\text{Thermoelastic effect}} = \frac{\rho C_v \kappa_T \sqrt{\varepsilon}}{3c\alpha\beta_p}\,\frac{1}{t_r}$$
$$\frac{\text{Polarization effect}}{\text{Thermoelastic effect}} = \frac{\sqrt{\varepsilon}}{c\alpha}\,\frac{1}{t_r} \qquad (21)$$

One sees that the second and the third driving forces may be larger than the thermoelastic term if the microwave is rapidly modulated, contrary to the estimate by previous theory that the electrostrictive effect is two orders of magnitude smaller[20]. For water at 30 °C, ρ = 1 gm/cm^3, $C_p = 1.013\cdot C_v = 4.186\times10^7$ erg/gm°C, $\kappa_T = 4.46\times10^{-11}$ cm^2/dyne, $\beta_p = 2.8\times10^{-4}$ °C^{-1}, and, at 3 GHz, $\alpha = 0.88$ cm^{-1} and $\varepsilon = 80$. The above ratios are then, respectively:

$$\frac{\text{Electrostrictive effect}}{\text{Thermoelastic effect}} = \frac{0.75 \text{ nanosec}}{t_r}$$
$$\frac{\text{Polarization effect}}{\text{Thermoelastic effect}} = \frac{0.34 \text{ nanosec}}{t_r} \qquad (22)$$

One may conclude that, for water, a rise time of 1 nanosecond is the marginal modulation rate, beyond which the electrostrictive term and the polarization term contribute more to the pressure waves than the thermoelastic term.

Comparison with Experimental Measurements

Pressure measurements were made at WRAIR in air-water system similar to the models in our theoretical computation. Pressure waves were measured in both air and saline liquid for two types of vessels placed in an WR 975 exposure system. The first vessel was ca. one inch on each side with a 1/8 inch wall thickness. The second vessel was circular in cross section, one inch in outer diameter, 1/8 inch wall thickness, and made of acrylic plastic. Both were filled with phosphate buffed saline. These vessels were placed into the WR 975 via the same waveguide below cut-off window as the actual lenticular exposure chamber. The two vessels extended beyond the waveguide to provide a liquid column for coupling of the acoustic wave into regions where the hydrophone would not be subject to direct influence of the electromagnetic field. Each vessel was separately matched to the microwave source with the triple stub tuner. Typical return losses were ca. -15 to -20 dB for either vessel. All liquid based pressure measurements are expressed in dB relative to 0 dB = 1 micro Pascal, and all air based pressure measurements are made in dB relative to 0 dB = 20 micro Pascal. Both air and water pressure measurements were tested for direct electromagnetic field effects. The results of the measurements appeared to be in agreement with our theoretical calculation.[6]

4.3. Microwave Scattering, Inverse Scattering, and Dosimetry

An important practical aspect of microwave biological damage concerns the dosimetry of microwaves in biological bodies. Biological bodies are complicate dielectric structures and multiple scattering and reflection from dielectric interfaces often make it impossible to predict microwave dose distribution in the bodies. Experimental measurements using insertion technique are used, but the instruments often produce unpredictable disturbances on the electromagnetic field and thus render the measurements inaccurate. Therefore non-invasive measurement techniques are much desired. Our effort in this subject has been to develop an inverse scattering approach to accomplish microwave dosimetry by measuring scattered fields.

There are two aspects in this subject. One is the determination of scattered fields from the dielectric profile of a dielectric object, and another concerns the determination of the electric fields inside the target from measurement of the scattered fields in a limited region outside the target. Both aspects have been under intensive investigation by many researchers. On the determination of scattered fields from dielectric profiles of scattering objects, previous approaches by other investigators included: 1) Born approximation, of which the accuracy was limited,[28] 2) the moment method by Richmond, which applied to only two-dimensional objects, viz., objects with cylindrical symmetry,[29,30] and 3) linear parameter technique with moment method, which approximated the field inside the scatterer by a linear combination of some basis functions and then numerically solved the linear coefficients. Therefore our main effort on this aspect has been to extend Richmond's moment method to three-dimensional object with arbitrary geometry and dielectric profile. Our effort has been quite successful. We have developed the following algorithm to compute the scattered field of arbitrary three-dimensional dielectric objects from their dielectric profile. As to the second problem, viz., determination of electric fields inside a target from measurement of scattered fields in a limited region outside the target, it is the problem of inverse scattering, and is also related to microwave imaging; once the field inside the target is known, one may then obtain a dielectric image in terms of the profile of dielectric permittivity of the target. On this subject, we also developed two inverse scattering approaches. The first approach utilizes a method of "soft focusing" of scattering data to reconstruct qualitative dielectric images with negligible computing time. The second approach utilizes a method of converting the integral wave equation to matrix equation and reconstructs images by matrix inversion. This method provides images with resolution limited only by signal-to-noise ratio and computer power, and not by wavelength. Both algorithms achieve three-dimensional imaging by measuring scattered waves in the near zone where the wave structure is correlated to the "depth" of the target.

Microwave Scattering

The objective of this problem was to develop a method to compute scattered microwave fields from an arbitrary three-dimensional inhomogeneous object. Our approach is to convert the integral equation into a matrix equation by digitizing the target space and the measurement space. First, denote by V_o the region occupied by the dielectric object, and by V_α a region outside of V_o in which scattered fields are measured. We divide both V_o and V_α into a number of small cells, say, N cells, and denote by $\mathbf{x}_i$ and $\mathbf{y}_i$, respectively, the centers of the ith cell in V_α and V_o. Let $f_o^{(i)}$ be a N-dimensional vector representing the incident field in the N cells inside the dielectric body V_o, and let $f_\alpha^{(s)}$ be a N-dimensional vector representing the scattered fields in the N cells inside the measurement region V_α. Then we have developed the following formula to compute $f_\alpha^{(s)}$ from the incident field $f_o^{(i)}$:

$$|f_\alpha^{(s)}\rangle = G_\alpha(S^{-1} - G_o)^{-1}|f_o^{(i)}\rangle \tag{23}$$

where S, G_o, and G_α are, respectively, dielectric profile of the scattering body, Green's matrix inside V_o, and correlated Green's matrix between V_α and V_o; $f_o^{(i)}$ is the incident field inside the target, which is known and readily obtainable in analytic form. Note that, since we are dealing with vector fields, each element of the N-dimensional vectors is itself a 3-dimensional vector, and each element of the N x N matrices is a 3 x 3 matrix. Explicitly, the matrix S is given by:

$$S_{ij} = \frac{-1}{\varepsilon_m}[\varepsilon(\mathbf{y}_i) - \varepsilon_m]\,\delta_{ij} \qquad (\mathbf{y}_i \subset V_o) \tag{24}$$

As to G_o and G_α, we have been successful in developing analytical formulas for these matrices, and thereby avoided making any Born approximation or linear parameterization. Denoting by k_m the wave number in the background medium, a the radius of a sphere of volume equal to that of the cells, $\mathbf{y}_i$ and $\mathbf{y}_j$, respectively, the centers of the ith and jth cells inside V_o, and $\mathbf{x}_i$ the center of the ith cell in V_α, the results are, for the matrix G_o:

$$i = j: \quad (G_o)_{ij} = \vec{\mathbf{I}}\left(1 + \frac{2}{3}a^2\frac{d}{da}\left[\frac{\exp(ik_m a)}{a}\right]\right) \qquad (\mathbf{y}_i, \mathbf{y}_j \subset V_o)$$

$$i \neq j: \quad (G_o)_{ij} = a\frac{\exp(ik_m|\mathbf{y}_i-\mathbf{y}_j|)}{|\mathbf{y}_i-\mathbf{y}_j|}\cdot[\cos(k_m a) - \frac{1}{k_m a}\cdot\sin(k_m a)] \qquad (\mathbf{y}_i, \mathbf{y}_j \subset V_o) \tag{25}$$

$$\times\left(\vec{\mathbf{I}}\left(1 - \frac{1}{ik_m|\mathbf{y}_i-\mathbf{y}_j|} + \frac{1}{(ik_m|\mathbf{y}_i-\mathbf{y}_j|)^2}\right) - \frac{(\mathbf{y}_i-\mathbf{y}_j)(\mathbf{y}_i-\mathbf{y}_j)}{|\mathbf{y}_i-\mathbf{y}_j|\cdot|\mathbf{y}_i-\mathbf{y}_j|}\left(1 - \frac{3}{ik_m|\mathbf{y}_i-\mathbf{y}_j|} + \frac{3}{(ik_m|\mathbf{y}_i-\mathbf{y}_j|)^2}\right)\right)$$

and, for the correlated matrix G_α between V_α and V_o:

$$(G_\alpha)_{ij} = a\frac{\exp(ik_m|\mathbf{x}_i-\mathbf{y}_j|)}{|\mathbf{x}_i-\mathbf{y}_j|}\cdot[\cos(k_m a) - \frac{1}{k_m a}\cdot\sin(k_m a)] \qquad (\mathbf{x}_i \subset V_\alpha,\ \mathbf{y}_j \subset V_o) \tag{26}$$

$$\times\left(\vec{\mathbf{I}}\left(1 - \frac{1}{ik_m|\mathbf{x}_i-\mathbf{y}_j|} + \frac{1}{(ik_m|\mathbf{x}_i-\mathbf{y}_j|)^2}\right) - \frac{(\mathbf{x}_i-\mathbf{y}_j)(\mathbf{x}_i-\mathbf{y}_j)}{|\mathbf{x}_i-\mathbf{y}_j|\cdot|\mathbf{x}_i-\mathbf{y}_j|}\left(1 - \frac{3}{ik_m|\mathbf{x}_i-\mathbf{y}_j|} + \frac{3}{(ik_m|\mathbf{x}_i-\mathbf{y}_j|)^2}\right)\right)$$

Details of description of these quantities and derivation of the formulas are given in Appendix C.

Microwave Dosimetry and Quantitative Microwave Imaging by Matrix Inversion

The Green's matrix approach described above also allowed us to solve the second aspect of dosimetry problem, viz., the determination of the electric field inside the target from measurement of the scattered field in a limited region outside the target. We have derived the following equations relating the scattered fields in V_o and in V_α to the total fields inside the dielectric body, V_o:

$$|f_o^{(s)}\rangle = G_o S|f_o\rangle \tag{27}$$

$$|f_\alpha^{(s)}\rangle = G_\alpha S|f_o\rangle \tag{28}$$

where f_o is a N-dimensional vector representing the total fields in the N cells of the dielectric body. Applying the inverse of G_α to both sides of the second equation and substituting the result to the first equation, and then adding the incident fields $f_o^{(i)}$ to both sides, one gets:

$$|f_o> = |f_o^{(i)}> + G_o G_\alpha^{-1} |f_\alpha^{(s)}> \tag{29}$$

which gives the total field inside the dielectric body in terms of the measured scattered field in any region, say V_α, outside the body. With this formula, we have accomplished the principal goal of non-invasive dosimetry.

The above approach may also be extended to microwave imaging. Once the field is known inside the target V_o, one may then derive the dielectric profile inside the target. To this end, we first derived the following relationship:

$$S[|f_o^{(i)}> + G_o G_\alpha^{-1} |f_\alpha^{(s)}>] = G_\alpha^{-1} |f_\alpha^{(s)}> \tag{30}$$

from which we obtained the dielectric profile inside the target in terms of the scattered field outside the target:

$$S_{ii} = \frac{-1}{\varepsilon_m}[\varepsilon(\mathbf{y}_i) - \varepsilon_m] = \frac{\sum_j (G_\alpha^{-1})_{ij} f_\alpha^{(s)}(\mathbf{x}_j)}{f_o^{(i)}(\mathbf{y}_i) + \sum_{jk} (G_o)_{ij} (G_\alpha^{-1})_{jk} f_\alpha^{(s)}(\mathbf{x}_k)} \tag{31}$$

The above equation gives the dielectric permittivity of the i^{th} cell, S_{ii}, in the target in terms of the scattering fields $f_\alpha^{(s)}(\mathbf{x}_j)$ in any scattering space, V_α, outside the scatterer, and the incident fields $f_o^{(i)}$ inside the scatterer. The incident fields inside the scatterer, $f_o^{(i)}(\mathbf{x}_j)$, are known analytically.

There is still one problem that needs further study. It concerns the data stability of the inverse of the matrix G_α. Our dosimetry algorithm, as described by the above equation, requires computation of the inverse of G_α. If this matrix is almost singular, then computation of its inverse may be unstable with respect to noises and errors in the data of its matrix elements. Therefore, further effort on non-invasive dosimetry must be focused on developing techniques to stabilize the inverse of G_α.

Microwave Dosimetry and Qualitative Microwave Imaging by "Soft Focusing"

The objective of inverse scattering is to reconstruct the target from the scattered field. From Maxwell's electromagnetic theory, if one knows the scattered field everywhere in space, the source of the field, which is the induced charge-current distribution in the target, can be derived completely. However, in practice, one can only measure the scattered field exterior to the target and only at a limited number of points in space which are often confined in a small region. The question is then how much information on the scattering target one can infer based on a limited knowledge of the scattered field. Here we remark that the term "scattering field" differs from the conventional definition in the sense that it refers to a field anywhere outside of the target; it does not need to be far away from the target. Indeed, the fields for image reconstruction must be close to the target in order to contain information on the depth of the target.

Our approach to inverse scattering with a limited number of data is to use a soft focusing technique to focus the scattering data back to the target. Mathematically, soft focusing is similar to regular focusing of radiation, which we call "hard focusing". In hard focusing, the substance is some sort of radiation, the tool is a lens, and the focal point is where the radiation energy converges. In parallel, the substance of soft focusing is a set of information data, the focusing tool is some algorithm, and the focal point is where the information consolidates. The soft focusing technique is based on an inverse scattering theorem that we have formulated:[5,31]

$$\frac{c}{\varepsilon_m}\iiint_{V_o}\left[-(\nabla\cdot\mathbf{A}_w)\left(\nabla\cdot\frac{\chi-\chi_m}{\chi}\mathbf{P}\right)+k_m^2\mathbf{A}_w\cdot\frac{\chi-\chi_m}{\chi}\mathbf{P}\right]d\mathbf{x} = \sum_n \mathbf{J}_n\cdot\mathbf{E}_{scatt}(\mathbf{x}_n) \tag{32}$$

where the quantities are defined as below:

c	Speed of light in vacuum.
V_o	Space occupied by the target.
ε_m, χ_m	Dielectric susceptibility and dielectric permittivity, respectively, of water, which is the background medium.
$\chi = \chi(\mathbf{x})$	Dielectric susceptibility of the target.
$k_m = \sqrt{\varepsilon_m}\omega/c$	Wave number of the probing microwave in the background medium.
$\omega/2\pi$	Microwave frequency.
$\mathbf{P} = \mathbf{P}(\mathbf{x})$	Induced dielectric polarization in the target.
$\mathbf{x}_n$	Coordinate of the n^{th} element of the receiving array.
$\mathbf{E}_{scatt}(\mathbf{x}_n)$	Electric field of the scattered wave measured by the n^{th} element of the receiving array.
$\mathbf{J}_n$	Weighing factor to be applied to the n^{th} element of the array.
$\mathbf{A}_w = \mathbf{A}_w(\mathbf{x})$	Vector field that would be produced by a set of current elements equivalent to the set of weighing factors $\{\mathbf{J}_n\}$.

The theorem described above may be considered as a generalization of Lorentz reciprocity theorem.[32,33,34] So, multiplying the measured scattered field at each of the array element with a weighing factor, then the sum of the products is c/ε_m times the sum of the integrals of $\nabla\cdot[(1-\chi_m/\chi)\mathbf{P}]$ and $[(1-\chi_m/\chi)\mathbf{P}]$ weighted by, respectively, $-\nabla\cdot\mathbf{A}_w$ and $k_m^2\mathbf{A}_w$. The weighing field $\mathbf{A}_w$ is equal to the vector field that would be produced by a set of current distribution equal to the weighing factors, $\{\mathbf{J}_n\}$, so it is given by:

$$\mathbf{A}_w(\mathbf{x}) = \sum_n \frac{\exp(ik_m|\mathbf{x}-\mathbf{x}_n|)}{|\mathbf{x}-\mathbf{x}_n|}\mathbf{J}_n \tag{33}$$

The integral on the left hand side of eq. 32 is to integrate over only the target, therefore it will not be affected by the values of $\mathbf{A}_w$ outside the target. This gives us a free hand to select the weighing factors $\{\mathbf{J}_n\}$. To retrieve dielectric property of the target at a focal point, say $\mathbf{x}_f$, one then finds a set of weighing factors $\{\mathbf{J}_n\}$ such that the corresponding vector field $\mathbf{A}_w$ has a sharp peak at $\mathbf{x}_f$, and negligibly small elsewhere inside the target. We have found that this is possible by selecting the magnitude of the vector $\mathbf{J}_n$ to be the phase-amplitude conjugation corresponding to the path from the element $\mathbf{x}_n$ to the desired focal point, $\mathbf{x}_f$:

$$|\mathbf{J}_n(\mathbf{x}_f)| = c|\mathbf{x}_n-\mathbf{x}_f|\cdot\exp(-ik_m|\mathbf{x}_n-\mathbf{x}_f|) \tag{34}$$

As to the direction of $\mathbf{J}_n$, if only one direction of the scattered field is measured by the array elements, then $\mathbf{J}_n$ may be chosen to be in that direction only, so that the sum on the right hand side of eq. 32 can be calculated from the measured field.

To summarize our approach of soft focusing, one first acquires the scattered fields at each of the array elements at $\{\mathbf{x}_n\}$, a qualitative dielectric property of the target at any point, say $\mathbf{x}_f$, is given by:

$$\text{Qualitative dielectric property at } \mathbf{x}_f = \sum_n \mathbf{J}_n \cdot \mathbf{E}_{scatt}(\mathbf{x}_n) \tag{35}$$

where the magnitude of $\mathbf{J}_n$ is given by eq. 34, and its direction is taken to be that of the field being measured. If only one direction, say, y-direction, of $\mathbf{E}_{scatt}$ is measured, then take $\mathbf{J}_n$ to be only in y-direction, so that only the measured part of the field enters the above equation. The set of factors $\{\mathbf{J}_n\}$ works like a synthetic soft lens for focusing the scattering data, and the weighing field, $\mathbf{A}_w(\mathbf{x})$, gives the equivalent field pattern of the soft lens. Therefore, the quality of the soft lens may be evaluated by analyzing the field pattern of $\mathbf{A}_w(\mathbf{x})$. Note that, given any lens $\{\mathbf{J}_n\}$, the corresponding field $\mathbf{A}_w(\mathbf{x})$ will have all sorts of peaks outside some finite region. These peaks will contribute to the integral on the left hand side of eq. 32 unless they are outside the target. Therefore, some *a priori* knowledge on the geometrical extent of the target is a necessary condition of the applicability of the above "soft focusing" method.

We have made numerical computation and modeling to analyze the sensitivity of the above "soft focusing" technique. The computation is based on a water-immersed medical imaging system that we studied for the Walter Reed Army Institute of Research (WRAIR). The receiving antenna has hexagonal lattice structure with 127 waveguide-fed antenna elements, each of size 4 mm × 7 mm (see Figures 1a-1c of Appendix E or reference 5). The system operates at 3 GHz in water. These results show a 3 dB focusing resolution of about 5 mm in the transverse direction, and 11 mm in the longitudinal direction (see Figures 2-5 and Table 1 of Appendix E or reference 5).

REFERENCES

1. T. C. Guo and W. W. Guo, "Dielectric Acoustic Response to Microwave Pulses Through Thermoacoustic and Electrostrictive Effects," Annual Report of the Conference on Electrical Insulation and Dielectric Phenomena, pp. 152-158, Washington, D.C., October 1987, IEEE Publication 87CH2462-0, Library of Congress No. 79-649806.

2. T. C. Guo and W. W. Guo, "Generation of Acoustic Waves at Dielectric Interface by Microwave Pulses," IEE Proceedings of the Fifth International Conference on Dielectric Materials, Measurements, and Applications, June 1988, Canterbury, England (in press).

3. T. C. Guo and W. W. Guo, "Scattering of Vector Waves by Arbitrary Three-Dimensional Dielectric Objects," Proceedings of the 1987 International Microwave Symposium, pp. 307-312, Rio de Janeiro, Brazil, July 1987, IEEE Publication 87TH0183-4, Library of Congress No. 87-80089.

4. T. C. Guo and W. W. Guo, "Physics of Image Formation by Microwave Scattering," SPIE Proceedings **767**, pp. 30-39, February 1987.

5. T. C. Guo, W. W. Guo, and L. E. Larsen, "Recent Development in Microwave Medical Imagery - Phase and Amplitude Conjugations and the Inverse Scattering Theorem," in Medical Applications of Microwave Imaging, ed. L. E. Larsen and J. H. Jacobi, pp. 167-183, IEEE Press, 1986.

6. T. C. Guo, W. W. Guo, and L. E. Larsen, "Microwave Induced Thermoelastic Process in Dielectrics - Theory and Experiments," International Journal of Infrared and Millimeter Waves, Plenum Press, **6**, 405-422 (1985).

7. T. C. Guo and W. W. Guo, "A Transient-State Theory of Dielectric Relaxation and the Curie-von Schweidler's Law," J. Phys. C: Solid State Phys., vol. 16, pp. 1955-1960, 1983.

8. T. C. Guo and W. W. Guo, "A Transient-State Theory of Dielectric Relaxation and Some Empirical Laws," Annual Report of the Conference on Electrical Insulation and Dielectric Phenomena, pp. 29-38, Amherst, Massachusetts, October 1982, IEEE Publication 82CH1773-1, Library of Congress No. 79-649806.

9. T. C. Guo and W. W. Guo, "A Transient-State Model of Dielectric Response Accounting for Lag of Many- Body Effects," J. Electrostatics, vol. 12, pp. 229-234, Elsevier Sci. Pub. Co., 1982.

10. T. C. Guo and W. W. Guo, "Transient Dielectric Response to Radiation Pulses Under Non-Steady State Condition," Proc. 2nd Int'l Symp. Radiation Phys., Penang, Malaysia, pp. 190-197, May 1982.

11. I. S. Gradshteyn and I. M. Ryzhik, Table of Integrals, Series, and Products, 4th ed., p. 1045, Academic Press, New York, 1965.

12. G. S. Edwards, C. C. Davis, and M. L. Swicord, Phys. Rev. Lett., Vol. 53, p. 1284, 1984.

13. C. C. Davis, G. S. Edwards, and M. L. Swicord, Proc. Symp. Linear and Non-linear Phenomena in Biological and Synthetic Polymers, Hayashibana Forums, Okayama, Japan, 1985.

14. H. Kliem and B. Schumacher, "Time-Dependent Dielectric Susceptibility in High Electric Fields," IEEE Trans. Elec. Insul., Vol. EI-32, p. 219, 1987.

15. K. R. Foster and E. E. Finch, "Microwave hearing: Evidence for thermoacoustical auditory stimulation by pulsed microwaves," Science **185**, pp. 256-258 (1974).

16. J. C. Lin, "Further studies on the microwave auditory effect," IEEE Trans. Microwave Theory Tech. **MTT-25**, pp. 938-943 (1977).

17. Borth, D. E., and Cain, C. A., "Theoretical analysis of acoustic signal generation in materials irradiated with microwave energy," IEEE Trans. Microwave Theory Tech., MTT-25, pp. 944-954, 1977.

18. P. V. K. Brown and N. C. Wyeth, "Laser interferometer for measuring microwave-induced motion in eye lenses in vitro," Rev. Sci. Instrum., 54, pp. 85-89 (1983).

19. P. J. Stewart-DeHaan, M. O. Creighton, L. E. Larsen, J. H. Jacobi, W. M. Ross, M. Sanwal, T. C. Guo, W. W. Guo, and J. R. Trevithick, "In Vitro Studies of Microwave-Induced Cataract: Separation of Field and Heating Effects," Exp. Eye Res., 36, pp. 75-90 (1983).

20. J. C. Lin, Microwave Auditory effects and Applications, Spring-field, IL: C. C. Thomas, 1978.

21. See reference 20, Table XIII, p. 126.

22. See reference 20, pp. 115-118.

23. Oscar, K. J., "Interaction of Electromagnetic Energy with Absorptive Materials by Thermally Inducing Elastic Stress Wave," The American University Ph.D. Dissertation, University Microfilms International 8017445, 1980.

24. T. C. Guo, W. W. Guo, and L. E. Larsen, "Microwave Induced Thermoacoustic Effect in Dielectrics and Its Couplings to External Medium - A Thermodynamical Formulation," IEEE Trans. Microwave Theory Tech., vol. MTT-32, pp. 835-843, 1984.

25. Our earlier estimate, as published in reference 6, gave a specific absorption rate (SAR) of 30 kW/gram to produce an acoustic wave of this peak pressure; the estimate neglected the m=-1 term.

26. Our earlier estimate, as published in reference 24, gave a specific absorption rate (SAR) of 13 kW/gram to produce an acoustic wave of this peak pressure; the estimate neglected the m=-1 term.

27. L. D. Landau, E. M. Lifshitz, and L. P. Pitaevskii, Electrodynamics of Continuous Media, pp. 59-62, Oxford: Pergamon Press, 1984.

28. J. B. Keller, "Accuracy and validity of the Born and Rytov approximations," J. Opt. Soc. America **59**, pp. 1003-1004 (1969).

29. J. H. Richmond, "Scattering by a Dielectric Cylinder of Arbitrary Cross-Section," IEEE Trans. **AP-13**, pp. 334-341 (1965).

30. J. H. Richmond, "TE-Wave Scattering by a Dielectric Cylinder of Arbitrary Cross Section Shape," IEEE Trans. **AP-14**, pp. 460-464 (1966).

31. T. C. Guo, W. W. Guo, and L. E. Larsen, "Microwave Imagery of Biological Objects - An Inverse Scattering Approach," Proc. 8th Int'l Symp. Infrared and Millimeter Waves, December 1983, Florida, IEEE Publication 83CH1917-4, Library of Congress No. 83-81469.

32. J. R. Carson,"Reciprocaltheoremsinradiocommunication,"Proc.IRE**17**,pp. 952-956(1929).

33. J. H. Richmond, "A reaction theorem and its application to antenna impedance calculations," IRE Trans. Antenna and Propagation **AP-9**, pp. 515-520 (1961).

34. L. D. Landau and E. M. Lifshitz, Electrodynamics of Continuous Media, Pergamon Press, Oxford, 1960.

APPENDICES - Reprints from Publications

Appendix A. Dielectric Acoustic Response to Microwave Pulses Through Thermoacoustic and Electrostrictive Effects, reprint from Annual Report of the Conference on Electrical Insulation and Dielectric Phenomena, IEEE Publication 87CH2462-0, Library of Congress No. 79-649806, October 1987.

Appendix B. Generation of Acoustic Waves at Dielectric Interface by Microwave Pulses, preprint of a publication in IEE Proceedings of the Fifth International Conference on Dielectric Materials, Measurements, and Applications, June 1988, Canterbury, England (in press).

Appendix C. Scattering of Vector Waves by Arbitrary Three-Dimensional Dielectric Objects, reprint from the Proceedings of the 1987 International Microwave Symposium, July 1987.

Appendix D. Physics of Image Formation by Microwave Scattering, reprint from SPIE Proceedings, Vol. 767, February 1987.

Appendix E. Recent Development in Microwave Medical Imagery - Phase and Amplitude Conjugations and the Inverse Scattering Theorem, reprint from Medical Applications of Microwave Imaging, ed. L. E. Larsen and J. H. Jacobi, IEEE Press, 1986.

Appendix F. Microwave Induced Thermoelastic Process in Dielectrics - Theory and Experiments, reprint from International Journal of Infrared and Millimeter Waves, Plenum Press, **6**, 1985.

APPENDIX A

DIELECTRIC ACOUSTIC RESPONSE TO MICROWAVE PULSES THROUGH THERMOACOUSTIC AND ELECTROSTRICTIVE EFFECTS

Theodore C. Guo and Wendy W. Guo
Department of Physics, The Catholic University of America
Washington, D.C. 20064

INTRODUCTION

Acoustic waves generated by pulsed microwaves have been cited as a mechanism for microwave hearing [1],[2],[3]. More recently it has been demonstrated that acoustic waves are transduced in dielectric objects simulating the ocular lens when exposed to pulsed microwaves [4]. The effect has also been cited as the operant mechanism for cellular damage in studies of the murine ocular lens in vitro [5]. Three theories on the microwave auditory mechanism have been reviewed and compared by Lin [6], viz., the radiation pressure theory, the electrostrictive theory, and the thermoacoustic theory. Among them it was found that only the thermoacoustic mechanism could produce elastic waves of magnitude large enough to explain the experimental observations. Comparing to the magnitude of acoustic pressure generated in typical biological tissues, the electrostrictive effect was found to be about two orders of magnitude smaller, while the radiation pressure three orders of magnitude smaller [7].

Previous theories on microwave electrostrictive process and microwave thermoacoustic process are based on a linear wave equation with a generating function derived from the microwave pulses. Pressure waves are thereby generated in a way similar to a forced harmonic oscillator. In the case of the thermoacoustic process, the generating function is derived from an inhomogeneous heating by the microwaves, whereas in the case of the electrostrictive process, it is derived from stress due to dielectric polarization [8],[9]. This approach fails to consider the proper balance of the distribution of the absorbed microwave energy among the internal thermal energies and the bulk kinetic energy, and the effect of thermal or dielectric discontinuities at medium interface. Also neglected is the coupling between the thermoacoustic process and electrostrictive process, which may result from dependency of dielectric permittivity on various thermodynamical coefficients,

Reprint from the Annual Report of the 1987 IEEE Conference on Electrical Insulation and Dielectric Phenomena.

such as mass density, temperature, and pressure; this coupling may further enhance the electrostrictive effect.

Earlier, we have developed a thermodynamical formulation of the process of microwave absorption and its coupling to the internal thermal energy and mechanical bulk energy in the dielectrics [10]. It was shown that acoustic waves may be generated by microwave pulses if there are discontinuities in thermodynamical characteristics in the dielectrics, or discontinuities in microwave absorptions. Numerical results for a one-dimensional system and a spherical system with water as the absorbing dielectric have been compared consistently with experimental results, which included measurement of pressure waves in a cylinder filled with an aqueous solution of electrolytes exposed to pulsed microwaves and estimation of the coupling efficiency between the liquid dielectric and the adjacent air [11]. However, these studies did not include electrostrictive force in the dielectric and the dielectric interface. In this paper, we reformulate the problem to include electrostrictive stress and show that it may play an important role in the generation of pressure waves by microwave pulses in dielectrics with thermal or dielectric discontinuities. We also show that, in the first-order linear approximation, the effect of the electrostrictive force on the acoustic velocity is negligible.

THEORY OF MICROWAVE ACOUSTICS

Our approach to derive the coupling from microwave pulses to acoustic waves is to start from the laws of the conservation of mass, the conservation of momentum, the conservation of energy, and the thermodynamic equation of state. When a dielectric system is exposed to microwave radiation, microwave energy is absorbed into the dielectric through the work of the electric field on the electric polarization: $\mathbf{E}\cdot d\mathbf{P}$, which is then partially converted into the internal energy U_I and partially into the bulk kinetic energy U_k via thermal expansion and other elastic vibrations. The process is complex and irreversible; however, we shall assume that the time domain which concerns us is much greater than the time it takes to reach a quasi-steady state and that every microscopically small part of the system is in local equilibrium so that thermodynamic variables may be defined.

Reprint from the Annual Report of the 1987 IEEE Conference on Electrical Insulation and Dielectric Phenomena.

The time domain of our interest is the width of the microwave pulse, which is in the order of microseconds and is too short for any heat conduction and convective flow to take place. On the other hand, the time cycle of electric field is in the range of subnanosecond, which is much shorter than the time domain of our concern. Therefore, we may average all variables over a microwave cycle. The resulting time-average of $\mathbf{E}\cdot d\mathbf{P}$ gives the microwave energy absorbed by the dielectric, δQ_P, and the electrostrictive work on the dielectric, δW_P. Thus, the first law of thermodynamics gives:

$$\delta Q_P + \delta W_P = d(U_I + U_k) + \delta W \qquad (1)$$

where δW is the mechanical work done by the dielectric; heat flow by conduction and convection have been ignored, as explained earlier. Denote by p_{ij} the stress tensor in the dielectric, and by σ_{ij} the electrostrictive stress tensor on the dielectric by the electromagnetic field, then $\iiint \partial_j p_{ij} dV$ and $\iiint \partial_j \sigma_{ij} dV$ are, respectively, the force on the dielectric volume element by the surrounding body and the force on the element by the electromagnetic field. The total stress tensor experienced by the dielectric is then the sum of p_{ij} and σ_{ij}, which will be denoted by s_{ij}:

$$s_{ij} = p_{ij} + \sigma_{ij}$$

If ε is the dielectric permittivity, then [12]

$$\sigma_{ij} = \frac{\mathbf{E}^2}{8\pi}\left[\varepsilon - \rho\left(\frac{\partial \varepsilon}{\partial \rho}\right)_T\right]\delta_{ij} - \frac{\varepsilon}{4\pi} E_i E_j \qquad (2)$$

Averaging over the microwave cycle, the terms $E_i E_j$ vanish except for i=j, and the above equation gives:

$$\sigma_{ij} = \left[\frac{|\mathbf{E}|^2}{16\pi}\left[\varepsilon - \rho\left(\frac{\partial \varepsilon}{\partial \rho}\right)_T\right] - \frac{\varepsilon}{8\pi}|E_i|^2\right]\delta_{ij} \qquad (3)$$

In order to convert eq. (1) into a differential equation with respect to space and time, we start from a general form of the equation of conservation. Let g be a thermodynamic extensive quantity, S_g be the rate of production of g, which may be due to internal production or external input, and $\mathbf{v}$ be the bulk velocity function, then the equation of conservation for g is:

Reprint from the Annual Report of the 1987 IEEE Conference on Electrical Insulation and Dielectric Phenomena.

$$\partial_t g + g\nabla\cdot\mathbf{v} = S_g \tag{4}$$

where we have ignored the second order term $\mathbf{v}\cdot\nabla g$ by assuming that both g and $\mathbf{v}$ are small. The first term on the left represents the rate of increase of g per unit volume, and the second term is the rate of outgoing flow of g. Taking g to be, respectively, the mass density, the stress tensor s_{ij}, and energy density, eq. (4) gives

$$\partial_t \rho + \rho\nabla\cdot\mathbf{v} = 0 \tag{5}$$

$$\rho\partial_t v_i - \partial_j s_{ij} = 0 \tag{6}$$

$$\rho\partial_t U_I - s_{ij}\partial_j v_i = \rho P(\mathbf{x},t) \tag{7}$$

where P is the specific absorption rate (SAR) of microwaves, and U_I is the internal energy density. Short of an analytic expression for the internal energy, we shall express $\partial_t U_I$ in terms of empirical coefficients. In terms of the heat capacities C_p and C_v, isothermal compressibility tensor $(\kappa_T)_{ij}$, and isobaric thermal expansion coefficient β_p, it may be shown that:

$$\partial_t U_I = -\left[\frac{C_p}{\beta_p} + \frac{p_{ij}\partial_j v_i}{\rho^2\nabla\cdot\mathbf{v}}\right]\frac{\partial_t\rho}{\rho} - \frac{C_v}{\beta_p}(\kappa_T)_{ij}\partial_t p_{ij} + \partial_t\left[\frac{(\varepsilon-1)|\mathbf{E}|^2}{8\pi\rho}\right]$$

Note that, while the total stress on the dielectric is $s_{ij} = p_{ij} + \sigma_{ij}$, it is the material stress p_{ij} which is responsible for the material strain, and therefore accountable in the thermal internal energy. Indeed, in the presence of an electromagnetic field, the material stress automatically adjusts itself in reaction to the electrostrictive stress. Therefore, the above equation does not include σ_{ij}. To obtain $\partial_t U_I$ in terms of $\partial_t s_{ij}$, we replace, in the above equation, p_{ij} by $s_{ij}-\sigma_{ij}$ and use eq. (3) for σ_{ij}, and replace $\nabla\cdot\mathbf{v}$ by $-\partial_t\rho/\rho$. It gives:

$$\begin{aligned}\partial_t U_I = &-\left[\frac{C_p}{\rho\beta_p}\right]\partial_t\rho + \frac{s_{ij}\partial_j v_i}{\rho} - \frac{C_v(\kappa_T)_{ij}}{\beta_p}\partial_t s_{ij} \\ &+\left[\frac{|\mathbf{E}|^2}{16\pi\rho}\left[\frac{\varepsilon}{\rho} - \left(\frac{\partial\varepsilon}{\partial\rho}\right)_T\right]\right]\partial_t\rho + \frac{\varepsilon}{8\pi\rho}\cdot|E_i|^2\partial_i v_i + \partial_t\left[\frac{(\varepsilon-1)|\mathbf{E}|^2}{8\pi\rho}\right] \\ &+\frac{C_v}{\beta_p}(\kappa_T)_{ii}\partial_t\left[\frac{|\mathbf{E}|^2}{16\pi}\left[\varepsilon - \rho\left(\frac{\partial\varepsilon}{\partial\rho}\right)_T\right] - \frac{\varepsilon}{8\pi}|E_i|^2\right]\end{aligned} \tag{8}$$

Eqs. (5)-(8) are the equations of the system.

Reprint from the Annual Report of the 1987 IEEE Conference on Electrical Insulation and Dielectric Phenomena.

THE LINEAR APPROXIMATION

The above system equations may be mutually substituted to eliminate the terms involving $\mathbf{v}$ and ρ and thereby yield a wave equation for s_{ij}. However, it is rather difficult to eliminate the term $\Sigma(|E_i|^2 \partial_i v_i)$ (summing over i) in eq. (8), which is highly anisotropic. One may select a coordinate system such that $|E_i|$ in all three directions are equal, but then it will complicate the boundary conditions. Nevertheless, we shall make a crude approximation that $|E_i|^2 = |\mathbf{E}|^2/3$. Then $\Sigma(|E_i|^2 \partial_i v_i) = (1/3)|\mathbf{E}|^2 \nabla\cdot\mathbf{v}$, which, by eq. (5), is $-(1/3)|\mathbf{E}|^2(\partial_t \rho/\rho)$. With this approximation, the electrostrictive tensor σ_{ij} in eq. (3) becomes isotropic: $\sigma_{ij} = -\sigma\cdot\delta_{ij}$, where σ is the electrostrictive pressure defined as:

$$\sigma = -\left[\frac{|\mathbf{E}|^2}{16\pi} \left[\frac{\varepsilon}{3} - \rho\left(\frac{\partial \varepsilon}{\partial \rho}\right)_T \right] \right] \tag{9}$$

Neglecting terms involving second order products of P, σ_{ij}, $|\mathbf{E}|$, and derivatives of all thermal quantities, we arrive at the following wave equation for the stress tensor s_{ij}:

$$\partial_i\left[\frac{1}{\rho} \partial_j s_{ij} \right] - \partial_t\left[\frac{C_p}{\beta_p} + \frac{\sigma}{\rho} \right]^{-1}\left[\frac{C_v}{\beta_p}(\kappa_T)_{ij}\partial_t s_{ij} \right] \tag{10}$$

$$= \left[\frac{C_p}{\beta_p} + \frac{\sigma}{\rho} \right]_o^{-1}\left[\partial_t P + \left[\frac{C_v}{\beta_p}(\kappa_T)_{ii} \right]_o \partial_t{}^2\sigma - \partial_t{}^2\left[\frac{(\varepsilon-1)|\mathbf{E}|^2}{8\pi\rho}\right]\right]$$

where the subscript o signifies that the quantity is evaluated at its ambient equilibrium value. For an isotropic dielectric, $s_{ij} = -s\delta_{ij}$ and $(\kappa_T)_{ij} = \kappa_T/3$, so $\Sigma(\kappa_T)_{ii}$ (sum over i) is κ_T, the above wave equation is then further reduced to

$$\nabla^2 s - \left[\frac{C_p}{\beta_p} + \frac{\sigma}{\rho} \right]_o^{-1}\left[\frac{\rho C_v \kappa_T}{\beta_p} \right]_o \partial_t{}^2 s \tag{11}$$

$$= -\left[\frac{C_p}{\beta_p} + \frac{\sigma}{\rho} \right]_o^{-1}\left[\rho_o \partial_t P + \left[\frac{\rho C_v \kappa_T}{\beta_p} \right]_o \partial_t{}^2\sigma - \partial_t{}^2\left[\frac{(\varepsilon-1)|\mathbf{E}|^2}{8\pi}\right]\right]$$

Equation (11) is a typical linear wave equation with the velocity

$$u = \left[1 + \frac{\sigma\beta_p}{\rho C_p} \right]_o^{1/2}\left[\frac{C_p}{\rho C_v \kappa_T} \right]_o^{1/2} = \left[1 + \frac{\sigma\beta_p}{\rho C_p} \right]_o^{1/2}\cdot u_o \tag{12}$$

Reprint from the Annual Report of the 1987 IEEE Conference on Electrical Insulation and Dielectric Phenomena.

where u_o denotes the acoustic velocity in the dielectric in the absence of the electromagnetic waves. To estimate the magnitude of the change of acoustic velocity by electrostrictive pressure σ, we consider water at room temperature as the dielectric, for which $\rho = 1$ gm/cm^3, $C_p = 4.186\times10^7$ erg/gm°C, $\beta_p = 2.8\times10^{-4}$ °C^{-1}, and $\varepsilon = 80$. We also assume that the dielectric permittivity is linearly proportional to the mass density, so $(\partial\varepsilon/\partial\rho)_T = \varepsilon/\rho$, then eq. (9) gives $\sigma = (\varepsilon|\mathbf{E}|^2)/(24\pi)$. Assume a plane electromagnetic wave of intensity $I = 1$ kW/cm^2, then its field magnitude is $|\mathbf{E}|^2 = 8\pi I/(c\sqrt{\varepsilon}) = 0.94$ erg/cm^3, where c is the speed of light in vacuum. Then $\sigma = 1$ dyne/cm^2, and the correction term is $(\sigma\beta_p)/(\rho C_p) \approx 6.7\times10^{-12}$, which is insignificant.

PRESSURE WAVE GENERATION *

As illustrated at the end of the last paragraph, for most dielectrics and for microwave intensity up to gigawatts/cm^2, the term σ/ρ on both sides of eq. (11) may be neglected. Eq. (11) may then be rewritten as

$$\nabla^2 s - \frac{1}{u^2}\partial_t{}^2 s = -\frac{\beta_p}{C_p}\,\partial_t\left[\rho_o P + \left[\frac{\rho C_v \kappa_T}{\beta_p}\right]_o \partial_t\sigma - \partial_t\left[\frac{(\varepsilon-1)|\mathbf{E}|^2}{8\pi}\right]\right] \tag{13}$$

where $u = [C_p/\rho C_v \kappa_T]^{1/2}$ is the speed of sound in the dielectric. The three terms inside the brackets on the right hand side are the generating forces of pressure waves. The first term represents the thermoelastic effect, the second term is the electrostrictive force, and the third term comes from the electromagnetic energy of dielectric polarization. We shall compare the sizes of these three driving forces by expressing them in terms of $|\mathbf{E}|^2$. Let α be the attenuation coefficient of microwave intensity as defined by the equation $I(x) = I_o e^{-\alpha x}$. Then the first term is $\rho_o P = \alpha I = (\alpha c\sqrt{\varepsilon}/8\pi)|\mathbf{E}|^2$. If the dielectric permittivity is linear in ρ, then $(\partial\varepsilon/\partial\rho)_T = \varepsilon/\rho$, so eq. (9) gives $\sigma = (\varepsilon|\mathbf{E}|^2)/(24\pi)$ and the electrostrictive term gives $[(\rho\varepsilon C_v\kappa_T)/(24\pi\beta_p)]\partial_t|\mathbf{E}|^2$. Denote by t_r the rise time of a microwave pulse, then $\partial_t|\mathbf{E}|^2 \sim |\mathbf{E}|^2/t_r$. Thus, the relative magnitudes of these three terms are, respectively,

---

* The first paragraph in this section was inadvertently missed from the manuscript submitted to CEIDP.

Reprint from the Annual Report of the 1987 IEEE Conference on Electrical Insulation and Dielectric Phenomena.

$$1, \quad \frac{\rho C_v \kappa_T \sqrt{\varepsilon}}{3c\alpha\beta_p} \cdot \frac{1}{t_r}, \quad \frac{\sqrt{\varepsilon}}{c\alpha} \cdot \frac{1}{t_r}. \tag{14}$$

One sees that the second and the third driving forces may be larger than the thermoelastic term if the microwave is rapidly modulated, contrary to the estimate by previous theory that the electrostrictive effect is two orders of magnitude smaller [6]. For water at 30 °C, ρ = 1 gm/cm^3, $C_p = 4.186 \times 10^7$ erg/gm°C, $\kappa_T = 4.46 \times 10^{-11}$ cm^2/dyne, $\beta_p = 2.8 \times 10^{-4}$ °C^{-1}, and, at 3 GHz, $\alpha = 0.88$ cm^{-1} and $\varepsilon = 80$. The relative magnitudes are, respectively:

$$1, \quad \frac{C_v}{C_p} \cdot \frac{0.75 \text{ nanosec}}{t_r}, \quad \frac{0.34 \text{ nanosec}}{t_r}. \tag{15}$$

One may conclude that, for water, a rise time of 1 nanosecond is the marginal modulation rate, beyond which the electrostrictive term and the polarization term contribute more to the pressure waves than the thermoelastic term.

In the absence of the electrostrictive force, the wave equation for the pressure waves reduces to the one developed for thermoacoustic process [10,11]. While we have not yet completed calculations on the pressure waves generated by the electrostrictive effect, pressure waves from the thermoacoustic effects have been reported [10,11], and measurement on the amplitude and pulse characteristics have also been made [11]. Contrary to previous theory that thermoacoustic pressure waves were generated mainly by inhomogeneous distribution of microwaves in dielectrics [6], it was found that pressure waves are generated whenever there is a discontinuity in thermal or dielectric parameters in the medium. Equations (10) and (11) also indicate this effect for electrostrictive pressure waves. With an air-water system and neglecting the electrostrictive force, it was found that a peak SAR of 4.5 kW/gram sufficed to generate a pressure wave of peak pressure equivalent to about 10% of the ambient atmospheric pressure, which is the upper limit of linear approximation.

ACKNOWLEDGEMENT

This work is partially supported by Potomac Research, Inc., Potomac, Maryland, and by Walter Reed Army Institute of Research through the Office of Naval Research under the Contract N00014-85-K-0475.

REFERENCES

[1] Foster, K. R., and Finch, E. E., "Microwave hearing: Evidence for thermoacoustical auditory stimulation by pulsed microwaves," Science, 185, pp. 256-258, 1974.

[2] Lin, J. C., "Further studies on the microwave auditory effect," IEEE Trans. Microwave Theory Tech., MTT-25, pp. 938-943, 1977.

[3] Borth, D. E., and Cain, C. A., "Theoretical analysis of acoustic signal generation in materials irradiated with microwave energy," IEEE Trans. Microwave Theory Tech., MTT-25, pp. 944-954, 1977.

[4] Brown, P. V. K., and Wyeth, N. C., "Laser interferometer for measuring microwave-induced motion in eye lenses in vitro," Rev. Sci. Instrum., 54, pp. 85-89, 1983.

[5] Stewart-DeHaan, P. J., Creighton, M. O., Larsen, L. E., Jacobi, J. H., Ross, W. M., Sanwal, M., Guo, T. C., Guo, W. W., and Trevithick, J. R., "In Vitro Studies of Microwave-Induced Cataract: Separation of Field and Heating Effects," Exp. Eye Res., 36, pp. 75-90, 1983.

[6] Lin, J. C., Microwave Auditory Effects and Applications, Springfield, IL: C. C. Thomas, 1978.

[7] See reference 6, Table XIII, p. 126.

[8] See reference 6, pp. 115-118.

[9] Oscar, K. J., "Interaction of Electromagnetic Energy with Absorptive Materials by Thermally Inducing Elastic Stress Wave," The American University Ph.D. Dissertation, University Microfilms International 8017445, 1980.

[10] Guo, T. C., Guo, W. W., and Larsen, L. E., "Microwave Induced Thermoacoustic Effect in Dielectrics and Its Couplings to External Medium - A Thermodynamical Formulation," IEEE Trans. MTT-32, pp. 835-843, 1984.

[11] Guo, T. C., Guo, W. W., and Larsen, L. E., "Microwave Induced Thermoelastic Process in Dielectrics - Theory and Experiments," Int'l J. Infrared & Millimeter Waves, 6, pp. 405-422, 1985.

[12] Landau, L. D., Lifshitz, E. M., and Pitaevskii, L. P., Electrodynamics of Continuous Media, pp. 59-62, Oxford: Pergamon Press, 1984.

Reprint from the Annual Report of the 1987 IEEE Conference on Electrical Insulation and Dielectric Phenomena.

Report to WRAIR via ONR
Contract No. N00014-85-K-0475
Transient Interaction of Electromagnetic Pulses
in Dielectrics and Microwave Biophysics
by Theodore C. Guo and Wendy W. Guo

GENERATION OF ACOUSTIC WAVES AT DIELECTRIC INTERFACE BY MICROWAVE PULSES

APPENDIX B

Theodore C. Guo and Wendy W. Guo

Department of Physics, The Catholic University of America, Washington, D.C. 20064, U.S.A.
and
Potomac Research, Inc., Potomac, Maryland 20854, U.S.A.

INTRODUCTION

Acoustic waves generated by pulsed microwaves have been cited as a mechanism for microwave hearing (1,2,3). More recently it has been demonstrated that acoustic waves are transduced in dielectric objects simulating the ocular lens when exposed to pulsed microwaves (4). The effect has also been cited as the operant mechanism for cellular damage in studies of the murine ocular lens in vitro (5). Three theories on the microwave auditory mechanism have been reviewed and compared by Lin (6), viz., the radiation pressure theory, the electrostrictive theory, and the thermoacoustic theory. Among them it was found that only the thermoacoustic mechanism could produce elastic waves of magnitude large enough to explain the experimental observations. Comparing to the magnitude of acoustic pressure generated in typical biological tissues, the electrostrictive effect was found to be about two orders of magnitude smaller, while the radiation pressure three orders of magnitude smaller (7).

Previous theories on microwave electrostrictive process and microwave thermoacoustic process are based on a linear wave equation with a generating function derived from the microwave pulses. Pressure waves are thereby generated in a way similar to a forced harmonic oscillator. In the case of the thermoacoustic process, the generating function is derived from an inhomogeneous heating by the microwaves, whereas in the case of the electrostrictive process, it is derived from stress due to dielectric polarization (8,9). This approach fails to consider the proper balance of the distribution of the absorbed microwave energy among the internal thermal energies and the bulk kinetic energy, and the effect of thermal or dielectric discontinuities at medium interface. Also neglected is the coupling between the thermoacoustic process and electrostrictive process, which may result from dependency of dielectric permittivity on various thermodynamical coefficients, such as mass density, temperature, and pressure; this coupling may further enhance the electrostrictive effect.

Earlier, we have developed a thermodynamical formulation of the process of microwave absorption and its coupling to the internal thermal energy and mechanical bulk energy in the dielectrics (10). It was shown that acoustic waves may be generated by microwave pulses if there are discontinuities in thermodynamical characteristics in the dielectrics, or discontinuities in microwave absorptions. Numerical results for a one-dimensional system and a spherical system with water as the absorbing dielectric have been compared consistently with experimental results, which included measurement of pressure waves in a cylinder filled with an aqueous solution of electrolytes exposed to pulsed microwaves and estimation of the coupling efficiency between the liquid dielectric and the adjacent air (11). However, these studies did not include electrostrictive force in the dielectric and the dielectric interface. In this paper, we reformulate the problem to include electrostrictive stress and show that it may play an important role in the generation of pressure waves by microwave pulses in dielectrics with thermal or dielectric discontinuities. We also show that, in the first-order linear approximation, the effect of the electrostrictive force on the acoustic velocity is negligible.

THEORY OF MICROWAVE ACOUSTICS

Our approach to derive the coupling from microwave pulses to acoustic waves is to start from the laws of the conservation of mass, the conservation of momentum, the conservation of energy, and the thermodynamic equation of state. When a dielectric system is exposed to microwave radiation, microwave energy is absorbed into the dielectric through the work of the electric field on the electric polarization: $\mathbf{E}\cdot d\mathbf{P}$, which is then partially converted into the internal energy U_I and partially into the bulk kinetic energy U_k via thermal expansion and other elastic vibrations. The process is complex and irreversible; however, we shall assume that the time domain which concerns us is much greater than the time it takes to reach a quasi-steady state and that every microscopically small part of the system is in local equilibrium so that thermodynamic variables may be defined.

The time domain of our interest is the width of the microwave pulse, which is in the order of microseconds and is too short for any heat conduction and convective flow to take place. On the other hand, the time cycle of electric field is in the range of subnanosecond, which is much shorter than the time domain of our concern. Therefore, we may average all variables over a microwave cycle. The resulting time-average of $\mathbf{E}\cdot d\mathbf{P}$ gives the microwave energy absorbed by the dielectric, δQ_P, and the electrostrictive work on the dielectric, δW_P. Thus, the first law of thermodynamics gives:

$$\delta Q_P + \delta W_P = d(U_I + U_k) + \delta W \qquad (1)$$

where δW is the mechanical work done by the dielectric; heat flow by conduction and convection have been ignored, as explained earlier. Denote by p_{ij} the stress tensor in the dielectric, and by σ_{ij} the electrostrictive stress tensor on the dielectric by the electromagnetic field, then $\iiint \partial_j p_{ij} dV$ and $\iiint \partial_j \sigma_{ij} dV$ are, respectively, the force on the dielectric volume element by the surrounding body and the force on the element by the electromagnetic field. The total stress tensor experienced by the dielectric is then the sum of p_{ij} and σ_{ij}, which will be denoted by s_{ij}:

$$s_{ij} = p_{ij} + \sigma_{ij}$$

To appear in the IEE Proceedings of the Fifth International Conference on Dielectric Materials, Measurements, and Applications, June 1988, Canterbury, England

If ε is the dielectric permittivity, then (12)

$$\sigma_{ij} = \frac{\mathbf{E}^2}{8\pi}\left[\varepsilon - \rho\left(\frac{\partial\varepsilon}{\partial\rho}\right)_T\right]\delta_{ij} - \frac{\varepsilon}{4\pi}E_iE_j \qquad (2)$$

Averaging over the microwave cycle, the terms E_iE_j vanish except for $i=j$, and the above equation gives:

$$\sigma_{ij} = \left[\frac{|\mathbf{E}|^2}{16\pi}\left[\varepsilon - \rho\left(\frac{\partial\varepsilon}{\partial\rho}\right)_T\right] - \frac{\varepsilon}{8\pi}|E_i|^2\right]\delta_{ij} \qquad (3)$$

In order to convert eq. (2) into a differential equation with respect to space and time, we start from a general form of the equation of conservation. Let g be a thermodynamic extensive quantity, S_g be the rate of production of g, which may be due to internal production or external input, and $\mathbf{v}$ be the bulk velocity function, then the equation of conservation for g is:

$$\partial_t g + g\nabla\cdot\mathbf{v} = S_g \qquad (4)$$

where we have ignored the second order term $\mathbf{v}\cdot\nabla g$ by assuming that both g and $\mathbf{v}$ are small. The first term on the left represents the rate of increase of g per unit volume, and the second term is the rate of outgoing flow of g. Taking g to be, respectively, the mass density, the stress tensor s_{ij}, and energy density, eq. (5) gives

$$\partial_t\rho + \rho\nabla\cdot\mathbf{v} = 0 \qquad (5)$$

$$\rho\partial_t v_i - \partial_j s_{ij} = 0 \qquad (6)$$

$$\rho\partial_t U_I - s_{ij}\partial_j v_i = \rho P(\mathbf{x},t) \qquad (7)$$

where P is the specific absorption rate (SAR) of microwaves, and U_I is the internal energy density of the dielectric system.

Equations (5)-(7) all together contain four unknowns, viz., ρ, $\mathbf{v}$, $\overleftrightarrow{s}$, and U_I. One more equation is needed to complete the system, which will be furnished by the thermodynamic equation of state:

$$U_I = U_{th}(\rho, \overleftrightarrow{p}) + \left(\frac{1}{\rho}\right)\left(\frac{\varepsilon-1}{8\pi}\right)|\mathbf{E}|^2 \qquad (8)$$

where the first term on the right hand side is the thermodynamical energy, whereas the second term is the electrical energy in the dielectric that arises from electric polarization. Since the electric energy density averaged over a microwave cycle is $(1/8\pi)\mathrm{Re}(\mathbf{P}\cdot\mathbf{E}) = (1/8\pi)\mathrm{Re}(\varepsilon-1)|\mathbf{E}|$, ε in eq. (8) represents only the real part of the dielectric permittivity; the imaginary part of ε contributes to ρP in eq. (7), the energy absorption by the dielectric. As there is no analytic expression for the thermodynamical energy, U_{th}, we shall try to express it in terms of other empirical coefficients, such as density ρ, specific heats C_v and C_p, isobaric thermal expansion coefficient β_p, and isothermal compressibility tensor $(\kappa_T)_{ij}$. As a thermodynamical system, the dielectric has two independent thermodynamic variables, which may be any pair among the variables ρ, T, $\overleftrightarrow{p}$, and U_{th}, and all other variables may be considered as functions of the pair. Since ρ and $\overleftrightarrow{p}$ are the variables in eqs. (5)-(7), they are selected as the independent variables. A differential of U_{th} may be expressed as:

$$dU_{th} = (\partial_\rho U_{th})_{p_{ij}}d\rho + (\partial_{p_{ij}}U_{th})_\rho dp_{ij} \qquad (9)$$

It is remarked that, while the total stress on the dielectric is $s_{ij} = p_{ij} + \sigma_{ij}$, it is the material stress p_{ij} which is responsible for the material strain, and therefore accountable in the thermal internal energy. Indeed, in the presence of an electromagnetic field, the material stress automatically adjusts itself in reaction to the electrostrictive stress by the field, therefore, the above equation does not include σ_{ij}.

We would like to express the partial derivatives of U_{th} with respect to ρ and p_{ij} in terms of known empirical quantities such as specific heat and compressibility. Utilizing the Jacobian method of relating one partial derivative to another, one may derive from eq. (9) the following equation:

$$\partial_t U_{th} = \left[-\frac{C_p}{\beta_p}\cdot\frac{1}{\rho} + \frac{p}{\rho^2}\right]\partial_t\rho + \left[\frac{C_v\kappa_T}{\beta_p}\right]\partial_t p \qquad (10)$$

where C_v and C_p are the specific heat (per mass) at constant volume and constant pressure, respectively; β_p is the isobaric thermal expansion coefficient, and κ_T the isothermal compressibility. It is straightforward to generalize the above result to include the stress tensor. Noting that the sign of p_{ij} is generally defined such that, for an isotropic case, $p_{ij} = -p\delta_{ij}$, where p is positive when it is a pressure, and negative when it is a tension. Eq. (10) then takes the form:

$$\partial_t U_{th} = -\left[\frac{C_p}{\rho\beta_p} + \frac{p_{ij}}{\rho^2}\cdot\frac{\partial_j v_i}{\nabla\cdot\mathbf{v}}\right]\partial_t\rho - \frac{C_v(\kappa_T)_{ij}}{\beta_p}\partial_t p_{ij} \qquad (11)$$

where C_p is given by:

$$C_p = \left[\partial_T U_{th}\right]_{\rho,\mathbf{v}} - \left[\partial_T\frac{p_{ij}\partial_j v_i}{\nabla\cdot\mathbf{v}}\right]_{\rho,\mathbf{v}}$$

and $(\kappa_T)_{ij}$ is the compressibility tensor defined as

$$(\kappa_T)_{ij} = \frac{1}{V}\left[\frac{\partial V}{\partial p_{ij}}\right]_T$$

In deriving the above equation, we have used the generalized first law of thermodynamics for mechanically anisotropic media:

$$\delta Q = dU_{th} - \frac{p_{ij}\partial_j v_i}{\nabla\cdot\mathbf{v}}dV.$$

The electromagnetic terms are not included because the thermodynamical quantities, C_v, C_p, β_p, and $(\kappa_T)_{ij}$, are generally measured in the absence of electromagnetic fields. To understand the above equation, we consider δQ as the total heat input to a material element of unit mass during time dt, during which the total energy is increased by dU. The total work done by the element is equal to $-\nabla\cdot(\mathbf{v}\cdot\overleftrightarrow{p})dt$ times the volume, $1/\rho$. On the other hand, from eq. (5), the increment in volume during dt is $dV = d(1/\rho) = (1/\rho)\nabla\cdot\mathbf{v}dt$. Therefore the work done associated with a volume increment dV is $-[\nabla\cdot(\mathbf{v}\cdot\overleftrightarrow{p})/\nabla\cdot\mathbf{v}]dV$, which may be separated into two terms:

$$-(p_{ij}\partial_j v_i/\nabla\cdot\mathbf{v})dV - (v_i\partial_j p_{ij}/\nabla\cdot\mathbf{v})dV,$$

of which the second term cancels with the bulk kinetic energy U_k, so only the first term is accounted for in the above equation.

To appear in the IEE Proceedings of the Fifth International Conference on Dielectric Materials, Measurements, and Applications, June 1988, Canterbury, England

As explained earlier, it is the material stress p_{ij} which is responsible for the material strain, and therefore accountable in the thermal internal energy U_{th}. On the other hand, the acoustic wave equation is the equation for the total stress s_{ij}. To obtain $\partial_t U_{th}$ in terms of $\partial_t s_{ij}$, we replace, in the above equation, p_{ij} by $s_{ij}-\sigma_{ij}$ and substitute (3) for σ_{ij}. Eq. (11) then gives:

$$\partial_t U_{th} = -\left[\frac{C_p}{\rho\beta_p} + \frac{s_{ij}\partial_j v_i}{\rho^2 \nabla\cdot\mathbf{v}}\right]\partial_t\rho - \frac{C_v}{\beta_p}(\kappa_T)_{ij}\partial_t s_{ij}$$
$$+\left[\frac{|\mathbf{E}|^2}{16\pi}\left[\varepsilon - \rho\left(\frac{\partial\varepsilon}{\partial\rho}\right)_T\right] - \frac{\varepsilon}{8\pi}\cdot\frac{|E_i|^2\partial_i v_i}{\nabla\cdot\mathbf{v}}\right]\cdot\frac{\partial_t\rho}{\rho^2}$$
$$+\frac{C_v}{\beta_p}(\kappa_T)_{ii}\partial_t\left[\frac{|\mathbf{E}|^2}{16\pi}\left[\varepsilon - \rho\left(\frac{\partial\varepsilon}{\partial\rho}\right)_T\right] - \frac{\varepsilon}{8\pi}|E_i|^2\right]$$

By eq. (5), the factor $\nabla\cdot\mathbf{v}$ in the denominator may be replaced by $-\partial_t\rho/\rho$, the above equation then becomes:

$$\partial_t U_{th} = -\left[\frac{C_p}{\rho\beta_p}\right]\partial_t\rho + \frac{s_{ij}\partial_j v_i}{\rho} - \frac{C_v}{\beta_p}(\kappa_T)_{ij}\partial_t s_{ij}$$
$$+\left[\frac{|\mathbf{E}|^2}{16\pi}\left[\varepsilon - \rho\left(\frac{\partial\varepsilon}{\partial\rho}\right)_T\right]\right]\cdot\frac{\partial_t\rho}{\rho^2} + \frac{\varepsilon}{8\pi\rho}\cdot|E_i|^2\partial_i v_i$$
$$+\frac{C_v}{\beta_p}(\kappa_T)_{ii}\partial_t\left[\frac{|\mathbf{E}|^2}{16\pi}\left[\varepsilon - \rho\left(\frac{\partial\varepsilon}{\partial\rho}\right)_T\right] - \frac{\varepsilon}{8\pi}|E_i|^2\right] \quad (12)$$

We may now substitute eq. (12) for the term U_{th} in eq. (8) to obtain an expression for $\partial_t U_I$. With some rearrangement of terms, one obtains:

$$\partial_t U_I = \left[-\frac{C_p}{\rho\beta_p} + \frac{|\mathbf{E}|^2}{16\pi\rho}\left[\frac{\varepsilon}{\rho} - \left(\frac{\partial\varepsilon}{\partial\rho}\right)_T\right]\right]\partial_t\rho$$
$$+\frac{\partial_j v_i}{\rho}s_{ij} - \frac{C_v(\kappa_T)_{ij}}{\beta_p}\partial_t s_{ij} \quad (13)$$
$$+\frac{\varepsilon}{8\pi\rho}\cdot|E_i|^2\partial_i v_i + \partial_t\left[\frac{(\varepsilon-1)|\mathbf{E}|^2}{8\pi\rho}\right]$$
$$+\frac{C_v}{\beta_p}(\kappa_T)_{ii}\partial_t\left[\frac{|\mathbf{E}|^2}{16\pi}\left[\varepsilon - \rho\left(\frac{\partial\varepsilon}{\partial\rho}\right)_T\right] - \frac{\varepsilon}{8\pi}|E_i|^2\right]$$

Eqs. (5)-(7) and (13) are the equations of the system. To summarize, we list these equations below (summation over repeated indices):

$$d_t\rho + \rho\nabla\cdot\mathbf{v} = 0 \quad (14)$$

$$\rho d_t v_i - \partial_j s_{ij} = 0 \quad (15)$$

$$\rho d_t U_I - s_{ij}\partial_j v_i = \rho P(\mathbf{x},t) \quad (16)$$

$$\partial_t U_I = \left[-\frac{C_p}{\rho\beta_p} + \frac{|\mathbf{E}|^2}{16\pi\rho}\left[\frac{\varepsilon}{\rho} - \left(\frac{\partial\varepsilon}{\partial\rho}\right)_T\right]\right]\partial_t\rho$$
$$+\frac{\partial_j v_i}{\rho}s_{ij} - \frac{C_v(\kappa_T)_{ij}}{\beta_p}\partial_t s_{ij} \quad (17)$$
$$+\frac{\varepsilon}{8\pi\rho}\cdot|E_i|^2\partial_i v_i + \partial_t\left[\frac{(\varepsilon-1)|\mathbf{E}|^2}{8\pi\rho}\right]$$
$$+\frac{C_v}{\beta_p}(\kappa_T)_{ii}\partial_t\left[\frac{|\mathbf{E}|^2}{16\pi}\left[\varepsilon - \rho\left(\frac{\partial\varepsilon}{\partial\rho}\right)_T\right] - \frac{\varepsilon}{8\pi}|E_i|^2\right]$$

THE LINEAR APPROXIMATION

The above system equations may be mutually substituted to eliminate the terms involving $\mathbf{v}$ and ρ and thereby yield a wave equation for s_{ij}. However, it is rather difficult to eliminate the term $\Sigma(|E_i|^2\partial_i v_i)$ (summing over i) in eq. (17), which is highly anisotropic. One may select a coordinate system such that $|E_i|$ in all three directions are equal, but then it will complicate the boundary conditions. Nevertheless, we shall make a crude approximation that $|E_i|^2=|\mathbf{E}|^2/3$. Then $\Sigma(|E_i|^2\partial_i v_i) = (1/3)|\mathbf{E}|^2\nabla\cdot\mathbf{v}$, which, by eq. (14), is $-(1/3)|\mathbf{E}|^2(\partial_t\rho/\rho)$. With this approximation, the electrostrictive tensor σ_{ij} in eq. (3) becomes isotropic: $\sigma_{ij} = -\sigma\cdot\delta_{ij}$, where σ is the electrostrictive pressure defined as:

$$\sigma = -\left[\frac{|\mathbf{E}|^2}{16\pi}\left[\frac{\varepsilon}{3} - \rho\left(\frac{\partial\varepsilon}{\partial\rho}\right)_T\right]\right] \quad (18)$$

Neglecting terms involving second order products of P, σ_{ij}, $|\mathbf{E}|$, and derivatives of all thermal quantities, we arrive at the following wave equation for the stress tensor s_{ij}:

$$\partial_i\left[\frac{1}{\rho}\partial_j s_{ij}\right] - \partial_t\left[\frac{C_p}{\beta_p} + \frac{\sigma}{\rho}\right]^{-1}\left[\frac{C_v}{\beta_p}(\kappa_T)_{ij}\partial_t s_{ij}\right]$$
$$= \left[\frac{C_p}{\beta_p} + \frac{\sigma}{\rho}\right]_o^{-1} \quad (19)$$
$$\times\left[\partial_t P + \left[\frac{C_v}{\beta_p}(\kappa_T)_{ii}\right]_o\partial_t^2\sigma - \partial_t^2\left[\frac{(\varepsilon-1)|\mathbf{E}|^2}{8\pi\rho}\right]\right]$$

where the subscript o signifies that the quantity is evaluated at its ambient equilibrium value. *For an isotropic dielectric,* $s_{ij} = -s\delta_{ij}$ and $(\kappa_T)_{ij} = \kappa_T/3$, so $\Sigma(\kappa_T)_{ii}$ (sum over i) is κ_T, the above wave equation is then further reduced to

$$\nabla^2 s - \left[\frac{C_p}{\beta_p} + \frac{\sigma}{\rho}\right]_o^{-1}\left[\frac{\rho C_v\kappa_T}{\beta_p}\right]_o\partial_t^2 s$$
$$= -\left[\frac{C_p}{\beta_p} + \frac{\sigma}{\rho}\right]_o^{-1} \quad (20)$$
$$\times\left[\rho_o\partial_t P + \left[\frac{\rho C_v\kappa_T}{\beta_p}\right]_o\partial_t^2\sigma - \partial_t^2\left[\frac{(\varepsilon-1)|\mathbf{E}|^2}{8\pi}\right]\right]$$

Equation (20) is a typical linear wave equation with the velocity

$$u = \left[1 + \frac{\sigma\beta_p}{\rho C_p}\right]_o^{1/2}\left[\frac{C_p}{\rho C_v\kappa_T}\right]_o^{1/2} = \left[1 + \frac{\sigma\beta_p}{\rho C_p}\right]_o^{1/2}\cdot u_o \quad (21)$$

where u_o denotes the acoustic velocity in the dielectric in the absence of the electromagnetic waves. To estimate the magnitude of the change of acoustic velocity by electrostrictive pressure σ, we consider water at room temperature as the dielectric, for which ρ = 1 gm/cm^3, $C_p = 4.186\times10^7$ erg/gm·C, $\beta_p = 2.8\times10^{-4}\cdot C^{-1}$, and $\varepsilon = 80$. We also assume that the dielectric permittivity is linearly proportional to the mass density, so $(\partial\varepsilon/\partial\rho)_T = \varepsilon/\rho$, then eq. (18) gives $\sigma = (\varepsilon|\mathbf{E}|^2)/(24\pi)$. Assume a plane electromagnetic wave of intensity I = 1 kW/cm^2, then its field magnitude is $|\mathbf{E}|^2 = 8\pi I/(c\sqrt{\varepsilon}) = 0.94$ erg/cm^3, where c is the speed of light in vacuum. Then σ = 1 dyne/cm^2, and the correction term is $(\sigma\beta_p)/(\rho C_p) = 6.7\times10^{-12}$, which is insignificant.

To appear in the IEE Proceedings of the Fifth International Conference on Dielectric Materials, Measurements, and Applications, June 1988, Canterbury, England

PRESSURE WAVE GENERATION

As illustrated at the end of the last paragraph, for most dielectrics and for microwave intensity up to gigawatts/cm^2, the term σ/ρ on both sides of eq. (20) may be neglected. Eq. (20) may then be rewritten as

$$\nabla^2 s - \frac{1}{u^2}\cdot\partial_t{}^2 s = -\frac{\beta_p}{C_p}\,\partial_t\left[\rho_o P + \left[\frac{\rho C_v \kappa_T}{\beta_p}\right]_o \partial_t\sigma - \partial_t\left[\frac{(\varepsilon-1)\,|\mathbf{E}|^2}{8\pi}\right]\right] \tag{22}$$

where $u = [\rho C_v \kappa_T / C_p]^{1/2}$ is the speed of sound in the dielectric. The three terms inside the brackets on the right hand side are the generating forces of pressure waves. The first term represents the thermoelastic effect, the second term is the electrostrictive force, and the third term comes from the electromagnetic energy of dielectric polarization. We shall compare the sizes of these three driving forces by expressing them in terms of $|\mathbf{E}|^2$. Let α be the attenuation coefficient of microwave intensity as defined by the equation $I(x) = I_o e^{-\alpha x}$. Then the first term is $\rho_o P = \alpha I = (\alpha c\sqrt{\varepsilon}/8\pi)\,|\mathbf{E}|^2$. If the dielectric permittivity is linear in ρ, then $(\partial\varepsilon/\partial\rho)_T = \varepsilon/\rho$, so eq. (18) gives $\sigma = (\varepsilon|\mathbf{E}|^2)/(24\pi)$ and the electrostrictive term gives $[(\rho\varepsilon C_v\kappa_T)/(24\pi\beta_p)]\,\partial_t|\mathbf{E}|^2$. Denote by t_r the rise time of a microwave pulse, then $\partial_t|\mathbf{E}|^2 \sim |\mathbf{E}|^2/t_r$. Thus, the relative magnitudes of the electrostrictive and polarization terms with respect to the thermoelastic term are, respectively,

$$\frac{\text{Electrostrictive effect}}{\text{Thermoelastic effect}} = \frac{\rho C_v \kappa_T \sqrt{\varepsilon}}{3c\alpha\beta_p}\cdot\frac{1}{t_r}, \qquad \frac{\text{Polarization effect}}{\text{Thermoelastic effect}} = \frac{\sqrt{\varepsilon}}{c\alpha}\cdot\frac{1}{t_r}. \tag{23}$$

One sees that the second and the third driving forces may be larger than the thermoelastic term if the microwave is rapidly modulated, contrary to the estimate by previous theory that the electrostrictive effect was two orders of magnitude smaller (6). For water at 30 °C, ρ = 1 gm/cm^3, $C_v = 0.987\cdot C_p = 4.132\times10^7$ erg/gm·C, $\kappa_T = 4.46\times10^{-11}$ cm^2/dyne, $\beta_p = 2.8\times10^{-4}$ °C^{-1}, and, at 3 GHz, $\alpha = 0.88$ cm^{-1} and $\varepsilon = 80$, the above ratios are then, respectively:

$$\frac{\text{Electrostrictive effect}}{\text{Thermoelastic effect}} = \frac{0.75\ \text{nanosec}}{t_r}, \qquad \frac{\text{Polarization effect}}{\text{Thermoelastic effect}} = \frac{0.34\ \text{nanosec}}{t_r}. \tag{24}$$

One may conclude that, for water, a rise time of 1 nanosecond is the marginal modulation rate, beyond which the electrostrictive term and the polarization term contribute more to the pressure waves than the thermoelastic term.

In the absence of the electrostrictive force, the wave equation for the pressure waves reduces to the one developed for thermoacoustic process (10,11). While we have not yet completed calculations on the pressure waves generated by the electrostrictive effect, pressure waves from the thermoacoustic effects have been reported (10,11), and measurement on the amplitude and pulse characteristics have also been made (11). Contrary to previous theory that thermoacoustic pressure waves were generated mainly by inhomogeneous distribution of microwaves in dielectrics (6), it was found that pressure waves are generated whenever there is a discontinuity in thermal or dielectric parameters in the medium. Equations (19) and (20) also indicate this effect for electrostrictive pressure waves. With an air-water system and neglecting the electrostrictive force, it was found that a peak SAR of 4.5 kW/gram sufficed to generate a pressure wave of peak pressure 10^4 pascal (i.e., 10^5 dynes/cm^2), which is equivalent to about 10% of the ambient atmospheric pressure. This level of peak pressure may be considered as the upper limit of linear approximation. As to the ratio of electrostrictive effect to thermoacoustic effect, it depends on the rise time of the microwave pulse, being greater than one for rise time shorter than a nanosecond, and smaller than one for rise time longer than a nanosecond. This result is in contrary to previous estimate based on a simpler theory, which gave a ratio of the order of 10^{-2}, and independent of the rise time of microwave pulses.

ACKNOWLEDGEMENT

This work is supported by Potomac Research, Inc., Potomac, Maryland, U.S.A.

REFERENCES

1. Foster, K. R., and Finch, E. E., 1974, Science, 185, 256-258.
2. Lin, J. C., 1977, IEEE MTT, 25, 938-943.
3. Borth, D. E., and Cain, C. A., 1977, IEEE MTT, 25, 944-954.
4. Brown, P. V. K., and Wyeth, N. C., 1983, Rev. Sci. Instrum., 54, 85-89.
5. Stewart-DeHaan, P. J., Creighton, M. O., Larsen, L. E., Jacobi, J. H., Ross, W. M., Sanwal, M., Guo, T. C., Guo, W. W., and Trevithick, J. R., 1983. Exp. Eye Res., 36, 75-90.
6. Lin, J. C., 1978, Microwave Auditory Effects and Applications, C. C. Thomas, Springfield, IL, U.S.A.
7. See reference 6, Table XIII, p. 126.
8. See reference 6, pp. 115-118.
9. Oscar, K. J., "Interaction of Electromagnetic Energy with Absorptive Materials by Thermally Inducing Elastic Stress Wave," 1980, The American University Ph.D. Dissertation, University Microfilms International 8017445.
10. Guo, T. C., Guo, W. W., and Larsen, L. E., 1984, IEEE MTT, 32, 835-843.
11. Guo, T. C., Guo, W. W., and Larsen, L. E., 1985. Int'l J. Infrared & Millimeter Waves, 6, 405-422.
12. Landau, L. D., Lifshitz, E. M., and Pitaevskii, L. P., "Electrodynamics of Continuous Media," 1984, pp. 59-62, Oxford: Pergamon Press.

To appear in the IEE Proceedings of the Fifth International Conference on Dielectric Materials, Measurements, and Applications, June 1988, Canterbury, England

APPENDIX C

SCATTERING OF VECTOR WAVES BY ARBITRARY THREE-DIMENSIONAL DIELECTRIC OBJECTS

by

Theodore C. Guo and Wendy W. Guo
Department of Physics, The Catholic University of America
Washington, D. C. 20064

ABSTRACT

A formulation for scattering of electromagnetic fields by arbitrary three-dimensional dielectric objects is presented. The formulation also provides an inverse solution, viz., determination of the dielectric profile of scatterers through measurement of the scattered fields in a finite region outside of the target. Uniqueness of the inverse scattering solution is assured owing to the dissipativity of the propagation medium.

I. INTRODUCTION

Analytic expressions of scattering of electromagnetic fields may be obtained only in simple cases, such as the Mie scattering from a uniform dielectric sphere,[1] or scattering from concentric dielectric spheres, which may be treated as extension of Mie scattering. For arbitrary dielectric objects, numerical approach must be taken. Even so, there are many theoretical difficulties which require certain approximation schemes. The simplest among them is the Born approximation, which takes the first order term in the expansion of the scattered field by iteration.[2] A better approach was developed by Richmond which uses the moment method,[3,4] however, it applies to only two-dimensional objects, viz., objects with cylindrical symmetry. The moment method has also been used to evaluate the field inside an arbitrary three-dimensional dielectric body,[5,6] but it has been found that the numerical solutions tend to diverge with respect to the subdivision of cells.[7] Most recently, a testing procedure was developed to analyze the numerical stability and reduce the computation time.[8] These approaches approximated the field inside the scatterer by a linear combination of some basis functions and then numerically solve the linear coefficients. In this paper, we reformulate Richmond's moment method in an operator form and extend it to three dimensions. We then develope a method to calculate the integrals of the Green's function in analytic form, thereby provide a formula for the scattering field from three-dimensional scattering objects. The formulation provides a solution of the field anywhere, inside or outside the scatterer. Furthermore, it may be inverted to provide an inverse scattering formulation, from which one may develope a formula to obtain the three-dimensional dielectric profile from the measurement of the scattered field.

II. THE SCATTERING FORMULATION

Consider an arbitrary dielectric body placed in a homogeneous background medium. Let ε_m and μ_m denote, respectively, the dielectric permittivity and the magnetic permeability of the background medium, and let $\varepsilon(\mathbf{x})$ and $\mu(\mathbf{x})$ denote those inside the dielectric object. Thus the quantity $\varepsilon(\mathbf{x})-\varepsilon_m$ vanishes outside the scatterer. We shall limit our scattering problem to non-magnetic object such that $\mu(\mathbf{x}) = \mu_m$ for all $\mathbf{x}$. Consider now a plane wave incident upon

Reprint from the Proceedings of the 1987 International Microwave Symposium, IEEE Publication 87TH0183-4

the dielectric object. In the absence of free charge and current, the Maxwell's equations of the system may be written in the form: $M|f\rangle = 0$, where M represents the Maxwell's differential operators and f the field quantities. The total field may be expressed as the sum of the scattered field and the incident field: $f = f^{(s)} + f^{(i)}$. We also separate the operator M into two parts: $M = M_m - S$, with M_m representing the Maxwell's operator in a homogeneous background and -S the operator due to excess dielectric permittivity, $\varepsilon(\mathbf{x}) - \varepsilon_m$. Then the Maxwell's equations may be written as $M_m|f^{(i)}\rangle + M_m|f^{(s)}\rangle = S|f\rangle$. Since $f^{(i)}$ satisfies the Maxwell's equations in the homogeneous medium, so $M_m|f^{(i)}\rangle = 0$. The equation then becomes: $M_m|f^{(s)}\rangle = S|f\rangle$. Operating both sides by the inverse of M_m, denoted by G_m, one then gets:

$$|f^{(s)}\rangle = G_m S|f\rangle. \tag{1}$$

It is remarked that the Maxwell's operator, M_m, in general, has no inverse because it has a null space. However, we are only concerned with the scattered waves that contain the factor $\exp(ik_m r)$, which, owing to a positive imaginary part of k_m, vanishes at infinity faster than any power of r. Therefore, in the subspace of scattered waves, M_m has an inverse, which is the Green's function G_m. Here we also remark that, owing to the existence of the inverse of the Maxwell's operator in the dissipative medium, the inverse scattering problem will have a unique solution.

Thus the scattering problem has been reduced to a source-field problem in the homogeneous medium, with the source $S|f\rangle$. Adding $|f^{(i)}\rangle$ to both sides of eq. (1) and rearranging terms, the equation gives $(1 - G_m S)|f\rangle = |f^{(i)}\rangle$, or,

$$|f\rangle = (1 - G_m S)^{-1}|f^{(i)}\rangle \tag{2}$$

Eq. (2) gives the total field in terms of the incident field. Specific expressions of G_m and S depend on the choice of $|f\rangle$, which can be a one-dimensional potential $|\varphi\rangle$, or a three-dimensional electric field $|\mathbf{E}\rangle$, or a four-dimensional potential $|A\rangle = |\varphi, \mathbf{A}\rangle$. For any choice of $|f\rangle$, the operators are derivable from the Maxwell's equations. Once eq. (1) is obtained, one may re-factorize the product $G_m S$ to any pair of operators, (G_m', S'), such that $G_m' S' = G_m S$. So, for the case $|f\rangle$ being the electric field $|\mathbf{E}\rangle$, we first write the Maxwell's equations in the form: $M_m'|f^{(s)}\rangle = S'|f\rangle$, where, in the Gaussian system of electromagnetic unit, the operators M_m' and S' are as follows:

$$M_m' = [\nabla^2 + k_m^2]\cdot\overleftrightarrow{I} \tag{3}$$

$$S' = -\frac{1}{\varepsilon_m}[\nabla\nabla\cdot + k_m^2\cdot\overleftrightarrow{I}](\varepsilon - \varepsilon_m) \tag{4}$$

where a time-dependency of $e^{-i\omega t}$ has been assumed. From eq. (3) one obtains the $\mathbf{x}$-representation of the inverse of M_m':

$$G_m(\mathbf{x}, \mathbf{x}') = -\frac{1}{4\pi}\cdot\frac{\exp(ik_m|\mathbf{x} - \mathbf{x}'|)}{|\mathbf{x} - \mathbf{x}'|}\cdot\overleftrightarrow{I} \tag{5}$$

Since $[\nabla\nabla\cdot + k_m^2\cdot\overleftrightarrow{I}]$ commutes with M_m', it commutes with its inverse, G_m'. Therefore, from eq. (4), $G_m' S' = [\nabla\nabla\cdot + k_m^2\cdot\overleftrightarrow{I}]G_m'[-(\varepsilon - \varepsilon_m)/\varepsilon_m]$. Defining G_m as $[\nabla\nabla\cdot + k_m^2\cdot\overleftrightarrow{I}]G_m'$, we may re-factorize $G_m' S'$ to the product of the following pair of (G_m, S):

Reprint from the Proceedings of the 1987 International Microwave Symposium, IEEE Publication 87TH0183-4

$$G_m(\mathbf{x},\mathbf{x}') = -\frac{1}{4\pi}\,[\nabla\nabla\cdot + k_m^2\cdot\overleftrightarrow{I}]\,\frac{\exp(ik_m|\mathbf{x}-\mathbf{x}'|)}{|\mathbf{x}-\mathbf{x}'|} \tag{6}$$

$$S = -\frac{1}{\varepsilon_m}\,[\varepsilon(\mathbf{x}) - \varepsilon_m]\cdot\overleftrightarrow{I} \tag{7}$$

The operator S vanishes outside the scatterer and is diagonal in the sense that $S(\mathbf{x},\mathbf{x}') = S(\mathbf{x})\delta(\mathbf{x}-\mathbf{x}')$. In the next section, we shall convert the above integral equations to matrix equations by digitizing the operators G_m and S.

III. DIGITIZING THE SCATTERING EQUATION

To calculate the inverse of $(1 - G_mS)$ in eq. (2), we divide the space into small cells so that the integral operators G_m and S may be converted into matrix operators. We first divide the entire space into subspaces, V_α (α=0,1,2,...), with V_o being the region occupied by the scatterer. We further divide each of V_α into N small cells, labeled by τ_j, with j = 1, 2, ..., N. Assuming that each cell τ_j is small, the field $f^{(s)}$ and the dielectric permittivity ε inside each cell may be represented by their respective mean values inside the cells. This means that the dimension of the cells must be smaller than a fraction, say 1/4, of the electromagnetic wavelength inside the scattering object. Denoting by $\mathbf{x}_j$ the center of the cell τ_j, eq. (1) may then be converted into summation of integrals over cells τ_j as below:

$$\langle\mathbf{x}|f^{(s)}\rangle \approx \sum_j \left[\int_{\mathbf{x}'\varepsilon\tau_j\subset V_o}\langle\mathbf{x}|G_m|\mathbf{x}'\rangle d\mathbf{x}'\right] S(\mathbf{x}_j)\langle\mathbf{x}_j|f\rangle \tag{8}$$

where we have used the diagonality of the operator S; the integral $\int d\mathbf{x}'$ is carried over only the space V_o since $S(\mathbf{x}')$ vanishes for all $\mathbf{x}'$ outside of V_o.

Let $f_\alpha^{(s)}$ denote a N-dimensional vector (of which each element is a 3-dimensional electric field) representing the scattered field in the N cells in the region V_α, and f_o and $f_o^{(i)}$, respectively, the total field and the incident field in the N cells in the scattering body V_o. Also denote by G_α and S the N x N square matrices with the matrix elements defined as below:

$$(G_\alpha)_{ij} = \int_{\mathbf{x}'\varepsilon\tau_j\subset V_o} G(\mathbf{x}_i,\mathbf{x}')\,d\mathbf{x}' \qquad \text{with } \mathbf{x}_i\varepsilon\tau_i\subset V_\alpha \tag{9}$$

$$S_{ij} = \frac{-1}{\varepsilon_m}\,[\varepsilon(\mathbf{x}_i) - \varepsilon_m]\cdot\overleftrightarrow{I}\,\delta_{ij} \qquad \text{with } \mathbf{x}_{i,j}\varepsilon\tau_{i,j}\subset V_o \tag{10}$$

Then the eq. (8) may be abbreviated as:

$$|f_\alpha^{(s)}\rangle = G_\alpha S|f_o\rangle \qquad (\alpha = 0,1,2,\ \ldots) \tag{11}$$

Note that, for S_{ij}, both τ_i and τ_j belong to V_o, the scattering object, whereas for $(G_\alpha)_{ij}$, τ_j belongs to V_o and τ_i belongs to V_α, which may be inside (if α=0) or outside (if $\alpha\neq$0) the scatterer. Eq. (11) represents the part of eq. (1) for the subspace V_α. For α = 0, we derive the equivalence of eq. (2) from eq. (11), as we did in deriving eq. (2) from eq. (1). We get:

$$|f_o\rangle = (1 - G_oS)^{-1}|f_o^{(i)}\rangle \tag{12}$$

Reprint from the Proceedings of the 1987 International Microwave Symposium, IEEE Publication 87TH0183-4

To get the scattered field inside or outside the scatterer, we substitut. eq. (12) into eq. (11). With some simple manipulation, it gives:

$$|f_\alpha^{(s)}\rangle = G_\alpha(S^{-1} - G_o)^{-1}|f_o^{(1)}\rangle \quad (\alpha = 0, 1, 2, \ldots). \tag{13}$$

The above equation gives the scattered field in any region, V_α, in terms of the incident field and dielectric permittivity inside the scatterer. In the next section, we shall evaluate, in analytic form, the matrix elements of G_α and G_o in eq. (13), which are the integrals G_{ij} defined in eq. (9).

IV. CALCULATION OF THE GREEN'S FUNCTION INTEGRALS

The two matrices, G_o and G_α, in eq. (13) are kinetic quantities, in the *sense* that they depend only on the background medium. The matrix elements of these two matrices are defined in eq. (9) as integrals of the Green's function over the cells inside V_o, and with $\mathbf{x}_i$ being the center of the cell τ_i, which is inside V_o for the matrix G_o, or inside V_α for the matrix G_α. To derive the integrals, one substitutes eq. (6) for the integrand of eq. (9), the latter then gives:

$$(G_\alpha)_{ij} = -\frac{1}{4\pi}\int_{\varepsilon\tau_j\subset V_o} [\nabla_i\nabla_i\cdot + k_m^2\cdot\overleftrightarrow{I}]\,\frac{\exp(ik_m|\mathbf{x}_i - \mathbf{x}'|)}{|\mathbf{x}_i - \mathbf{x}'|}\,d\mathbf{x}' \tag{14}$$

where ∇_i represents the gradient operator with respect to $\mathbf{x}_i$. Since $\mathbf{x}_i$ in the integrand always comes with $\mathbf{x}'$ in the form of $\mathbf{x}_i-\mathbf{x}'$, we may replace ∇_i with the gradient operator with respect to the vector $\mathbf{x}_i-\mathbf{x}.'$ Assuming that the volume of the integral, τ_j, is sufficiently small such that it may be represented by a sphere of radius a, centered at $\mathbf{x}_j$, then the above integral depends on $\mathbf{x}_i-\mathbf{x}_j$, a, and k_m only. Denoting $|\mathbf{x}_i-\mathbf{x}'|$ by $|\mathbf{x}|$, the above equation then gives:

$$(G_\alpha)_{ij} = -\frac{1}{4\pi}\int_\tau [\nabla\nabla\cdot + k_m^2\cdot\overleftrightarrow{I}]\,\frac{\exp(ik_m|\mathbf{x}|)}{|\mathbf{x}|}\,d\mathbf{x} \tag{15}$$

where the origin of the coordinates is $\mathbf{x}_i$, and τ is a sphere of radius a centered at $\mathbf{x}_j$. Since $(\nabla^2 + k_m^2)\cdot[\exp(ik_m|\mathbf{x}|)/|\mathbf{x}|] = -4\pi\delta(\mathbf{x})$, so

$$(G_\alpha)_{ij} = -\frac{1}{4\pi}\int_\tau (\nabla\nabla - \overleftrightarrow{I}\nabla^2)\,\frac{\exp(ik_m|\mathbf{x}|)}{|\mathbf{x}|}\,d\mathbf{x} + \overleftrightarrow{I}\cdot\int_\tau \delta(\mathbf{x})'d\mathbf{x} \tag{16}$$

The second integral on the right hand side gives unity when the sphere τ includes the origin, i.e., when $i=j$, and vanishes otherwise. As to the first integrals, it may be evaluated with the help of the identity, $\nabla g(r) = \hat{\mathbf{x}}g'(r)$, and the generalized Gauss's theorem, which relates a volume integral to a surface integral. The above equation then gives:

$$(G_\alpha)_{ij} = \delta_{ij} - \frac{1}{4\pi}\oint_\tau (\hat{\mathbf{n}}\hat{\mathbf{x}} - \overleftrightarrow{I}\hat{\mathbf{n}}\cdot\hat{\mathbf{x}})\cdot\frac{d}{dr}\left[\frac{\exp(ik_m r)}{r}\right] dS$$

The evaluation of the above surface integral is straightforward; the result depends on whether the sphere of integration, τ, contains the origin (i.e., whether $i = j$.) Thus we have, for $\alpha = 0, 1, 2, \ldots$:

Reprint from the Proceedings of the 1987 International Microwave Symposium, IEEE Publication 87TH0183-4

$$i = j: \quad (G_\alpha)_{ij} = \Upsilon \left[1 + \frac{2}{3}\cdot a^2 \cdot \frac{d}{da}\left(\frac{\exp(ik_m a)}{a}\right)\right] \tag{17}$$

$$i \neq j: \quad (G_\alpha)_{ij} = a\cdot\frac{\exp(ik_m|\mathbf{x}_i-\mathbf{x}_j|)}{|\mathbf{x}_i-\mathbf{x}_j|}\cdot\left[\cos(k_m a) - \frac{1}{k_m a}\cdot\sin(k_m a)\right]$$
$$\cdot\left[\Upsilon\left(1 - \frac{1}{ik_m|\mathbf{x}_i-\mathbf{x}_j|} + \frac{1}{(ik_m|\mathbf{x}_i-\mathbf{x}_j|)^2}\right)\right.$$
$$\left. - \frac{\mathbf{x}_i-\mathbf{x}_j}{|\mathbf{x}_i-\mathbf{x}_j|}\,\frac{\mathbf{x}_i-\mathbf{x}_j}{|\mathbf{x}_i-\mathbf{x}_j|}\left(1 - \frac{3}{ik_m|\mathbf{x}_i-\mathbf{x}_j|} + \frac{3}{(ik_m|\mathbf{x}_i-\mathbf{x}_j|)^2}\right)\right] \tag{18}$$

With the above analytic expressions for the matrix elements $(G_\alpha)_{ij}$, and the expression for the matrix element S_{ij} given by eq. (10), one may then calculate the scattered field in any region, say, V_α, using eq. (13).

IV. SUMMARY AND CONCLUSION

We have developed a three-dimensional scattering formulation from which one may calculate the scattered vector field anywhere, inside or outside the scattering object; the scatterer may be of arbitrary three-dimensional shape with arbitrary dielectric profile. There are two practical problems that need further investigation. One is the stability of the inversion of the matrix $(S^{-1}-G_o)$ in eq. (13). Another is the size of the matrices G_o and G_α, viz., the number of cells into which the scattering object is divided. We shall discuss these two problems in the following paragraphs.

On the stability of matrix inversion, the question is: How stable is the inverse of $(S^{-1}-G_o)$ if there is an error in $(S^{-1}-G_o)$? This subject may be investigated by analyzing the so called condition number of the matrix $(S^{-1}-G_o)$, which is a measure of singularity of the matrix.[9] The singularity of a matrix may be reduced by eliminating symmetry of the matrix, viz., eliminating the interdependency between the columns or the rows. Therefore, owing to the term S^{-1}, there is not much stability problem if the dielectric profile of the scatterer is highly asymmetric. For a symmetric dielectric body, it may be necessary to reduce the symmetry by other means, such as making the division into N cells asymmetrically.

As to the size of the matrices, it is limited by two conditions. One is the desired resolution or degree of accuracy, and another is the approximation that we used to digitize the original integral equation. The first limitation is a subjective one which needs not be remarked. As to the second limitation, recall that in deriving eq. (8), it was assumed that the values of the total field and the dielectric permittivity inside each cell of the scattering object do not vary much. For the field to remain constant inside each cell, the cell must be smaller than a quarter wavelength inside the scattering dielectric. In this aspect, the computation time increases with the cube of the frequency of the scattering waves. It is worth noting that, as some investigators have found, higher symmetry in the division of cells may facilitate the computation by consideration using group algebra;[10] this argument applies only to the computation involving the matrices G_α since they do not involve the dielectric properties of the scatterer, which may be quite asymmetric. On the other hand, as we mentioned above, higher symmetry may increase the condition number of the matrices and thereby reduce the accuracy of the result. For scatterers with some symmetric properties, it is possible, however, to utilize both arguments to benefit the computation. One may start

Reprint from the Proceedings of the 1987 International Microwave Symposium, IEEE Publication 87TH0183-4

by using a higher symmetric division of cells and then block-diagonalize the matrices G_α and $(S^{-1}-G_o)$ of eq. (13) to irreducible forms. The computing time is reduced by the diagonalizing operation while, since each diagonal block is highly asymmetric, the stability of the data may be preserved. However, rigorous proof and further investigation on this argument are needed.

Finally we remark that the formulation described in this paper may be inverted to provide an inverse scattering formula.[11,12] Briefly, the approach is to make as many scatterings with independent incident waves as there are number of cells in the target. For each scattering, we have a pair of $f_\alpha^{(s)}$ and $f_o^{(i)}$ that satisfy eq. (13). Lining up the column vectors representing $f_\alpha^{(s)}$ and $f_o^{(i)}$, respectively, we obtain two N x N square matrices, $F^{(i)}$ and $F^{(s)}$. Then eq. (13) gives: $F_\alpha^{(s)} = G_\alpha(S^{-1} - G_o)^{-1}F_o^{(i)}$. The equation may then be inverted to yield an expression of S^{-1} in terms of the $F^{(s)}$.

ACKNOWLEDGEMENT

This work was supported Potomac Research, Inc., Potomac, Maryland, U.S.A., and by Walter Reed Army Institute of Research through the Office of Naval Research under the Contract N00014-85-K-0475.

REFERENCES

1. M. Born and E. Wolf, Principles of Optics, pp. 633-656, Macmillan, 1964.
2. J. B. Keller, "Accuracy and validity of the Born and Rytov approximations," J. Opt. Soc. America **59**, pp. 1003-1004 (1969).
3. J. H. Richmond, "Scattering by a Dielectric Cylinder of Arbitrary Cross-Section," IEEE Trans. **AP-13**, pp. 334-341 (1965).
4. J. H. Richmond, "TE-Wave Scattering by a Dielectric Cylinder of Arbitrary Cross Section Shape," IEEE Trans. **AP-14**, pp. 460-464 (1966).
5. R. H. Harrington, Field Computations by Moments Methods, McGraw-Hill, New York, 1968.
6. D. E. Livesay and K.-M. Chen, "Electromagnetic Fields Induced Inside Arbitrarily Shaped Biological Bodies," IEEE Trans. **MTT-22**, pp. 1273-1280 (1974).
7. H. Massoudi, C. H. Durney, and M. F. Iskander, "Limitations of the Cubical Block Model of Men in Calculating SAR Distributions," IEEE Trans. **MTT-32**, pp. 746-752 (1984).
8. C. T. Tsai, H. Massoudi, C. H. Durney, and M. F. Iskander, "A Procedure for Calculating Fields Inside Arbitrarily Shaped, Inhomogeneous Dielectric Bodies Using Linear Basis Functions with the Moment Method," IEEE Trans. **MTT-34**, pp. 1131-1139 (1986).
9. G. E. Forsythe, M. A. Malcolm, and C. D. Moler, Computer Methods for Mathematical Computation, p. 41, Prentice-Hall, 1977.
10. D. K. Ghodgaonkar and O. P. Gandhi, "A Computationally-Efficient Method for Estimation of Complex Permittivities of 3-D Inhomogeneous Biological Bodies," preprint of Elec. Eng. Dept., University of Utah, 1985.
11. T. C. Guo, W. W. Guo, and L. E. Larsen, "Microwave Imagery of Biological Objects - An Inverse Scattering Approach," Proc. Eighth Int'l Sym. Infrared and Millimeter Waves, December 1983, IEEE Pub. 83CH1917-4, 1983.
12. T. C. Guo, W. W. Guo, and L. E. Larsen, "Recent Development in Microwave Medical Imagery - Phase and Amplitude Conjugations and the Inverse Scattering Theorem," in Medical Applications of Microwave Imaging, ed. L. E. Larsen and J. H. Jacobi, pp. 167-183, IEEE Press, 1986.

Reprint from the Proceedings of the 1987 International Microwave Symposium, IEEE Publication 87TH0183-4

Report to WRAIR via ONR
Contract No. N00014-85-K-0475
Transient Interaction of Electromagnetic Pulses
in Dielectrics and Microwave Biophysics
by Theodore C. Guo and Wendy W. Guo

APPENDIX D

A Reprint from the

PROCEEDINGS

Of SPIE-The International Society for Optical Engineering

Volume 767

Medical Imaging

1 6 February 1987
Newport Beach, California

Physics of image formation by microwave scattering

Theodore C. Guo, Wendy W. Guo
Department of Physics, The Catholic University of America
Washington, D.C. 20064

Physics of image formation by microwave scattering

Theodore C. Guo and Wendy W. Guo

Department of Physics, The Catholic University of America
Washington, D. C. 20064

Abstract

The complex permittivities of three-dimensional inhomogeneous biological bodies can be extracted from microwave scattering data by inverse scattering approach. A water-immersed microwave system is used to contract the wavelength to millimeter range and to enhance impedance matching with the biological body. Contraction of the wavelength increases the image resolution, while impedance matching promotes the microwave penetration. Scattered fields are measured using an array of 127 dipole elements and a total size of approximately 15cm x 18cm with operating frequency at 3 GHz. Two inverse scattering approaches have been developed. One approach, which has been published earlier,[1,2] utilizes an inverse scattering theorem which may be considered as a generalization of the Lorentz reciprocity theorem to dissipative media. The other approach, which is presented in this article, takes scattering measurement by an array with various directions of incident wave; the wave equation is converted to a matrix equation by dividing the dielectric body into a number of cells, the dielectric data is then obtained by inverting the matrix equation. In both approaches, uniqueness is assured owing to the dissipativity of the propagation medium.

Introduction

Microwave for medical imaging[3,4,5] provides many advantages over current techniques. The underlying idea here is to reconstruct a three-dimensional dielectric image based on the scattering data. The technique is relatively safe since only non-ionizing radiation is used. Comparing to all existing techniques, it provides the best contrast between soft tissues in terms of pathological information since it is the dielectric constant that is imaged. Simply by analyzing the dielectric image, it can also be used to provide temperature mapping in soft tissues with a resolution of one-tenth of a degree Celsius. Economically, the cost of a microwave imaging system is expected to be much less than those using the existing imaging techniques. As to the resolution, it depends on the number of elements in the detection array and the image reconstruction method. On a system of 127 array elements that is being developed, we have achieved a transverse resolution (3 dB width) of about 5.3 mm, which is about half-wavelength in water, and an axial resolution of about 11.7 mm, which is about one wavelength in water.[2,6,7]

In order to reduce reflection of the incident microwave from the target, both transmitting and detecting arrays are submerged in water. Submerging the arrays in water not only provides impedance matching, but also contracts the wavelength and thereby improves the resolution. Another advantage of submerging the arrays in water is elimination of multipath signals (viz., signals scattered from surrounding equipments outside of the target,) and thereby improving signal-to-noise ratio. There are a few methods to further improve the resolution, all of them require additional scattering data collection. However, increasing the amount of data does not always improve the imaging resolution since, depending on the reconstruction methods, redundancy and inter-dependency of reconstruction algorithm may negate the additional information input. The primary concern of this article is on the algorithm of image reconstruction from the measurements of scattered field.

The objective of microwave imagery is to determine the dielectric characteristics of a target from the microwave field pattern exterior of the target. For far-field and intermediate zones, the traditional approaches are the Fraunhofer and Frenel diffractions based on the theory of Fourier transformation. In many applications, particularly in medical imagery, the target must be in the vicinity of the microwave detector, then these approaches are not applicable since neither the field pattern of the target nor the field pattern of the receiving antenna may be characterized by a Fourier transform of the structure of the target or the antenna. Though this aspect complicates the mathematical problem of near-field imageries, development of some near-field approach may provide a possibility of three-dimensional focusing which is not achievable in either Fraunhofer or Frenel diffractions.

An important theoretical problem in imageries concerns the uniqueness of the target reconstruction. The dielectric structure of the target is part of the source of the field exterior to the target. In particular, apart from undesirable noises, it is the sole source of the scattered field. The Maxwell's equations guarantee a unique solution of the field once the source and the boundary condition are specified. However, the reverse is not true.

Indeed, a simple consideration of the field due to charges on a conducting sphere shows that the same field exterior to the sphere may be given by many possible distributions within the sphere, for example, a distribution of surface charges on a sphere of smaller radius, or a point charge at the center of the sphere. Therefore, theoretically, knowing the field everywhere exterior to an imaging target does not guarantee a unique solution of the dielectric structure within the target. In this paper we shall show that if the background medium is dissipative, then the inverse scattering has a unique solution. One may then argue that, for theoretical calculation, even in a non-dissipative medium, one can add a small dissipative part in the dielectric constant to start with and later set it to zero. The problem is that, even though the solution is theoretically unique, to reconstruct the target requires a large number of independent data. The smaller is the imaginary part of the dielectric constant, the more redundancy in the measured data. On the other hand, the stronger the dissipation of the background medium is, the weaker the scattered signal is, and therefore the smaller is the signal-to-noise ratio. Thus, we are faced with a practical problem of optimizing the dissipativity of the background medium.

Another practical aspect further complicates the issue: in reality, one can measure the field only at a limited number of points exterior to the target. The problem is a typical inverse scattering problem, viz., how much information on the dielectric structure of the target can one infer from a set of limited data of the field exterior to the target? Previously, we developed an inverse scattering theorem[1,2] and a method of phase and amplitude conjugation techniques[2,4] to reconstruct the target dielectric profile, with which a transverse resolution of $\lambda/2$ and an axial resolution of λ were obtained. In this paper, we present another method which is based on discretely sampling the Green's function and then converting it to a matrix (referred to as the Green's matrix). With this approach, the resolution can be improved unlimitedly; the resolution improves linearly with the number of sampling points of the scattered field anywhere outside of the target.

The scattering formulation

In this section we describe the logic of the formulation and present the scattering formula. First, we mention a few words about the notation. Since we are dealing with scattering of electromagnetic fields by three-dimensional objects, spatial coordinates are three-dimensional vectors while field quantities may be three-dimensional, such as the electric field, or four-dimensional, such as the charge-current density. To distinguish three-dimensional quantities from four-dimensional ones, we denote the former with bold face letters while use normal letters for the latter. We shall also use Dirac bra-ket, say, $|f\rangle$, to denote a field quantity f, and $\langle \mathbf{x}|f\rangle$ to denote the function $f(\mathbf{x})$, which is f in the x-representation. Thus, an operator, say, the Green's function G, takes the form $\langle \mathbf{x}|G|\mathbf{x}'\rangle = G(\mathbf{x},\mathbf{x}')$ in the x- representation. Unless otherwise stated, all products between vectors and between operators and vectors are vector products, namely, the products are to sum over either the 3 or the 4 components without the Σ notation; we reserve the Σ notation for summation over the number of cells in discrete sampling of data. On the electromagnetic equations, we shall use the Gaussian system of electromagnetic unit; conversion of equations between the Gaussian system and the MKS system may be found at the end of the text book by Jackson.[6]

Consider an arbitrary dielectric body, which will be our scattering object, occupying a region V_o in a homogeneous background medium. Let ϵ_m and μ_m denote respectively the dielectric permittivity and the magnetic permeability of the background medium, and let $\epsilon(\mathbf{x})$ and $\mu(\mathbf{x})$ denote those inside V_o. Thus the quantity $\epsilon(\mathbf{x})-\epsilon_m$ is localized in the sense that it vanishes outside V_o. We shall limit our system to non-magnetic object such that $\mu(\mathbf{x}) = \mu_m$ for all $\mathbf{x}$ inside V_o.

Consider now a plane wave incident upon the target. In the absence of free charge and current, the Maxwell's equations of the system may be written in the following form:

$$M|f\rangle = 0 \qquad (1)$$

where M, which is a function of $\epsilon(\mathbf{x})$, represents the Maxwell's differential operators and f the field quantities. The total field may be expressed as the sum of the scattered field and the incident field: $f = f^{(s)} + f^{(i)}$. In order to express the scattered field in terms of the incident field and the dielectric distribution of the target, we separate the operator M into two parts: M_m and -S. The first part, M_m, represents the Maxwell's operator in a homogeneous background medium and is independent of $\epsilon(\mathbf{x})$. The second part,

$$-S = M - M_m \qquad (2)$$

represents the operator due to excess dielectric permittivity, $\epsilon(\mathbf{x})-\epsilon_m$. Then eq. (1) may be written as $M_m|f^{(i)}\rangle + M_m|f^{(s)}\rangle = S|f\rangle$. Since $f^{(i)}$ satisfies the Maxwell's equations in the homogeneous medium, so $M_m|f^{(i)}\rangle = 0$. Eq. (1) then reduces to

$$M_m |f^{(s)}\rangle = S|f\rangle \tag{3}$$

Thus the scattering problem has been reduced to a source-field problem in the homogeneous medium, where the scattered field corresponds to the field due to a source distribution $S|f\rangle$. However, the quantity $|f\rangle$ on the right hand side still contains the unknown field $|f^{(s)}\rangle$. To remove the scattering field from the right hand side of eq. (3), we operate both sides of the equation by the inverse of M_m. Note that, since the operator M_m has a null space, it in general has no inverse. However, since we are only concerned with the outgoing fields that contain the factor $\exp(ik_m r)$, which, owing to the imaginary part of k_m, vanish at infinity faster than any power of r, we may then limit ourselves to the subspace of such fields. In such subspace, M_m has an inverse, which is the Green's function G_m. Since $|f^{(s)}\rangle$ is an outgoing scattered wave, so $G_m M_m |f^{(s)}\rangle = |f^{(s)}\rangle$. Then eq. (3) gives:

$$|f^{(s)}\rangle = G_m S|f\rangle. \tag{4}$$

Adding $|f^{(i)}\rangle$ to both sides, it then becomes $|f\rangle = G_m S|f\rangle + |f^{(i)}\rangle$, or,

$$(1 - G_m S)|f\rangle = |f^{(i)}\rangle \tag{5}$$

It can be proven that the operator $(1-G_m S)$ on the left hand side has an inverse. Therefore the above equation gives

$$|f\rangle = (1 - G_m S)^{-1}|f^{(i)}\rangle \tag{6}$$

Subtract the incident field $|f^{(i)}\rangle$ from both sides of the above equation, one then obtains the scattered field $|f^{(s)}\rangle$:

$$|f^{(s)}\rangle = [(1 - G_m S)^{-1} - 1]|f^{(i)}\rangle. \tag{7}$$

Eq. (7) gives the scattered field in terms of the incident field. In the next section we shall develop a technique to evaluate the inverse of $(1-G_m S)$.

So far we have described the scattering formulation in general terms. Specific expressions of these equations depend on the choice of the quantity $|f\rangle$; $|f\rangle$ can be the one-dimensional scalar potential $|\Phi\rangle$, or the three-dimensional electric field $|\mathbf{E}\rangle$, or the four-dimensional potential $|A\rangle = |\Phi, \mathbf{A}\rangle$. For any choice of the field $|f\rangle$, the operators are derived from the Maxwell's equations. In below we list the results for the case where $|f\rangle$ is $|A\rangle$, and for the case where $|f\rangle$ is $|\mathbf{E}\rangle$. Details of the derivation will be given in a forthcoming paper.

We shall assume a time-dependency of $e^{-i\omega t}$ and replace $\partial/\partial t$ with $-i\omega$. If the field $|f\rangle$ is the 4-dimensional vector potential, we shall use the following notation to represent matrix operation:

$$\begin{bmatrix} \times \\ | \end{bmatrix} = \begin{bmatrix} \times & \text{———} \\ | & \square \end{bmatrix} \begin{bmatrix} \times \\ | \end{bmatrix}$$

where $\times$ denotes the 1-dimensional time component of a 4-dimensional vector, and (———) denotes the 3-dimensional space component. Then the operators M_m and S may be represented as below:

$$M_m = (\nabla^2 + k_m^2) \begin{bmatrix} 1 & 0 \\ 0 & \bar{I} \end{bmatrix} \tag{8}$$

$$S = -\frac{1}{c} \begin{bmatrix} -\frac{1}{\epsilon_m} \nabla\cdot(\epsilon-\epsilon_m)\nabla & -\frac{i\omega}{\epsilon_m} \nabla\cdot(\epsilon-\epsilon_m) \\ i\omega\mu_m(\epsilon-\epsilon_m)\nabla & \frac{\omega^2\mu_m}{c}(\epsilon-\epsilon_m)\,\bar{I} \end{bmatrix} \tag{9}$$

Note also that the operator ∇ on the left of $(\epsilon-\epsilon_m)$ inside the matrix not only operates on $(\epsilon-\epsilon_m)$, but also operates on whatever quantity to be operated by S. Since M_m is a differential operator, its inverse, G_m, is an integral operator. In the $\mathbf{x}$-representation, G_m may be explicitly expressed as below:

$$G_m(\mathbf{x},\mathbf{x}') = \langle \mathbf{x}|G_m|\mathbf{x}'\rangle = -\frac{1}{4\pi}\frac{\exp(ik_m|\mathbf{x}-\mathbf{x}'|)}{|\mathbf{x}-\mathbf{x}'|} \begin{bmatrix} 1 & 0 \\ 0 & \bar{I} \end{bmatrix} \tag{10}$$

The above expression means that, in the $\mathbf{x}$-representation, G_m is an integral operator:

$$\langle \mathbf{x}|G_m|f\rangle = \int G_m(\mathbf{x},\mathbf{x}')f(\mathbf{x}')d\mathbf{x}'$$

Note that the definitions of operators G_m and S are not unique in the sense that, once eq. (4) is obtained, one may re-factorize the product G_mS to any pair of operators, (G_m', S'), such that $G_m'S' = G_mS$. This is exactly what we shall do for the case where the field $|f\rangle$ is the electric field $|E\rangle$. We shall first derive a pair denoted by G_m' and S', where G_m' corresponds to the Maxwell's operator M_m', then re-factorize the pair to another pair G_m and S. The re-factorization will not affect the results of scattered fields or inverse scattering image reconstruction, but simplifies the scattering and inverse scattering formulation. Thus, for the case where $|f\rangle$ is the electric field, $|E\rangle$, we first derive from the Maxwell's equations M_m' and S':

$$M_m' = [\nabla^2 + k_m^2]\cdot\bar{I} \tag{11}$$

$$S' = -\frac{1}{\epsilon_m}[\nabla\nabla\cdot + k_m^2\cdot\bar{I}](\epsilon - \epsilon_m) \tag{12}$$

From eq. (11) we obtain the $\mathbf{x}$-representation of the inverse of M_m':

$$G_m'(\mathbf{x},\mathbf{x}') = -\frac{1}{4\pi}\frac{\exp(ik_m|\mathbf{x}-\mathbf{x}'|)}{|\mathbf{x}-\mathbf{x}'|}\cdot\bar{I} \tag{13}$$

Since $[\nabla\nabla\cdot + k_m^2\cdot\bar{I}]$ in eq. (12) commutes with $M_m' = [\nabla^2 + k_m^2]\cdot\bar{I}$, so it commutes with its inverse, G_m'. Therefore, from eq. (12), $G_m'S' = -G_m'[\nabla\nabla\cdot + k_m^2\cdot\bar{I}](\epsilon - \epsilon_m)/\epsilon_m = [\nabla\nabla\cdot + k_m^2\cdot\bar{I}]G_m'[-(\epsilon - \epsilon_m)/\epsilon_m]$. Then we define the pair G_m and S as $[\nabla\nabla\cdot + k_m^2\cdot\bar{I}]G_m'$ and $-\bar{I}\cdot(\epsilon - \epsilon_m)/\epsilon_m$, respectively:

$$G_m(\mathbf{x},\mathbf{x}') = -\frac{1}{4\pi}[\nabla\nabla\cdot + k_m^2\cdot\bar{I}]\frac{\exp(ik_m|\mathbf{x}-\mathbf{x}'|)}{|\mathbf{x}-\mathbf{x}'|} \tag{14}$$

$$S = -\frac{1}{\epsilon_m}[\epsilon(\mathbf{x}) - \epsilon_m]\cdot\bar{I} \tag{15}$$

The operator S in eq. (15) is diagonal in the sense that, in the $\mathbf{x}$-representation, $S(\mathbf{x},\mathbf{x}') = S(\mathbf{x})\delta(\mathbf{x}-\mathbf{x}')$. It also vanishes outside of the target region V_o. It is the diagonal elements of this operator that we wish to recover from the scattering data. In the next section, we shall covert the above integral equations to matrix equations by digitizing the operators G_m and S.

Digitizing the scattering equation

In this section, we describe a numerical method to calculate the inverse of $(1 - G_mS)$, and thus the scattered field $f^{(s)}$ using eq. (7), for the case when $f^{(s)}$ is the electric field, $E^{(s)}$. In this case, G_m and S are given by eqs. (14) and (15). Our approach will be to divide the space into small cells so that the integral operator G_m may be converted to a matrix operator. To this end, we divide the entire space into subspaces, and label each subspace by V_α, with V_o being the entire region occupied by the target. We further divide each of V_α into N small cells, labeled by τ_j, with $j = 1, 2, \ldots, N$. We assume that each cell τ_j is small enough that the field $f^{(s)}$ and the dielectric permittivity ϵ inside each cell may be represented by their respective mean values inside the cell. This means that the dimension of the cell must be smaller than a fraction, say 1/4, of the microwave wavelength inside the target. We shall denote by $\mathbf{x}_j$ the center of the cell τ_j. Then eq. (4) may be converted into summation of integrals over cells τ_j as below:

$$\begin{aligned}\langle \mathbf{x}|f^{(s)}\rangle &= \int\int \langle \mathbf{x}|G_m|\mathbf{x}'\rangle\langle \mathbf{x}'|S|\mathbf{x}''\rangle\langle \mathbf{x}''|f\rangle d\mathbf{x}'d\mathbf{x}'' = \int\int \langle \mathbf{x}|G_m|\mathbf{x}'\rangle\cdot S(\mathbf{x}')\delta(\mathbf{x}'-\mathbf{x}'')\langle \mathbf{x}''|f\rangle d\mathbf{x}'d\mathbf{x}'' \\ &= \int_{\mathbf{x}'\in V_o} \langle \mathbf{x}|G_m|\mathbf{x}'\rangle\cdot S(\mathbf{x}')\langle \mathbf{x}'|f\rangle d\mathbf{x}' = \sum_j \left[\int_{\mathbf{x}'\in\tau_j\subset V_o} \langle \mathbf{x}|G_m|\mathbf{x}'\rangle S(\mathbf{x}')\langle \mathbf{x}'|f\rangle d\mathbf{x}'\right] \\ &\approx \sum_j \left[\int_{\mathbf{x}'\in\tau_j\subset V_o} \langle \mathbf{x}|G_m|\mathbf{x}'\rangle d\mathbf{x}'\right] S(\mathbf{x}_j)\langle \mathbf{x}_j|f\rangle\end{aligned} \tag{16}$$

where the integral $\int d\mathbf{x}'$ is carried over only the space V_o since $S(\mathbf{x}')$ vanishes for all $\mathbf{x}'$ outside of V_o.

Denote by $G_{i,j}$ and $S_{i,j}$, respectively, the following quantities:

$$G_{i,j} = \int_{\mathbf{x}'\in\tau_j\subset V_o} G_m(\mathbf{x}_i,\mathbf{x}')d\mathbf{x}' \tag{17}$$

$$S_{i,j} = S(\mathbf{x}_i)\delta_{i,j} = -\frac{1}{\epsilon_m}[\epsilon(\mathbf{x}_i) - \epsilon_m]\,\delta_{i,j} \tag{18}$$

By approximating the integrated region τ_j with a sphere, the integral G_{ij} of eq. (17) may be calculated analytically; the analytic form is presented at the end of this section. With the definition of G_{ij} and S_{ij}, eq. (16) may be written as:

$$f_i^{(s)} = \sum_{j,k} G_{ij} S_{jk} f_k \tag{19}$$

In the matrix form, the above equation is:

$$\begin{bmatrix} f_1 \\ f_2 \\ f_3 \\ \cdot \\ \cdot \\ f_N \\ f_{N+1} \\ \cdot \\ \cdot \end{bmatrix}^S = \begin{bmatrix} G_{11} & G_{12} & G_{13} & \cdot & \cdot & G_{1N} & G_{1,N+1} & \cdot & \cdot \\ G_{21} & G_{22} & G_{23} & \cdot & \cdot & G_{2N} & G_{2,N+1} & \cdot & \cdot \\ G_{31} & G_{32} & G_{33} & \cdot & \cdot & G_{3N} & G_{3,N+1} & \cdot & \cdot \\ \cdot & \cdot & \cdot & \cdot & \cdot & \cdot & \cdot & \cdot & \cdot \\ \cdot & \cdot & \cdot & \cdot & \cdot & \cdot & \cdot & \cdot & \cdot \\ G_{N1} & G_{N2} & \cdot & \cdot & \cdot & G_{NN} & G_{N,N+1} & \cdot & \cdot \\ G_{N+1,1} & \cdot & \cdot & \cdot & \cdot & G_{N+1,N} & \cdot & \cdot & \cdot \\ \cdot & \cdot & \cdot & \cdot & \cdot & \cdot & \cdot & \cdot & \cdot \\ \cdot & \cdot & \cdot & \cdot & \cdot & \cdot & \cdot & \cdot & \cdot \end{bmatrix} \begin{bmatrix} S_1 & 0 & 0 & \cdot & \cdot & 0 & 0 & \cdot & \cdot \\ 0 & S_2 & 0 & \cdot & \cdot & 0 & 0 & \cdot & \cdot \\ 0 & 0 & S_3 & \cdot & \cdot & 0 & 0 & \cdot & \cdot \\ \cdot & \cdot & \cdot & \cdot & \cdot & \cdot & \cdot & \cdot & \cdot \\ \cdot & \cdot & \cdot & \cdot & \cdot & \cdot & \cdot & \cdot & \cdot \\ 0 & 0 & 0 & \cdot & \cdot & S_N & 0 & \cdot & \cdot \\ 0 & 0 & 0 & \cdot & \cdot & 0 & 0 & \cdot & \cdot \\ \cdot & \cdot & \cdot & \cdot & \cdot & \cdot & \cdot & \cdot & \cdot \\ \cdot & \cdot & \cdot & \cdot & \cdot & \cdot & \cdot & \cdot & \cdot \end{bmatrix} \begin{bmatrix} f_1 \\ f_2 \\ f_3 \\ \cdot \\ \cdot \\ f_N \\ f_{N+1} \\ \cdot \\ \cdot \end{bmatrix} \tag{20}$$

where subscripts 1 to N denote cells inside V_o, subscripts N+1 to 2N denote those inside V_1, etc. We may break the above equation into equations representing the operation for each subspace V_α. Thus, for the space V_o occupied by the target, the above equation gives:

$$\begin{bmatrix} f_1 \\ f_2 \\ f_3 \\ \cdot \\ \cdot \\ f_N \end{bmatrix}^S = \begin{bmatrix} G_{11} & G_{12} & G_{13} & \cdot & \cdot & G_{1N} \\ G_{21} & G_{22} & G_{23} & \cdot & \cdot & G_{2N} \\ G_{31} & G_{32} & G_{33} & \cdot & \cdot & G_{3N} \\ \cdot & \cdot & \cdot & \cdot & \cdot & \cdot \\ \cdot & \cdot & \cdot & \cdot & \cdot & \cdot \\ G_{N1} & G_{N2} & \cdot & \cdot & \cdot & G_{NN} \end{bmatrix} \begin{bmatrix} S_1 & 0 & 0 & \cdot & \cdot & 0 \\ 0 & S_2 & 0 & \cdot & \cdot & 0 \\ 0 & 0 & S_3 & \cdot & \cdot & 0 \\ \cdot & \cdot & \cdot & \cdot & \cdot & \cdot \\ \cdot & \cdot & \cdot & \cdot & \cdot & \cdot \\ 0 & 0 & 0 & \cdot & \cdot & S_N \end{bmatrix} \begin{bmatrix} f_1 \\ f_2 \\ f_3 \\ \cdot \\ \cdot \\ f_N \end{bmatrix} \tag{21}$$

and, for the subspaces V_α (α = 1, 2, ...), eq. (20) gives:

$$\begin{bmatrix} f_{\alpha N+1} \\ f_{\alpha N+2} \\ f_{\alpha N+3} \\ \cdot \\ \cdot \\ f_{\alpha N+N} \end{bmatrix}^S = \begin{bmatrix} G_{\alpha N+1,1} & G_{\alpha N+1,2} & G_{\alpha N+1,3} & \cdot & \cdot & G_{\alpha N+1,N} \\ G_{\alpha N+2,1} & G_{\alpha N+2,2} & G_{\alpha N+2,3} & \cdot & \cdot & G_{\alpha N+2,N} \\ G_{\alpha N+3,1} & G_{\alpha N+3,2} & G_{\alpha N+3,3} & \cdot & \cdot & G_{\alpha N+3,N} \\ \cdot & \cdot & \cdot & \cdot & \cdot & \cdot \\ \cdot & \cdot & \cdot & \cdot & \cdot & \cdot \\ G_{\alpha N+N,1} & G_{\alpha N+N,2} & G_{\alpha N+N,3} & \cdot & \cdot & G_{\alpha N+N,N} \end{bmatrix} \begin{bmatrix} S_1 & 0 & 0 & \cdot & \cdot & 0 \\ 0 & S_2 & 0 & \cdot & \cdot & 0 \\ 0 & 0 & S_3 & \cdot & \cdot & 0 \\ \cdot & \cdot & \cdot & \cdot & \cdot & \cdot \\ \cdot & \cdot & \cdot & \cdot & \cdot & \cdot \\ 0 & 0 & 0 & \cdot & \cdot & S_N \end{bmatrix} \begin{bmatrix} f_1 \\ f_2 \\ f_3 \\ \cdot \\ \cdot \\ f_N \end{bmatrix} \tag{22}$$

The above two equations may be abbreviated as:

$$|f_o^{(s)}\rangle = G_o S |f_o\rangle \tag{23}$$

$$|f_\alpha^{(s)}\rangle = G_\alpha S |f_o\rangle \tag{24}$$

where $|f_o^{(s)}\rangle$ and $|f_o\rangle$ represent, respectively, the scattered and total fields in V_o, the region occupied by the target; $|f_\alpha^{(s)}\rangle$ and $|f_\alpha\rangle$ represent those in V_α (α = 1, 2, ...), a subspace of any volume outside of the target. In the above two equations, the matrix elements of G_o, G_α, and S are as defined in eqs. (17) and (18) with the following assignments for $\mathbf{x}_i$ and $\mathbf{x}_j$:

$$(G_o)_{ij} = \int_{\mathbf{x}' \in \tau_j \subset V_o} G(\mathbf{x}_i, \mathbf{x}')\, d\mathbf{x}' \qquad \text{with} \quad \mathbf{x}_i \in \tau_i \subset V_o \tag{25}$$

$$(G_\alpha)_{ij} = \int_{\mathbf{x}' \in \tau_j \subset V_o} G(\mathbf{x}_i, \mathbf{x}')\, d\mathbf{x}' \qquad \text{with} \quad \mathbf{x}_i \in \tau_i \subset V_\alpha \tag{26}$$

$$S_{ij} = \frac{1}{\epsilon_m} [\epsilon(\mathbf{x}_i) - \epsilon_m]\, \delta_{ij} \qquad \text{with} \quad \mathbf{x}_{i,j} \in \tau_{i,j} \subset V_o \tag{27}$$

The values of the matrix elements S_{ij} in eq. (27) are the quantities to be reconstructed from the scattering data; the values of the matrix elements $(G_o)_{ij}$ and $(G_\alpha)_{ij}$ may be calculated from the analytic forms presented at the end of this section. Note that eq. (23) is similar to eq. (4). Indeed, it represents the part of eq. (4) for the subspace V_o, the region occupied by the scattering target. We may then derive the equivalence of eqs. (6) and (7) from eq. (23), as we did in deriving eqs. (6) and (7) from eq. (4). We then get:

$$|f_o\rangle = (1 - G_o S)^{-1} |f_o^{(1)}\rangle \tag{28}$$

$$|f_o^{(s)}\rangle = [(1 - G_o S)^{-1} - 1] |f_o^{(1)}\rangle \tag{29}$$

To get the scattered field outside the target, we substitute eq. (28) into eq. (24). With some simple manipulation, it gives:

$$|f_\alpha^{(s)}\rangle = G_\alpha (S^{-1} - G_o)^{-1} |f_o^{(1)}\rangle \quad (\alpha = 1, 2, \ldots). \tag{30}$$

The above equation gives the scattered field in any region, V_α, outside of the scattering target in terms of the incident field and dielectric permittivity inside the target. In the next section, we shall invert this equation to obtain the dielectric permittivity, S, inside the target in terms of the scattered field outside the target.

We shall summarize the scattering approach described in this section. One first divides the target into a number of cells, say, N cells. Then one calculates the incident field at the center of each cell and constructs a N-dimensional vector, $f_o^{(1)}$ (of which each element may still be a 3-dimensional vector, such as an electric field). One also constructs a N x N diagonal matrix, S, of which each diagonal element is given by the average value of the dielectric permittivity, ϵ, in each cell of the target. Then one calculates integrals $(G_o)_{i,j} = \int G(\mathbf{x}_i, \mathbf{x}') d\mathbf{x}'$, with $\mathbf{x}_i$ being the center of the cell τ_i and integrating $\mathbf{x}'$ over the cell τ_j; both τ_i and τ_j are inside the target. Thus one constructs the N x N square matrix, G_o, with matrix elements being the integrals $(G_o)_{i,j}$. Finally, to obtain the scattered field anywhere outside the target, say, in a region V_α, one divides the region into N cells and calculates the integrals $(G_\alpha)_{i,j} = \int G(\mathbf{x}_i, \mathbf{x}') d\mathbf{x}'$, with $\mathbf{x}_i$ being the center of the cell τ_i in V_α and integrating $\mathbf{x}'$ over the cell τ_j inside the target region, V_o. One thus constructs the N x N square matrix, G_α, with matrix elements being the integrals $(G_\alpha)_{i,j}$. The scattered fields inside V_α can then be obtained from eq. (30), with the ith element of the vector $f_\alpha^{(s)}$ representing the scattered field in the cell τ_i of V_α.

Finally, we present results of the integrals $(G_o)_{i,j}$ and $(G_\alpha)_{i,j}$ in analytic forms. We consider the case where the field of interest is the electric field, then $G(\mathbf{x}, \mathbf{x}')$ is given by eq. (14). The expressions for the integrals in eqs. (25) and (26) are then:

$$i = j: \quad (G_o)_{i,j} \text{ or } (G_\alpha)_{i,j} = \bar{I} \left[1 + \frac{2}{3} \cdot a^2 \cdot \frac{d}{da} \left(\frac{\exp(ik_m a)}{a} \right)\right] \tag{31}$$

$$i \neq j: \quad (G_o)_{i,j} \text{ or } (G_\alpha)_{i,j} = a \cdot \frac{\exp(ik_m |\mathbf{x}_i - \mathbf{x}_j|)}{|\mathbf{x}_i - \mathbf{x}_j|} \cdot \left[\cos(k_m a) - \frac{1}{k_m a} \cdot \sin(k_m a)\right]$$
$$\cdot \left[\bar{I} \left(1 - \frac{1}{ik_m |\mathbf{x}_i - \mathbf{x}_j|} + \frac{1}{(ik_m |\mathbf{x}_i - \mathbf{x}_j|)^2}\right) \right.$$
$$\left. - \frac{\mathbf{x}_i - \mathbf{x}_j}{|\mathbf{x}_i - \mathbf{x}_j|} \frac{\mathbf{x}_i - \mathbf{x}_j}{|\mathbf{x}_i - \mathbf{x}_j|} \left(1 - \frac{1}{ik_m |\mathbf{x}_i - \mathbf{x}_j|} + \frac{1}{(ik_m |\mathbf{x}_i - \mathbf{x}_j|)^2}\right) \right] \tag{32}$$

where we have assumed that each cell is of equal volume, and that the volume of the cells are small and may be approximated by a sphere of radius a. Note that the expressions for $(G_o)_{i,j}$ and for $(G_\alpha)_{i,j}$ are of the same form; the only difference is the value of $\mathbf{x}_i$: for G_o, $\mathbf{x}_i$ is inside the scattering target, whereas for G_α, $\mathbf{x}_i$ is outside the target; for both, $\mathbf{x}_j$ is inside the target. With the above expressions for $(G_o)_{i,j}$ and $(G_\alpha)_{i,j}$, eqs. (29) and (30) provide a formula for the scattered field anywhere, inside or outside of the scattering target. Previously, complete formula for scattered fields has been developed only for two-dimensional targets.[9,10] Formula for evaluating fields inside arbitrary three-dimensional dielectric bodies has been derived,[11,12] but it has been found that the numerical solutions tend to diverge with respect to the subdivision of cells.[13] Most recently, a testing procedure was developed to analyze the numerical stability and reduce the computation time.[14] However, all these approaches approximated the field inside the scatterer by a linear combination of some basis functions and then numerically solved the linear coefficients. This is the first time a complete formula is developed for the vector scattered fields from an arbitrary three-dimensional target.

Inverse scattering - Green's function approach

The scattering formulation presented in the last two sections provides a method to calculate the scattered field of an arbitrary target. In this section, we shall show that the result of the formulation may be inverted to provide a method to evaluate the dielectric permittivity distribution of an arbitrary target.

Consider eq. (30). If the incident field $f_o^{(i)}$ is changed, say, by changing the direction of the incident wave, then the resulting scattered field will be changed accordingly. Two incident fields with different incident directions are linearly independent. So, if the target is divided into N cells, we may produce N linearly independent vectors, $\{f_{o1}^{(i)}, f_{o2}^{(i)}, \ldots, f_{oN}^{(i)}\}$, each of which corresponds to an incident wave vector k_j ($j = 1, 2, \ldots, N$), and thereby construct a non-singular N x N square matrix $F_o^{(i)}$, the incident matrix:

$$F_o^{(i)} = [f_{o1}^{(i)}, f_{o2}^{(i)}, \ldots, f_{oN}^{(i)}] = \begin{bmatrix} f_{o11} & f_{o12} & f_{o13} & \cdots & f_{o1N} \\ f_{o21} & f_{o22} & f_{o23} & \cdots & f_{o2N} \\ f_{o31} & f_{o32} & f_{o33} & \cdots & f_{o3N} \\ \cdot & \cdot & \cdot & & \cdot \\ \cdot & \cdot & \cdot & & \cdot \\ \cdot & \cdot & \cdot & & \cdot \\ f_{oN1} & f_{oN2} & f_{oN3} & \cdots & f_{oNN} \end{bmatrix}^{i} \tag{33}$$

So, if the incident waves $f_{oj}^{(i)}$ are the plane waves $\exp(ik_j \cdot x)$, then the matrix elements of the incident matrix $F_o^{(i)}$ are:

$$(F_o^{(i)})_{ij} = \exp(ik_j \cdot x_i) \tag{34}$$

where x_i is the center of the ith cell.

The dielectric profile of the target will be obtained from the measurements of the scattered fields by inverting eq. (30). The measurements of the scattered fields may be made in any region outside the target, say, in the region V, which may be one of the V_α's defined at the beginning of the last section. Since V_o is divided into N cells, we also divide V into N cells and measure the scattered field at the center of each cell for each incident field. Denoting by $f_j^{(s)}$ the N-dimensional vector that represents the scattered fields in the N cells for the jth incident wave, we then construct a N x N scattered matrix, $F^{(s)}$:

$$F^{(s)} = [f_1^{(s)}, f_2^{(s)}, \ldots, f_N^{(s)}] = \begin{bmatrix} f_{11} & f_{12} & f_{13} & \cdots & f_{1N} \\ f_{21} & f_{22} & f_{23} & \cdots & f_{2N} \\ f_{31} & f_{32} & f_{33} & \cdots & f_{3N} \\ \cdot & \cdot & \cdot & & \cdot \\ \cdot & \cdot & \cdot & & \cdot \\ \cdot & \cdot & \cdot & & \cdot \\ f_{N1} & f_{N2} & f_{N3} & \cdots & f_{NN} \end{bmatrix}^{s} \tag{35}$$

With the N incident waves and the N scattered waves lined up as two N x N square matrices, eq. (30) gives:

$$F^{(s)} = G(S^{-1} - G_o)^{-1} F_o^{(i)} \tag{36}$$

where we have dropped the subscript α in the matrix G since no reference was made to any particular V_α for sampling the scattered field. In the above equation, each column of the matrix $F^{(s)}$ represents the scattered wave due to an incident wave represented by the corresponding column in $F_o^{(i)}$. Each element in a column of $F^{(s)}$ represents the scattered field at a cell in V, whereas each element in a column of $F_o^{(i)}$ represents the incident field of the corresponding cell inside the target V_o. Since $F_o^{(i)}$ is a non-singular matrix, we may invert it and bring eq. (36) to the following form:

$$F^{(s)}(F_o^{(i)})^{-1} = G(S^{-1} - G_o)^{-1} \tag{37}$$

which then gives

$$S^{-1} = G_o + F_o^{(i)}(F^{(s)})^{-1} G. \tag{38}$$

Eq. (38) is the final result of this inverse scattering approach; the inverse of each diagonal element of the matrix on the left hand side gives the negative relative excess dielectric permittivity, $-(\epsilon - \epsilon_m)/\epsilon_m$, in the corresponding cell of the target.

The inverse scattering approach may be summarized below. One first divides the target into a number of cells, say, N cells. Then one produces N incident fields, all of which have the same amplitude and frequency, but each has a different incident direction. For each incident field, one calculates the incident field at the center of each cell inside the target region and constructs a N-dimensional vector, $f_o^{(i)}$ (of which each element is a 3-dimensional electric field vector). Lining up all incident vectors for the incident waves as column vectors, one then forms a N x N square matrix, $F_o^{(i)}$, referred to as the incident matrix. Also, for each incident field, one measures the scattered field in each cell in any region V, which is outside the target; the measurement region, V, and its division into N

cells must be unchanged for all incident fields. The scattered matrix, $F^{(s)}$, may then be constructed from the measurement of the scattered fields, in the same way as the incident matrix $F_o^{(i)}$ was constructed from the incident fields. Then one calculates the integrals $(G_o)_{i,j} = \int G(\mathbf{x}_i,\mathbf{x}')d\mathbf{x}'$ given by eqs. (31) and (32), with $\mathbf{x}_i$ being the center of the cell τ_i inside the target and integrating $\mathbf{x}'$ over the cell τ_j, also inside the target. Thus one constructs the N x N square matrix, G_o, referred to as the target Green's matrix, with matrix elements being the integrals $(G_o)_{i,j}$. Similarly, one calculates the integrals $(G)_{i,j} = \int G(\mathbf{x}_i,\mathbf{x}')d\mathbf{x}'$ from eqs. (31) and (32), with $\mathbf{x}_i$ being the center of the cell τ_i in the measurement region, V, and integrating $\mathbf{x}'$ over the cell τ_j inside the target region, V_o. One thus constructs the N x N square matrix, G, referred to as the cross Green's matrix, with matrix elements being the integrals $(G)_{i,j}$. Finally, one substitutes these matrices into eq. (38) and calculates the matrix S^{-1}. Ideally, the result will be a diagonal matrix, of which the negative of the inverse of each diagonal element is the relative excess dielectric permittivity, $(\epsilon-\epsilon_m)/\epsilon_m$, in the corresponding cell of the target divided by the background dielectric constant, as described by eq. (18).

Conclusion

We have developed a three-dimensional scattering formulation from which one may calculate the scattered vector field anywhere outside the scattering target; the scattering target may be of arbitrary three-dimensional shape with arbitrary dielectric profile. We also developed an inverse scattering formulation by inverting the scattering equation. The inverse scattering formulation provides a formula to calculate the three-dimensional dielectric permittivity inside the scattering target from measured data of the scattered field in a chosen region outside the target. There are two crucial aspects that enable our formulation. One is the dissipativity of the background medium that makes the scattering problem invertible and provides the uniqueness of the inverse solution. Another is the conversion of the integral equation into matrix equation by digitizing the space. The dissipativity aspect is the theoretical basis of the formulation, whereas the space digitizing provides practical support. Though the formulation provides a neat equation for inverse scattering calculation, two practical problems still require further investigation. One is the stability of the matrix inversion of the scattered matrix $F^{(s)}$, which is defined in eq. (35). Another is the size of the matrices that are involved in the inverse scattering formula, viz., the number of cells into which the target is divided. We shall discuss these two problems in the following paragraphs.

On the stability of matrix inversion, the question is: How stable is the inverse of $F^{(s)}$ if there is an error in $F^{(s)}$? This subject may be investigated by analyzing the so called condition number of the matrix $F^{(s)}$, which is a measure of singularity of the matrix.[16] The singularity of a matrix may be reduced by eliminating symmetry of the matrix, viz., eliminating the interdependency between the columns or the rows. Each column of the scattered matrix, $F^{(s)}$, corresponds to an incident wave while each row corresponds to a cell in the scattering region, V. Note that, for all incident waves, the region V and its subdivision of cells remain the same. One way to increase asymmetry of the matrix is to select the incident directions in a random fashion, such as using three-dimensional directions with unequal angular spacings. Similarly, random division of the scattered region into the N cells may also increase asymmetry. The latter means that random placement of the elements of the receiving antenna array is better than symmetric placement.

As to the size of the matrices, it is limited by two conditions. One is the desired resolution, and another is the approximation that we used to digitize the original integral equation. The first limitation is a subjective one which needs not be remarked. As to the second limitation, recall that in deriving eq. (16), it was assumed that the values of the total field and the dielectric permittivity inside each cell in the target region do not vary much. For the field to remain constant inside each cell, the cell must be smaller than a quarter wavelength inside the target. For a 3 GHz incident wave, the wavelength inside a typical biological target is about 12 mm, so the dimension of each cell must be smaller than 3 mm. This will require an enormous computation task for a typical biological target of, say, 30 cm in size. One way to reduce the size of the matrices is to use a lower frequency source. Using a 1 GHz source will reduce the size of the matrix by a factor of 27, and thereby reduce the number of matrix elements by a factor of 729. Another approach is to divide the target into several regions for image reconstruction by shielding the microwave radiation to allow only limited exposure. Theoretically, a division into 2 regions reduces the matrix elements of each region by a factor of 4, thereby a net gain of 2 in computation reduction. However, from the engineering point of view, limiting the exposure requires additional technical consideration on inter-regional interference.

Acknowledgement

This work was supported in part by the Walter Reed Army Institute of Research through the Office of Naval Research under the Contract N00014-85-K-0475.

Notations

A	The 4-dimensional electromagnetic potential $(\phi, \mathbf{A})$.
$\mathbf{A}$	The 3-dimensional vector potential.
c	The speed of light in vacuum.
$\mathbf{E}$	The electric field.
$F^{(s)}$	The N x N square matrix constructed from the column vectors $[f_1^{(s)}, f_2^{(s)}, \ldots, f_N^{(s)}]$, where $f_j^{(s)}$ represents the measured scattered field, in any region V outside of the target, due to the jth incident field (see $f_{oj}^{(i)}$ and $f_j^{(s)}$ below.)
$F_o^{(i)}$	The N x N square matrix constructed from the column vectors $[f_{o1}^{(i)}, f_{o2}^{(i)}, \ldots, f_{oN}^{(i)}]$.
f	Any total field, i.e., an incident and its scattered fields $f^{(i)}+f^{(s)}$.
$f^{(i)}$	The incident field.
$f^{(s)}$	The scattered field.
f_j	The value of f in the jth cell.
$f_j^{(i)}$	The value of $f^{(i)}$ in the jth cell.
$f_j^{(s)}$	The value of $f^{(s)}$ in the jth cell. In some occasions the subscript j refers to the jth incident direction (see $f_{oj}^{(i)}$ below), then $f_j^{(s)}$ represents the N-dimensional column vector derived from measurements of the corresponding scattered field in any region V outside of the target which is divided into N cells for data sampling.
f_o	The N-dimensional vector representing the sampling of the total field in V_o.
$f_o^{(i)}$	The N-dimensional vector representing the sampling of the incident field in V_o.
$f_o^{(s)}$	The N-dimensional vector representing the sampling of the scattered field in V_o.
$f_{oj}^{(i)}$	The N-dimensional column vector f_o for the jth incident direction; incident fields are sampled for a total of N different cases ($j = 1, 2, \ldots N$), each with a different incident direction but otherwise same target setup.
f_α	The N-dimensional vector representing the sampling of the total field in V_α.
$f_\alpha^{(i)}$	The N-dimensional vector representing the sampling of the incident field in V_α.
$f_\alpha^{(s)}$	The N-dimensional vector representing the sampling of the scattered field in V_α.
G	The Green's matrix with matrix elements defined as $\int G_m(\mathbf{x}_i, \mathbf{x}')d\mathbf{x}'$ with $\mathbf{x}_i$ being the center of the cell τ_i and $d\mathbf{x}'$ integrated over the cell τ_j.
G_{ij}	The matrix element of G, defined as $\int G_m(\mathbf{x}_i, \mathbf{x}')d\mathbf{x}'$ with $\mathbf{x}_i$ being the center of the cell τ_i and $d\mathbf{x}'$ integrated over the cell τ_j.
G_m	Green's operator of M_m ($G_m M_m = M_m G_m = 1$ in the space of outgoing scattering fields.
G_m'	Another expression of G_m based on a different factorization of the product $G_m'S' = G_m S$.
$G_m(\mathbf{x}, \mathbf{x}')$	The Green's function of M_m, viz, G_m in the $\mathbf{x}$-representation.
$G_m'(\mathbf{x}, \mathbf{x}')$	The Green's function of M_m', viz, G_m' in the $\mathbf{x}$-representation.
G_o	The N x N square submatrix of G with the matrix elements G_{ij}, where both i and j refer to cells in V_o.
G_α	($\alpha = 1, 2, \ldots$) The N x N square submatrix of G with the matrix elements G_{ij}, where i refers to the cell τ_i in V_α and j refers to cell τ_j in V_o.
$\mathbf{k}_m$	The wave vector in the background medium.
$\mathbf{k}_j$	The jth incident wave vector in the background medium ($\lvert\mathbf{k}_j\rvert = \lvert\mathbf{k}_m\rvert$); if the target is divided into N cells, then N scattering waves are used, each with a different incident direction.
M	Maxwell operator with background medium and scattering target.
M_m	Maxwell operator in a homogeneous background medium.
M_m'	Another expression of M_m based on a different factorization of the product $G_m'S' = G_m S$, where G_m' and G_m are inverse of M_m' and M_m, respectively, in the subspace of all outgoing scattered waves.
N	Total number of cells into which the target, or a region outside of the target, is divided for data sampling.
S	Scattering part of M ($-S = M - M_m$); it depends on ϵ and μ. For the case where f is the electric field $\mathbf{E}$, then $S = -[\epsilon(\mathbf{x})-\epsilon_m]/\epsilon_m$.
S'	Another expression of S based on a different factorization of the product $G_m'S' = G_m S$.
S_j	Negative of the relative excess value of ϵ in the target with respect to the background medium, $-[\epsilon(\mathbf{x}_j)-\epsilon_m]/\epsilon_m$. It is the value of S in the jth cell for the case where f is the electric field $\mathbf{E}$.
$\mathbf{x}$	A three-dimensional vector representing a point in space.
$\mathbf{x}_j$	The vector representing the center of the jth cell.
V_o	The region occupied by the target; also represents its volume. V_o is divided into N cells for data sampling.
V_α	($\alpha = 1, 2, \ldots$) A region outside of the target in which the scattered field is sampled. V_α is divided into N cells for data sampling.
ϵ	A function of $\mathbf{x}$ representing the distribution of dielectric permittivity in space.
ϵ_m	Dielectric permittivity of the homogeneous background medium.
ϕ	The electric scalar potential.
μ	A function of $\mathbf{x}$ representing the distribution of magnetic permeability in space.

μ_m Magnetic permeability of the homogeneous background medium.
τ_j The jth cell in V_o or V_α; also represents its volume.

References

1. Guo, T. C., Guo, W. W., and Larsen, L. E., "Microwave Imagery of Biological Objects - An Inverse Scattering Approach," Proceedings of the Eighth International Symposium on Infrared and Millimeter Waves, December 1983, Florida, IEEE Publication 83CH1917-4. 1983.

2. Guo, T. C., Guo, W. W., and Larsen, L. E., "Recent Development in Microwave Medical Imagery - Phase and Amplitude Conjugations and the Inverse Scattering Theorem," in Medical Applications of Microwave Imaging, ed. L. E. Larsen and J. H. Jacobi, pp. 167-183, IEEE Press. 1986.

3. Larsen, L. E., and Jacobi, J. H., eds., Medical Applications of Microwave Imaging, IEEE Press 1986.

4. Bolomey, Ch., Izadnegahdar, A., Jofre, L., Pichot, Ch., Peronnet, G., and Solaimani, M., "Microwave diffraction tomography for biomedical applications," IEEE Trans. Microwave Theory Tech., Vol. MTT-30, pp. 1998-2000. 1982.

5. Schwan, H. P., "Radiation biology, medical applications, and radiation hazards," Microwave Power Engineering, Vol. 2, ed. E. C. Okress, pp. 215-232, Academic Press 1968.

6. Larsen, L. E., Jacobi, J. H., Guo, W. W., Guo, T. C., and Kak, A. C., "Microwave Imaging Systems for Medical Diagnostic Applications," Proceedings of the Sixth Annual Conference of IEEE Engineering in Medicine and Biology Society - Frontiers of Engineering and Computing in Health Care, pp. 532-539, ed. John L. Semmlow and Walter Welkowitz, Los Angeles, September 1984, IEEE Publication 84CH2058-6. 1984.

7. Guo, T. C., Guo, W. W., and Larsen, L. E. "A Local Field Study of a Water-Immersed Microwave Antenna Array for Medical Imaging and Therapy," IEEE Transactions on Microwave Theory and Techniques, Vol. MTT-32, pp. 844-854. 1984.

8. Jackson, J., Classical Electrodynamics, John Wiley and Sons, New York. 1962.

9. Richmond, J. H., "Scattering by a Dielectric Cylinder of Arbitrary Cross-Section," IEEE Transactions on Antennas and Propagation, Vol. AP-13, pp. 334-341. 1965.

10. Richmond, J. H., "TE-Wave Scattering by a Dielectric Cylinder of Arbitrary Cross Section Shape," IEEE Transactions on Antennas and Propagation, Vol. AP-14, pp. 460-464. 1966.

11. Harrington, R. H., Field Computations by Moments Methods, McGraw-Hill, New York, 1968.

12. Livesay, D. E., and Chen, K.-M., "Electromagnetic Fields Induced Inside Arbitrarily Shaped Biological Bodies," IEEE Trans. Microwave Theory Tech. Vol. MTT-22, pp. 1273-1280. 1974.

13. Massoudi, H., Durney, C. H., and Iskander, M. F., "Limitations of the Cubical Block Model of Men in Calculating SAR Distributions," IEEE Trans. Microwave Theory Tech., Vol. MTT-32, pp. 746-752. 1984.

14. Tsai, C. T., Massoudi, H., Durney, C. H., and Iskander, M. F., "A Procedure for Calculating Fields Inside Arbitrarily Shaped, Inhomogeneous Dielectric Bodies Using Linear Basis Functions with the Moment Method," IEEE Trans. Microwave Theory Tech., Vol. MTT-34, pp. 1131-1139. 1986.

15. Forsythe, G. E., Malcolm, M. A., and Moler, C. D., Computer Methods for Mathematical Computation, p. 41, Printice-Hall 1977.

APPENDIX F

International Journal of Infrared and Millimeter Waves, Vol. 6, No. 6, 1985

MICROWAVE INDUCED THERMOELASTIC PROCESS IN DIELECTRICS-THEORY AND EXPERIMENTS

Theodore C. Guo and Wendy W. Guo

Department of Physics, The Catholic University of America
Washington, D.C. 20064

and

Lawrence E. Larsen

Walter Reed Army Institute of Research
Washington, DC 20012

Received March 5, 1985

ABSTRACT

Theoretical and experimental studies on microwave pulse induced pressure waves are reported. A thermodynamical formulation of microwave interaction with dielectrics is summarized. It is shown that acoustic waves may be generated by pulsed microwaves even in the absence of inhomogeneity of microwave absorption, owing to discontinuities of thermodynamical variables and microwave exposure conditions across the dielectric interface. The formulation is applied to a spherical system and some numerical results are presented. Experimental results include measurement of pressure waves in a cylinder filled with an aqueous solution of electrolytes exposed to pulsed microwaves and estimation of the coupling efficiency between the liquid dielectric and the adjacent air. Pressure scaling with energy per pulse is aiso demonstrated.

INTRODUCTION

Previous derivations of the thermoelastic mechanism induced by microwave pulses in dielectrics were based on the linear elastic equation with an external excitation derived from the thermal expansion that was produced by an inhomogeneous absorption of microwave energy [1]. This approach did not consider the proper balance of the distribution of the absorbed microwave energy among the internal thermal energies and the bulk kinetic energy,

0195-9271/85/0600-0405$04.50

and thereby failed to define all thermal coefficients adequately. Furthermore, all analyses have been limited to either isolated systems or completely constrained systems, both of which exclude the possibility of coupling to the external medium.

To correct these deficiencies, we have approached the subject from thermodynamical considerations and established a thorough formulation of the macroscopic electromagnetic interactions in dielectrics [2]. Couplings across dielectric interfaces are included through discontinuities of the thermodynamical variables and conditions of microwave exposure. Results of these couplings may provide a method for experimental evaluation of the microwave generated pressure waves in small dielectric objects for which direct measurement is difficult. In this paper, the theoretical formulation is briefly summarized. It is then applied to a spherical water-air system and some dynamical data are thereby calculated. Failure of the linear approach under high peak power exposures is predicted.

These results have important implications for biosystems exposed to pulsed fields. For example, ocular lenses exposured to pulse modulated microwave fields exhibit histopathological changes which are quantitatively and qualitatively different from CW exposures of equal average power [3]. A leading mechanism of cellular injury which may be invoked by pulse modulation is thermoelastic transduction. A microwave pulse, upon absorption in water dominated dielectrics, produces a transient pressure wave. This transduction does not neccessarily depend upon microwave gradients within the dielectric [2]. The transduced pressure wave then propagates within the dielectric on the basis of mechanical (elastic) impedance subject to mechanical and thermodynamical boundary conditions. In order to investigate the role of such pressure waves, a series of experiments have been performed to study the effect of pulse parameters as well as temperature. A central theme in these studies is the role of energy per pulse as related to peak pressures induced by thermoelastic transductions.

Pressure measurements were made in saline filled vessels which maintain the geometric section and material properties of the chamber in which earlier ocular lens exposures took place [4]. In addition, measurements were also made in vessels of similar geometric section but different material properties. Pressure measurements were made outside of the waveguide where exposures took place. Pressure measurements were made both in the saline medium and in the air at the air/liquid interface, in order to investigate the coupling efficiency between the medium in which the transduction takes place (saline) and the adjacent non-

absorbing medium (air). Theoretical calculations for a one-dimensional case comparable to the vessel geometry have been published previously [2].

THE NON-LINEAR WAVE EQUATIONS

The objective is to derive the governing equations for the thermodynamical and mechanical variables, which include mass density ρ, stress tensor $\vec{p}$, thermodynamic internal energy U_I, bulk kinetic energy U_k, bulk velocity $\mathbf{v}$, temperature T, and microwave specific absorption rate (SAR) P. Since the details of the formulation have been published earlier [2], here we just give a brief summary. The time domain of our concern is the acoustic relaxation time, which, as we shall show, is of the order of milliseconds. We assume that this is much greater than the microwave pulse width, which in turn is much greater than the period of the microwave carrier and the time to reach a local equilibrium. We also assume that, as it will be verified later, the acoustic relaxation time is in general much smaller than the relaxation time to reach a thermal steady-state by heat conduction. Based on these assumptions, we shall ignore heat conduction, heat transfer by convective flow, and any dependency of U_I on electric polarization. To reduce complexity, we shall also ignore the internal energy associated with the anisotropicity of the strain tensor. It can then be shown that the thermoacoustic effect may essentially be derived from the laws of the conservation of mass, the conservation of momentum, the conservation of energy, and the thermodynamic equation of state:

$$d_t \rho + \rho \nabla \cdot \mathbf{v} = 0 \tag{1}$$

$$\rho d_t v_i + \partial_j p_{ij} = 0 \tag{2}$$

$$P_{ij} \partial_j v_i + \rho d_t U_I = \rho P \tag{3}$$

$$d_t U_I = \left[-C_p / (\rho \beta_p) + (1/\rho^2) p_{ij} \partial_j v_i / \nabla \cdot \mathbf{v} \right] d_t \rho + (C_v / \beta_p)(\kappa_T)_{ij} \, d_t p_{ij} \tag{4}$$

where $d_t \equiv \partial_t + \mathbf{v} \cdot \nabla$ is the convective derivative, C_v and C_p are the specific heat (per mass) at constant volume and constant pressure, respectively, β_p is the isobaric thermal expansion coefficient, and κ_T the isothermal compressibility. The last equation, which may be substituted by another thermodynamic equation of state, is derived from the general expression $U_I = U(\rho, \vec{p})$ by using the Jacobian method of relating one partial derivative to another and applying the first law of thermodynamics.

By mutual substitution among equations (1) through (4), one may obtain the wave equations for any of the thermodynamic quantities. In particular, if the strain tensor $\partial_i u_j$ is isotropic, one obtains the following wave equation for the stress tensor:

$$\partial_t[(\rho_o/\rho)^{1/3}(C_v/C_p)(\kappa_T)_{ij}\partial_t p_{ij}] - \partial_i[(\rho/\rho_o)^{1/3}(1/\rho)\partial_j p_{ij}] = \partial_t[(\rho_o/\rho)^{1/3}(\beta_p/C_p)P] \quad (5)$$

Similar wave equations for the mass density ρ or the velocity v may also be obtained. These equations must be supported by the respective boundary conditions, which are implicated in eqs. (1)–(3). All boundary conditions may be obtained by integrating each term of these equations across a thin layer of the boundary interface and applying the generalized Stoke's theorem. However, since the boundary surface is not stationary, one must first transform these equations to the Lagrangian specification to obtain the boundary conditions [2]. The wave equations and boundary conditions are greatly simplied in the one dimensional case. Note that in the one-dimensional case, the factor $(\rho_o/\rho)^{\pm 1/3}$ in eq.(5) is replaced by $(\rho_o/\rho)^{\pm 1}$. For our calculations later, we list the result for the pressure and the bulk velocity:

$$[\partial_x \frac{1}{\rho_o}\partial_x - \partial_t(\frac{\rho_o C_v \kappa_T}{\rho C_p})\partial_t]p(x,t) = -\partial_t(\frac{\rho_o \beta_p}{\rho C_p} P) \quad (6)$$

with the boundary conditions that

$$p(x,t) \quad \text{and} \quad \rho_o^{-1}\partial_x p(x,t)$$

are continuous across the dielectric interface, and,

$$[\partial_x(\frac{\rho C_p}{\rho_o C_v \kappa_T})\partial_x - \rho_o \partial_t^2]v(x,t) = \partial_x(\frac{\beta_p}{C_v \kappa_T} P) \quad (7)$$

with the boundary conditions that

$$v(x,t) \quad \text{and} \quad (\rho C_p \partial_x v - \rho_o \beta_p P)/(\rho_o C_v \kappa_T)$$

are continuous across the interface.

These wave equations show that acoustic waves are generated either by an inhomogeneity or temporal variation of the product of the microwave SAR and some thermodynamical variables.

LINEAR APPROXIMATION IN A SPHERICAL MODEL

To illustrate the implications of the wave equations and their respective boundary conditions, we consider a dielectric sphere of radius a surrounded by air at 1 atmospheric pressure. A square pulse of microwave of duration τ and amplitude P_0 is incident upon the sphere. The sphere is assumed to be small so that the microwave absorption exhibits no spatial variation. In the linear approximation eq. (5) gives, for the pressure waves in the frequency domain:

$$p_1(r,\omega) = -i\left(\frac{c^2\rho\beta_p}{C_p}\right)_1 \frac{P(\omega)}{\omega - i0} \times \left\{ \frac{j_0(k_1 r)}{j_0(k_1 a) - \tan\phi \dfrac{h_0(k_2 a)}{h_0'(k_2 a)}\, j_0'(k_1 a)} - 1 \right\} \tag{8}$$

and

$$p_2(r,\omega) = -i\left(\frac{c^2\rho\beta_p}{C_p}\right)_1 \frac{P(\omega)}{\omega - i0} \frac{h_0(k_2 r)}{h_0(k_2 a)} \times \left\{ \frac{j_0(k_1 a)}{j_0(k_1 a) - \tan\phi \dfrac{h_0(k_2 a)}{h_0'(k_2 a)}\, j_0'(k_1 a)} - 1 \right\} \tag{9}$$

where $j_n(x)$ and $h_n(x)$ are respectively the spherical Bessel and Hankel functions of the first kind of order n, the subscripts 1 and 2 label the dielectric and the air media, respectively; $c_{1,2}$ denotes the corresponding value of $\sqrt{C_p/(\rho C_v \kappa_T)}$ in either medium, which is the velocity of the acoustic wave in the medium, $\tan\phi = (\rho c)_2/(\rho c)_1$ is the ratio of the acoustic impedances of the air to the liquid, $k_{1,2} = \omega/c_{1,2}$ are the acoustic wavenumber in either medium, and $P(\omega)$ is the Fourier transform of the square pulse SAR, which is given by:

$$P(\omega) = -\sqrt{2\pi}\, P_0 \frac{1 - e^{i\omega\tau}}{2\pi i(\omega - i0)} \tag{10}$$

The factor $(\omega - i0)$ in the denominator represents a singularity at the origin immediately below the real axis of the complex ω-plane. Multiplying $p_{1,2}(r,\omega)$ by $e^{-i\omega t}$ and integrating over ω using the contour integration technique, eqs. (8) and (9) then give the pressure waves in the time domain:

$$p_1(r,t) = \sum_{n=0}^{\infty} -\sqrt{2\pi}\left(\frac{\rho\beta_p c^3}{C_p a}\right)_1 \frac{P(\omega_n)}{\omega_n} \exp(-i\omega_n t) \times \frac{(i - c_2/(\omega_n a))\, j_0(\omega_n r/c_1)/j_0(\omega_n a/c_1)}{(c_2/c_1 - \tan\phi)/(\omega_n a/c_1)^2 + \tan\phi\, \csc^2(\omega_n a/c_1)} \quad (11)$$

and

$$p_2(r,t) = \sum_{n=0}^{\infty} -\sqrt{2\pi}\left(\frac{\rho\beta_p c^3}{C_p a}\right)_1 \frac{P(\omega_n)}{\omega_n} \exp(-i\omega_n t) \times \frac{(i - c_2/(\omega_n a))\, h_0(\omega_n r/c_2)/h_0(\omega_n a/c_2)}{(c_2/c_1 - \tan\phi)/(\omega_n a/c_1)^2 + \tan\phi\, \csc^2(\omega_n a/c_1)} \quad (12)$$

where ω_n are the frequency eigenvalues which are given by the solutions of the equation

$$[1 - (\omega a/c_1)\cot(\omega a/c_1)]\tan\phi = c_2/c_1 - i(\omega a/c_1) \quad (13)$$

For a water–air system, $\tan\phi$ is about 3×10^{-4}, the above equation may then be solved by making the Taylor expansion for ω as a funcion of $\tan\phi$. One gets, to the first order in $\tan\phi$,

$$(n\neq 0) \quad \frac{\omega_n a}{c_1} = n\pi - \frac{(c_2/c_1)/(n\pi) + i}{1 + (c_2/c_1)^2/(n\pi)^2}\tan\phi$$

$$(n=0) \quad \frac{\omega_0 a}{c_1} = -i\left(\frac{c_2}{c_1} + \left(\frac{c_2}{c_1}\coth\frac{c_2}{c_1} - 1\right)\tan\phi\right) \quad (14)$$

which gives an acoustic relaxation time of $\tau = 1/\mathrm{Im}(\omega_1) = 11.2$ milliseconds for the fundamental mode in a water sphere with $2a = 1$ cm. This is much smaller than the time for the sphere to reach a thermal steady state by heat conduction, which is about 19.4 seconds [5]. Since the acoustic relaxation time is proportional to the radius a while the conductive relaxation time is proportional to a^2, the two relaxation times become closer as the size of the dielectric decreases, and they become equal when the radius is about 2.9 microns, beyond which thermal conduction becomes important.

To obtain the acoustic energy coupled to the air, one first calculates the solution for the velocity in the frequency domain,

which is given by $(-i/(\omega\rho))\nabla p_{1,2}(r,\omega)$:

$$v_1(r,\omega) = -\left(\frac{c\beta_p}{C_p}\right)_1 \frac{P(\omega)}{\omega - i0} \frac{j_0'(k_1 r)}{j_0(k_1 a) - \tan\phi \frac{h_0(k_2 a)}{h_0'(k_2 a)} j_0'(k_1 a)} \quad (15)$$

and

$$v_2(r,\omega) = -\left(\frac{c\beta_p}{C_p}\right)_1 \frac{P(\omega)}{\omega - i0} \frac{\frac{j_0'(k_1 a)}{h_0'(k_2 a)} h_0'(k_2 r)}{j_0(k_1 a) - \tan\phi \frac{h_0(k_2 a)}{h_0'(k_2 a)} j_0'(k_1 a)} \quad (16)$$

The total acoustic energy coupled into the air may be obtained by calculating the work done by the dielectric on the air at the interface. To the first order, the result is:

$$E_{air} = 4\pi a^2 p_0 \int_{-\infty}^{\infty} v_1(a,t)dt = 4\pi a^2 p_0 \sqrt{2\pi}\, v_1(a,\omega=0)$$

$$= \sqrt{2\pi}\, \frac{4\pi a^3}{3}\, p_0 \left(\frac{\beta_p}{C_p}\right)_1 P(\omega=0) \quad (17)$$

Comparing this to the total microwave absorption by the liquid, $E_{abs} = \sqrt{2\pi}(4\pi a^3/3)\rho_1 P(\omega=0)$, one obtains the coupling efficiency of the absorbed microwave energy to the acoustic energy in the air:

$$\eta_{air} = E_{air}/E_{abs} = p_0 \left(\frac{\beta_p}{\rho C_p}\right)_1 . \quad (18)$$

Take the dielectric to be water, so $\beta_p = 2.8 \times 10^{-4}\ ^{\circ}C^{-1}$ at 30 °C [6], $C_p = 4.186 \times 10^7$ erg/gm-°C, and $\rho = 1$ gm/cm^3. With the equilibrium pressure of the air, p_0, being 1 atm $= 1.01 \times 10^6$ dyne/cm^2, the coupling efficiency is then $\eta_{air} = 6.7 \times 10^{-6}$. This value, as we shall show in the next section, appears to agree with the results from pressure measurements.

PRESSURE MEASUREMENTS

Material and Methods

Pressure measurements were made in both air and saline media for two types of vessels placed in the WR 975 exposure system (cf. Fig. 1). The first vessel duplicated the cross section and material properties of the lens exposure chamber. That is, it was made of square quartz tubing ca. one inch on each side with a 1/8 inch wall thickness. The second vessel was circular in cross

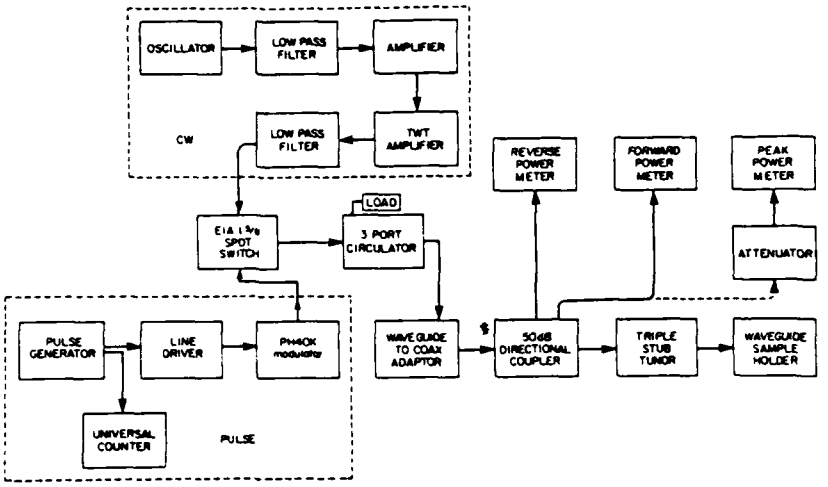

Fig. 1. Functional block diagram of the WR 975 exposure system.

section, one inch in outer diameter, 1/8 inch wall thickness, and made of acrylic plastic. Both were filled with phosphate buffered saline (PBS). These vessels were placed into the WR 975 via the same waveguide below cut-off window as the actual lenticular exposure chamber. The two vessels extended beyond the waveguide to provide a PBS column for coupling of the acoustic wave into regions where the hydrophone would not be subject to direct influence of the electromagnetic field. Each vessel was separately matched to the microwave source with the triple stub tuner. Typical return losses were ca. -15 to -20 dB for either vessel.

Pressure measurements made in the liquid were performed with the equipment illustrated in Fig. 2. The transducer was of Bruel and Kjaer manufacture, the type 8103 miniature hydrophone.

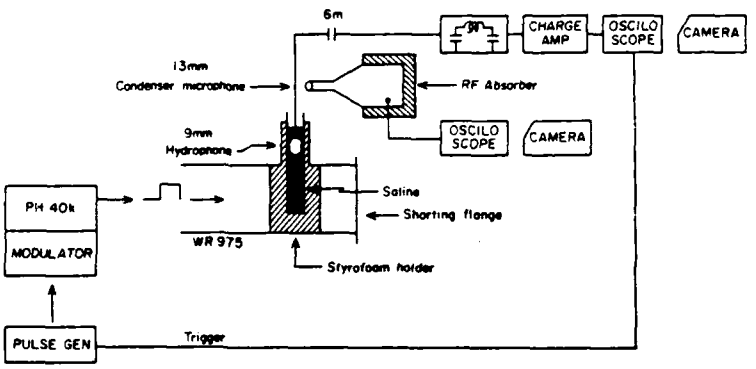

Fig. 2. Functional block diagram of the acoustic measurement system.

This transducer is of the piezoelectric type as shown in Fig. 3a. It is 9 mm in outer diameter with an integral waterproof connection to 6 meter of double shielded cable. The type 8103 has a 200 KHz bandwidth with a directivity response as shown in Fig. 3b. Since the hydrophone has serious lobing when used with axial incidence, an open mesh (ca 2 by 2 mm) fiberglass screen was loosely wrapped around the transducer to center it in the vessel's cross section. The hydrophone was calibrated with a B & K type 4223 hydrophone calibrator. All

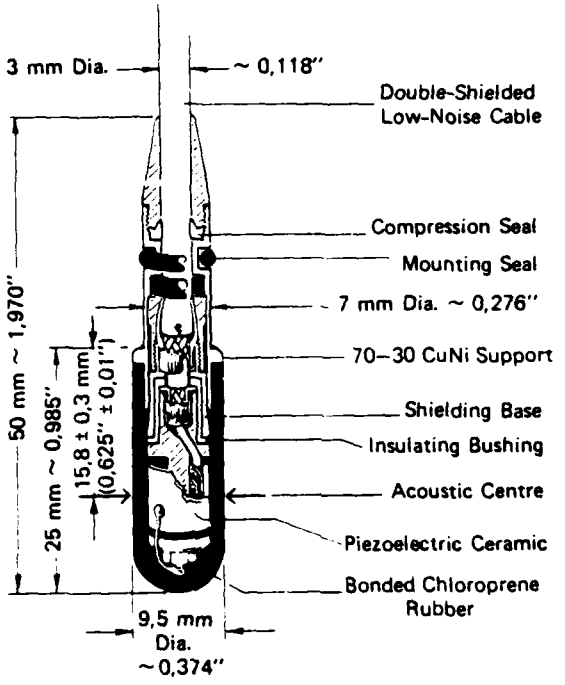

Fig. 3a. The hydrophone construction and dimensions.

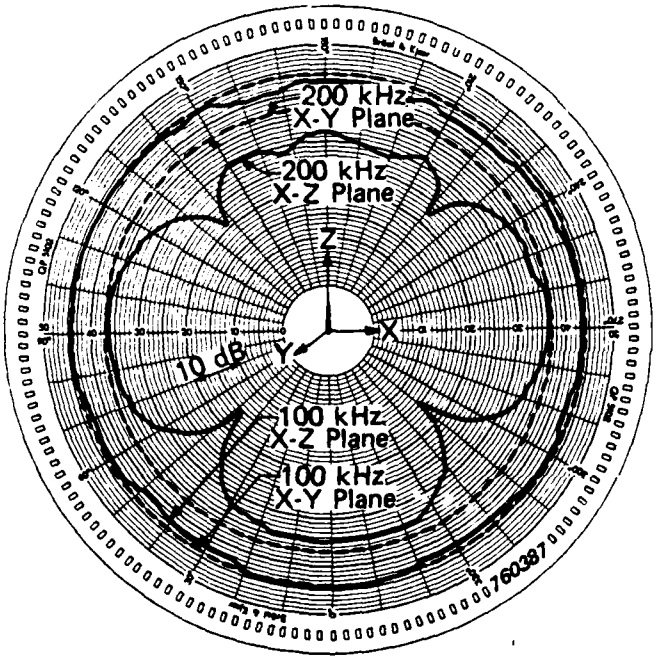

Fig. 3b. The axial and transverse patterns of the hydrophone.

water based measurements are expressed in dB relative to 0 dB = 1 micro Pascal. The hydrophone was interfaced to a charge amplifier also of B & K manufacture, the type 2650. This instrument allows insertion of the hydrophone calibration factor into the signal conditioning network just prior to the output amplifier. When used in the charge mode, the 2650 input amplifier is bypassed and the first stage becomes a band-pass filter. Prior to the 2650, the hydrophone cable was terminated by an Erie low pass filter with 30 dB rejection at 1 GHz. Hydrophone wave-forms were recorded by means of a Hewlett Packard 1740 osciloscope connected to the output of the B & K 2650. Photographs were made with a Hewlett Packard 197B osciloscope camera and Polaroid type 107 film. The photographic exposure duration was one second, thereby each photograph contains a total of 5 pulses superimposed.

Pressure measurements in air were made with a Bruel and Kjaer sound pressure level (SPL) meter, the type 2230. The microphone was a 0.5 inch condenser type of B & K manufacture, the type 4155. The SPL meter and microphone were shielded from direct influence of the electromagnetic field and ambient noise by a 1 m^3 enclosure of microwave absorber Eccosorb[1] EC-77. This combination was calibrated with a microphone calibrator the B & K type 4230 for an average SPL of 1 Pascal. All air based pressure measurements are made in dB relative to 0 dB = 20 micro Pascal. The 2230 must be used with the detector in the peak responding mode with display of the maximum value using broadband (lin) frequency response and fast time weighting. Electrical analogs of the pressure wave-forms are available from the 2.5 mm AC out minijack on the side of 2230. Waveform display and recording was performed using the same system described for the hydrophone measurements. Under these conditions, the rise time of the system is ca 30 microseconds.

The microwave pulse waveform (see Fig. 4) was measured from the forward power arm of the Dielectric Communications WR 975 directional coupler by means of a Hewlett-Packard directional detector HP type 423A. All RF pulses were monitored for rise time (ca 0.5 microseconds) and stated pulse widths are RF pulse widths rather than video pulse widths, i.e., the video rise time is excluded. The standard RF pulse was 10 microseconds in duration with a peak transmitted power of 10 KW at 918 MHz. This produced an energy density of ca 326 micro Joules/cm^2.

---

[1] Registered trademark, Emerson & Cumming, Canton, MA.

Fig. 4. A detected microwave pulse is shown with 5 μsec per horizontal division. The negative detector (HP type 423A) produces a downward pulse.

Both air and PBS pressure measurements were tested for direct electromagnetic field effects. In the case of air measurement this was accomplished by recording the SPL with blockage of the microphone air path by ca 20 dB with foam rubber. Also the SPL meter body was covered with EC-77. In the case of the PBS based measurements, the hydrophone transducer was removed from the PBS column with all other factors left constant, thus blocking the water path by ca 60 dB.

Results

The pressure measurements recorded with the hydrophone are shown in Fig. 5 as a function of position in the vessel. The peak

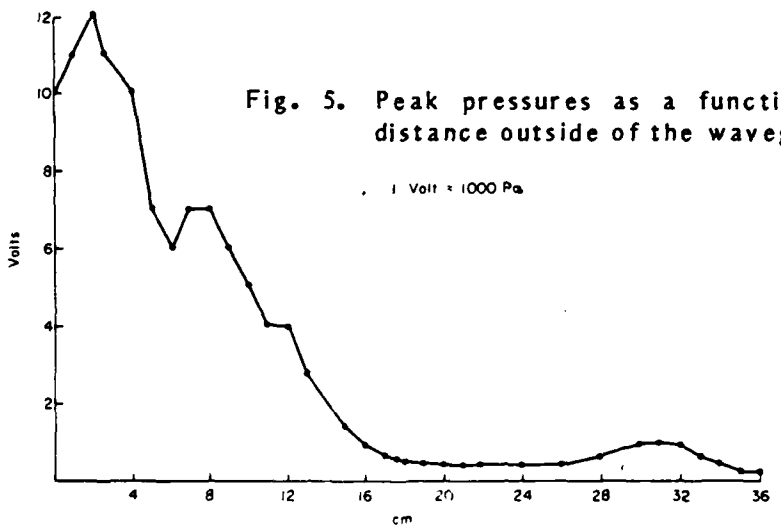

Fig. 5. Peak pressures as a function of distance outside of the waveguide.

pressures recorded were independent of the vessel material composition for equal net energy absorbed per unit volume of liquid. Note that no pressure measurements were made inside the wave guide. The pressure maximum (exclusive of the wave guide interior) was at a distance of about 1 cm up from the flange of the wave guide below cut-off window. At this location the pressure had a peak value of ca 10 kilopascals. The peak pressure declined nonmonotonically with distance to about 1 kilopascal at the air/water interface.

The pressure waveform recorded with the acoustical measurement system is shown in Fig. 6. The pressure wave rise time in the PBS is estimated in Fig. 7 to be ca 30 microseconds. This particular figure shows the pressure rise time for the 20 microsecond RF pulse, but that for the 10 microsecond RF pulse was substantially identical (probably due to the rise time limitations of the modulator and hydrophone systems). The pressure fall time to the abcissa is ca 30 milliseconds. This is followed by a slow (ca 50 milliseconds) pressure wave undershoot of modest amplitude before returning to the baseline.

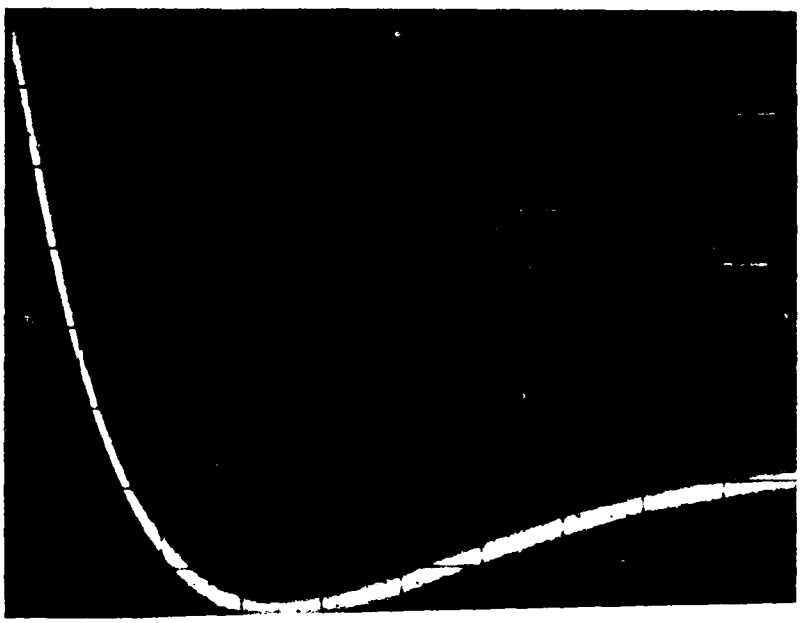

Fig. 6. The pressure waveform is shown above with 100 pascals per vertical division and 20 msec per horizontal division.

Pressure scaling with energy per pulse is demonstrated for the standard pulse and doubling the energy per pulse by doubling the pulse width from 10 to 20 microseconds (see Fig. 8). Similarly,

Fig. 7. The rise time of the pressure pulse in water. The vertical axis is 200 Pascals per division and the horizontal axis is 20 μsec per division.

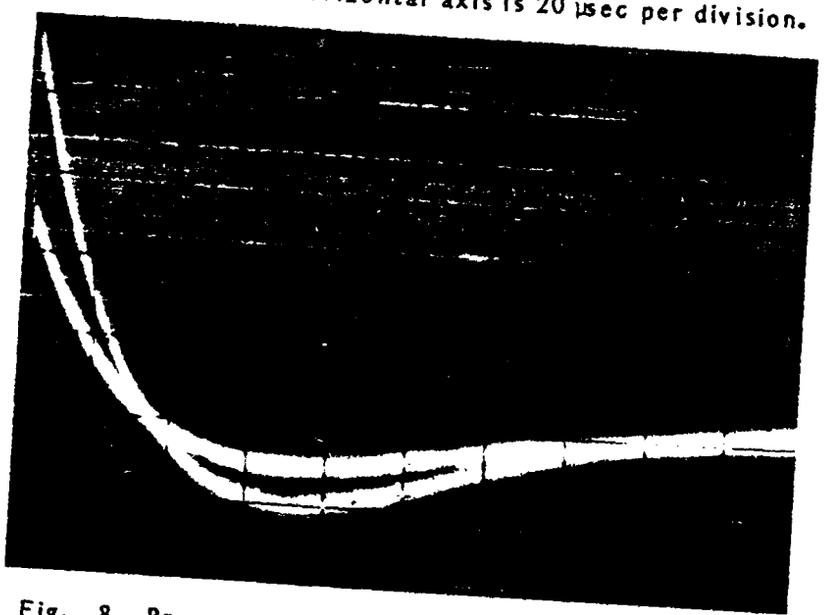

Fig. 8. Pressure scaling with energy/RF-pulse is shown for the case of doubling the RF pulse width from 10 to 20 μsec. The lower trace is 322 $\mu J/cm^2$ and the upper trace is 645 $\mu J/cm^2$. The vertical axis is 200 Pascals/division and the horizontal axis is 20 msec/division.

linear scaling of the peak pressure is demonstrated in Fig. 9 for doubling the energy per pulse by doubling the peak power leaving the pulse width constant at 10 microseconds. Such pressure scaling is consistent with the observation of increased histopathological damage with increased energy per pulse for fixed average power and total absorbed energy [7].

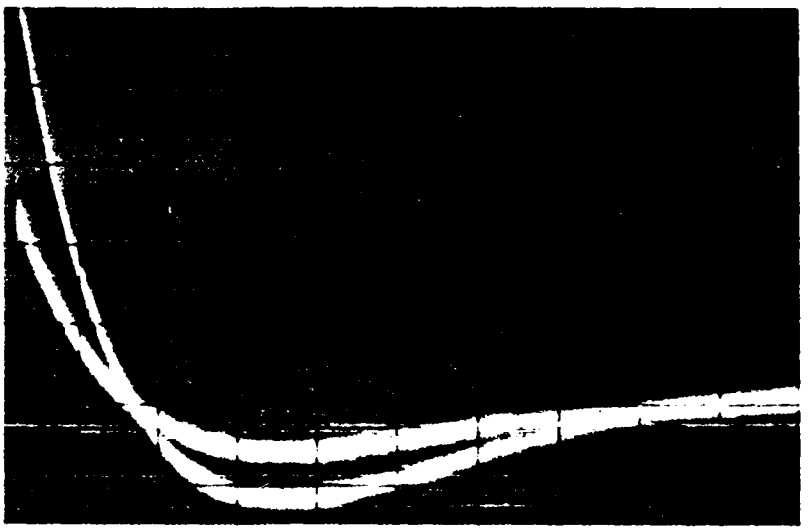

Fig. 9. Pressure scaling with energy per RF-pulse is shown for the case of doubling the peak power transmision from 10KW to 20KW. The axes and energy densities are those shown for Fig. 8.

The air pulse is shown in Fig. 10. The displayed maximum SPL in air was 90.4 dB, with standard deviation 2.26 dB. This suggests a ca 64 dB coupling factor from liquid pressure to air pressure across the interface. This confirms the predicted coupling efficiency presented earlier in this report. The rise time appears to be ca 5 microseconds (also probably limited by the SPL meter's band width) and a fall time of .5 milliseconds.

Fig. 10. The pressure pulse in the air, with 500 μsec per horizontal division and 0.2 volt per vertical division.

REMARKS AND DISCUSSIONS

We have shown that acoustic waves are generated if there is any spatial discontinuity in the dielectric medium, or temporal discontinuity in the microwave absorption. Coupling of the acoustic energy from an absorbing medium to a nonabsorbing medium has been formulated through the thermodynamic equations and the boundary conditions. The result may be useful for the evaluation of the pressure waves inside small biological objects by measuring the pressure waves or other thermodynamical quantities in the surrounding medium.

The result of the linear approximation indicates that the percentage of the absorbed microwave energy being coupled to a non-absorbing medium is proportional to the pressure in the nonabsorbing medium and, apart from that, is independent of its other thermodynamic properties. It is also independent of the microwave pulse width, so that total acoustic energy coupled to the air is proportional to the total microwave absorption cross section. The predicted value of 6.7×10^{-6} for the coupling efficiency (cf. eq. (18)) is exactly the same as the value derived previously for the one-dimensional case [2], which appears to agree with the experimental result of the pressure measurements described in the last section. Indeed, comparing eqs. (17) and (18) to the corresponding equations for the one-dimensional case, we arrive at the conclusion that the coupling efficiency is independent of the geometry of the system.

The formulation indicates that the microwave induced thermoacoustic effect is in general nonlinear. At low radiation density, one may make the linear approximation by ignoring all second and higher order terms. The validity of the linear approximation can be evaluated by calculating the generated pressure wave and comparing it to the initial equilibrium value. Taking an optimal pulse width of $\tau = \pi/\omega_0$, the amplitude for $p_1(r,t)$ in eq.(11) corresponding to the fundamental frequency component is equal to $(2a/\pi)(c\beta_p/C_p)_1 P_0$. Using the values of β_p and C_p for 30 °C as cited below eq. (18) and assuming 1 cm diameter of a water sphere surrounded by air of 1 atm pressure, a peak SAR of $P_0 = 30$ kW/gm results in a pressure wave of amplitude equal to 0.1 bar in the water, which is 10% of the initial equilibrium pressure. This fraction of variation in pressure will also result in at least equal fraction of error in the linear approximation. For the one dimensional case [2] with 4 cm length of water, which may be used to approximate the dielectric vessel described in the previous section, the same pressure amplitude is generated with a peak SAR of 3 kW/gm. The above estimate is based only on the fundamental

harmonic. Eq. (11) (as well as eq. 52 of ref. 2) shows that the pressure amplitudes of the higher harmonics are approximately inversely proportional to the frequency, so the sum does not converge rapidly. Therefore the total pressure amplitude could be much greater than that estimated with the fundamental harmonic alone. This is indeed evidenced by the pressure measurements described in the preceding section.

The experimental portion of this work is subject to some limitations which merit discussion. The first of these is the fact that no measurements were made inside of the waveguide. The reason for this exclusion was to reduce artifact due to direct electromagnetic coupling. The consequence, however, is that we have no measurement of pressure at the location where the ocular lens specimen was placed. We presume that pressures at that location may be higher than those recorded outside of the waveguide. Also the acoustic mode distribution in the vessel is complex as judged by the nonmonotonic pressure attneuation with increasing axial distance, and as evidenced by the marked pressure gradients in the transverse plane of the vessel. Work is presently in progress to develop a subminiature hydrophone based upon optical transduction mechanisms which will be free of direct electromagnetic influence. This probe will be used not only inside the waveguide, but also in vivo for direct pressure measurements.

Another instrumental limitation of importance is the bandwidth of the transducers. This imposes a lower limit in the pressure wave rise time estimates. Nevertheless, the recorded pressure rise time in PBS of 30 microseconds is remarkably fast when compared to pressure rise times in physiologic situations. It is also very fast compared to more common overpressure situations due to air conducted impulsive noise or blast effects. Of course, air conducted impulse noise is poorly coupled to internal organs such as the ocular lens where no air path exists (this stands in contrast to the situation of the so-called hollow viscus or air filled space such as the lungs.) We speculate that the pressure rise time may play a role in cellular damage that is separable from the peak pressure. This factor may not be examined in the present series of experiments since the exposure system is a power oscillator with fixed rise time of ca 0.5 microseconds.

The relationship of this work to that of Olsen and Lin [8] must also be discussed. The pressure measurements reported in that paper were directed primarily at a determination of the acoustic modes of the head of various experimental animals, rather than absolute pressure and air coupling measurements as was the case in our work. This is evidenced by the fact that Olsen and Lin

made no attempt to locate a pressure maximum. In fact, coupling was intentionally minimized to reduce artifact. Furthermore, no cognizance was taken of the spatial response pattern of the piezoelectric disk transducer or its directivity with respect to presumed acoustic generator centers. Nevertheless, a calibration curve was provided along with the transducer output signals. The calibration curve is somewhat difficult to interpret due to axis mislabeling, but if we assume that sensitivities (decibels referenced to one volt per micropascal) to be preceded by a negative sign, and that opposite label is Pascals per millivolt, then the pressure traces may be quantified. For example, the trace for rat 2 in figure five (ref. 8) demonstrates a peak of about 200 Pascals. Since Olsen and Lin used the same pulse width but ca 3.3 times lower peak power, their result would scale to ca 650 Pascals (neglecting the probable underestimation of a pressure peak). Our results show a peak of ca 1 kilopascal towards the distal end of the tube and much higher values as the flange of the waveguide below cut-off window is approached (cf. Fig. 5 of this paper). Based on the differences in geometry and the artifact problem, the measurements of Olsen and Lin are broadly consistent with ours, save those near the window flange. The measurements reported here, although confirming the coupling between the absorbing (saline) and nonabsorbing (air) media, can not be compared to our theoretical predictions in the case of the very high pressure values recorded near the window flange. On one hand this may be due to the fact that our numerical estimate is derived from only the contribution of the fundamental harmonic. On the other hand, until independent confirmation of these high values can be made with another transducer of better intrinsic decoupling from the incident field, the highest values must remain suspect.

The theory and experimental results presented here may represent the microwave analog of photoacoustic spectroscopy [9]. Some earlier works with microwave (X band) sources for electron paramagnetic resonance were reported by Diebold and McFadden [10]. They made neither measurements of coupling efficiency nor pressure measurements in the liquid phase. Also, the Rosencwaig-Gersho theory [9] appears to be derived from White [11] wherein the thermoacoustic elastic transduction process is assumed to derive from spatial inhomogeneity of microwave specific absorption rate.

ACKNOWLEDGEMENT

This work was supported in part by the Walter Reed Army Institute of Research through U.S. Army Medical R&D Command under the U.S. Naval Sea Systems Command Contract N00024-83-C-5301 to the Johns Hopkins University Applied Physics Laboratory.

REFERENCES

[1] J. C. Lin, Microwave Auditory Effects and Applications. Springfield, IL: C. C. Thomas, 1978.

[2] T. C. Guo, W. W. Guo, and L. E. Larsen, IEEE Trans. MTT-**32**, 835 (1984).

[3] P. J. Stewart-DeHaan, M. O. Creighton, L. E. Larsen, J. H. Jacobi, W. M. Ross, and J. R. Trevithick, 1980 IEEE MTT-S Int'l Microwave Symp. Digest, 341 (1980).

[4] P. J. Stewart-DeHaan, M. O. Creighton, L. E. Larsen, J. H. Jacobi, W. M. Ross, M. Sanwal, T. C. Guo, W. W. Guo, and J. R. Trevithick, Exp. Eye Res. **36**, 75 (1983).

[5] K. R. Foster et al, IEEE Trans. MTT-**30**, 1158 (1982).

[6] R. A. Horne, Water and Aqueous Solutions, p. 387, New York: Wiley-Interscience, 1974.

[7] L. E. Larsen, M. O. Creighton, M. Sanwal, and J. R. Trevithick, "A Comparative Study of Pulse and CW Microwave Exposures of the Murine Ocular Lens in Vitro," in preparation.

[8] R. G. Olsen and J. C. Lin, IEEE Trans. BME-**30**, 289 (1983).

[9] A. Rosencwaig, Photoacoustics and Photoacoustic Spectroscopy (Sections 8.5 and 9.2), Chemical Analysis Vol. 57, ed. P. J. Elving and J. D. Winefordner, John Wiley & Sons, New York, 1980.

[10] G. Diebold and D. L. McFadden, Appl. Phys. Lett. **29**, 447 (1976).

[11] R. M. White, J. Appl. Phys. **34**, 3559 (1963); also see reference 9, Section 9.6.

APPENDIX E

RECENT DEVELOPMENTS IN MICROWAVE MEDICAL IMAGERY—PHASE AND AMPLITUDE CONJUGATIONS AND THE INVERSE SCATTERING THEOREM

Theodore C. Guo, Wendy W. Guo, and Lawrence E. Larsen

Reprinted from Medical Applications of Microwave Imaging, IEEE PRESS, 1986

Recent Developments in Microwave Medical Imagery—Phase and Amplitude Conjugations and the Inverse Scattering Theorem

Theodore C. Guo,* Wendy W. Guo,* and Lawrence E. Larsen†

A theoretical analysis of the local field of microwave lattice radiation source and an inverse scattering theorem are presented. The results are applied to a water-immersed microwave array system for medical imaging. It is shown that, using a technique of phase and amplitude conjugations, a satisfactory three-dimensional focusing for a target located in the neighborhood of the array may be achieved. The focusing resolutions for transverse and longitudinal directions are approximately $\lambda/2$ and λ, respectively, where λ is the wavelength in the dielectric. By increasing the element spacing of the array, the resolutions can be as good as 5.3 mm and 11.7 mm, respectively, at the operating frequency of 3 GHz. Combining the technique of phase and amplitude conjugations with the inverse scattering theorem, the array will be able to provide a three-dimensional imaging system with satisfactory resolution.

I. INTRODUCTION

The use of imagery methods for microwave dosimetric analysis has many advantages. Chief among these are the non-invasive nature of the data collection and the ease with which imagery as a form of data display can be related to the medical traditions of anatomy and pathology. In fact, a considerable literature is being developed on the subject of medical applications of microwave technology in, e.g., the cardiovascular system as described elsewhere in this volume by Lin [1]–[13]. Nevertheless, medical imagery with microwave radiation faces a number of technical and theoretical problems. Historically, the most prominent technical problem has been the dilemma cast by the contradictory requirements of resolution and propagation loss with respect to the choice of the frequency of operation. When imagery is formed by sampling the scattered fields in air, system operation at frequencies below ca. 10 GHz produces unacceptably low spatial resolution whereas higher frequencies of operation impose excessive propagation loss [14]. Simultaneously, the use of air coupling in system design introduces two additional undesirable features: multipath contamination from propagation paths exterior to the target, including lateral or Beverage wave propagation at the air-dielectric interface [15]; and poor power transfer between the target and the antennas used for data collection [16]. These problems are solved by operation of the antennas in a medium of high permittivity and loss tangent comparable to the biologic target under study. The medium of choice is water since it provides a resolution enhancement by wave length contraction of nearly a factor of 9 at 3 GHz [3] while simultaneously the impedance match is improved and reflection is reduced in comparison to air coupling. Water coupled arrays offer all the advantages of water coupled elements plus the enormous increase in data collection speed made possible by electronic scanning and focusing. Additional discussion is presented in a companion paper by Foti *et al* elsewhere in this volume.

In spite of these operational advantages, water coupling introduces its own complications. The worst of these is the fact that the antennas must be placed in close proximity to the subject to reduce coupling losses. Thus, the antennas must operate within their reactive or local zone. This is especially troublesome in the case of array antennas since Fresnel or Fraunhofer diffraction theory cannot be used to effectively focus or stear the array. We address this problem in terms of a new method for array focusing which accommodates not only local-zone operation with 3-dimensional focus control, but also element-to-element variation in network parameters. This method is based on a phase-amplitude conjugation of fields sampled by the array when illuminated by a half-space omnidirectional radiator.

The major theoretical problem in medical application of microwave imagery is recovery of resolution in the direction of propagation for forward scattering (bistatic) based systems. In medical imagery from radiologic disciplines, this is known as the tomography problem; in microwave and

* Department of Physics, The Catholic University of America, Washington, D.C. 20064.
† Department of Microwave Research, Walter Reed Army Institute of Research, Washington, D.C. 20012.

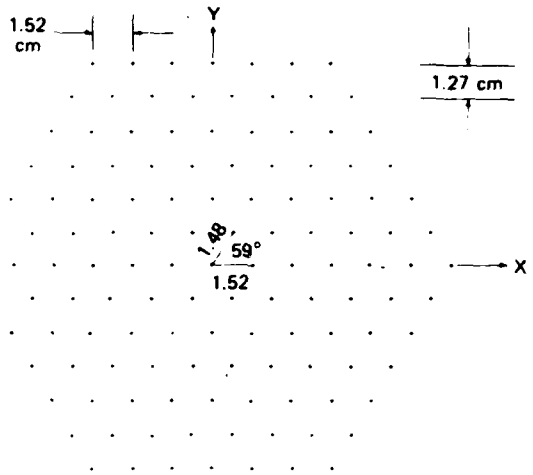

Fig. 1a. Lattice structure of the planar array of 127 elements.

electromagnetic propagation disciplines, this is the inverse scattering problem. A brief review of the inverse scattering problem and its historical solutions is presented elsewhere in this volume by Boerner and Chan. We express the problem chiefly in terms of axial resolution since usable resolution is obtainable in the transverse plane for isolated organs. Obviously, operation *in vivo* would require solution of the inverse scattering problem in any case. We present a new inverse scattering theorem which may be considered as a generalization of the Lorentz reciprocity theorem to the case of lossy media [19]–[21]. It is applied to forward scattered fields in combination with the phase-amplitude conjugation in a model data collection system which simulates the DART (Dosimetric Analysis by Radiofrequency Tomography) Mark 4 system under development at the Walter Reed Army Institute of Research [2], [3], [6]–[8], [12]–[13].

The next section provides a brief description of the DART system. It is followed by a theoretical analysis of the local field of the receiving array in Section 3. Section 4 introduces the topic of phase-amplitude conjugation and the application to three-dimensional focusing. Section 5 presents the new inverse scattering theorem and its use in combination with the phase-amplitude conjugation method for image reconstruction. The proof of the new inverse scattering theorem is given in Section 6 and concluding remarks appear in Section 7.

2. DESCRIPTION OF THE SYSTEM

The system is composed of two antenna arrays, one for transmission and another for reception, submerged in a cylindrical water container of about 3 feet in diameter and 3 feet high. Both antenna arrays are of hexagonal shape. The elements are placed in a brick-staggered arrangement, corresponding to a planar lattice with one lattice vector at 59° from another and 0.97 times the length (Fig. 1a). The receiving array is composed of 127 elements whereas the transmitting array contains 151 elements. Each element is a short, water-filled waveguide. The cross section, 4 mm × 7 mm, is that of a degenerate ellipse (see Fig. 1b). The feed structure consists of waveguide-to-coaxial adapter with an insulated end feed which is shorted to the broad wall of the waveguide as shown in Fig. 1c. This element differs from the one described by Foti *et al* (elsewhere in this volume) in that it is more amenable to series production in a monobloc array by numerically controlled milling machines. It is designed for fixed tuning (VSWR ≤ 1.5) over a 1GHz band centered on 3GHz.

At an axial distance of 5 cm or farther, the underwater field pattern of each element in the forward direction is similar to that of a dipole. Both transmitting and receiving antennas are mounted in adjustable frames, facing each other for forward scattering imagery. The target is to be placed between the two antennas. The axial distance between the antennas and the target may be adjusted from as close as 5 cm to a distance of about 35 cm. Other engineering details on water coupled antennas for medical microwave imagery may be found in Ref. [3].

In order to compensate for the differences of the distance from each of the elements to the target, a method of phase and amplitude conjugations is used. That is, a factor which includes both phase and amplitude is applied to each element depending on its distance to each focal point [see Section 4, cf. Eq. (25)]. Instead of applying the conjugations to the transmitting array, which would require RF attenuators and phase shifters, the conjugations are applied to the receiving elements in the form of off-line data processing,

Fig. 1b. Subarray in a stainless steel monobloc

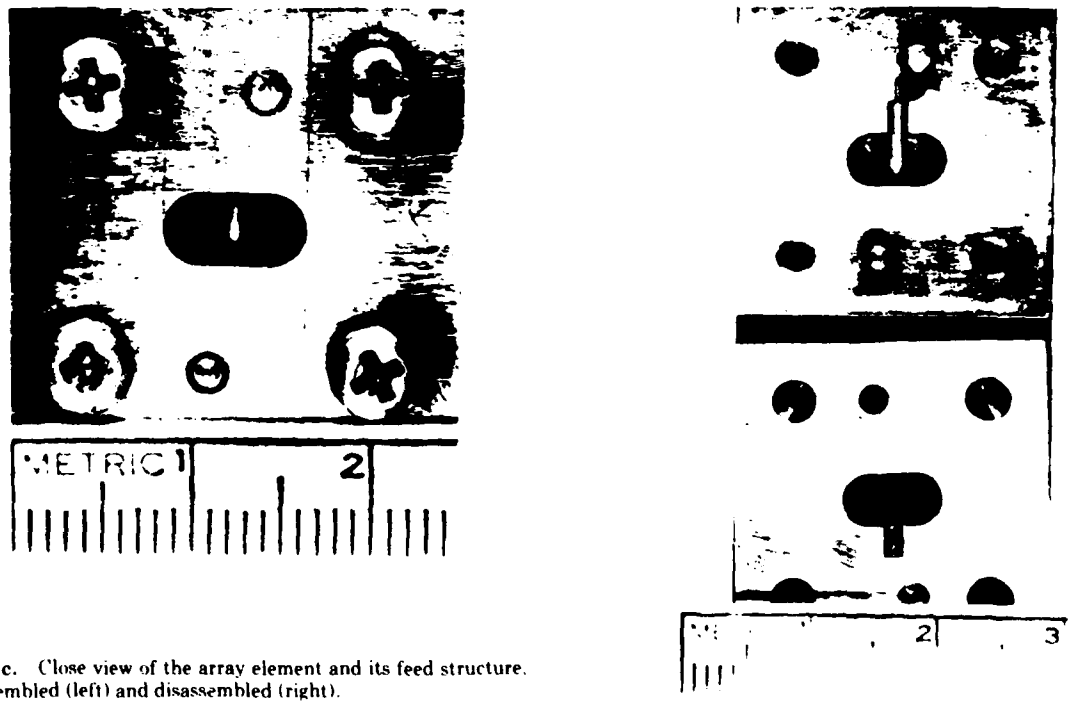

Fig. 1c. Close view of the array element and its feed structure, assembled (left) and disassembled (right).

i.e., by multiplying the received complex field amplitude for each element by a complex factor that corresponds to the conjugation of the phase and amplitude of the scattering parameter S_{21} [17] measured for each element illuminated by an omnidirectional source (this will be described in detail in Section 5). On the other hand, the phasing of the emitting array is designed to produce a near plane-wave. Alternatively, sequentially overlapping subarrays may be energized to provide illumination of selected areas of the target.

In order to describe the application of this technique to a water coupled microwave imaging system, a brief digression into the design of a multiplex receiver is necessary. The receiver consists of 127 open ended waveguide elements with 127 coax lines are routed to 23 6P1T diode switches in a 3-tier reverse corporate power divider network. This network provides the switching to connect each receiver array element to a harmonic converter. Two low noise amplifiers of 20 dB gain are inserted under operator selection prior to the harmonic converter to compensate for path losses through the coupling medium. The local oscillator for the harmonic converter is derived via a directional coupler from a digital synthesizer which serves as the signal source for the transmitting array. The RF port of the harmonic converter is attached to each element of the receiver array via the switch matrix. The IF port returns the down-converted receiver signal to a complex ratiometer which compares another sample of the transmitted signal with the IF signal from the receiver.

The amplitude and phase conjugation, therefore, includes not only element-to-element variations in the array geometry, but also path length and insertion loss variations in the switch matrix enroute to the harmonic converter. The complex ratiometer provides this measurement by estimating S_{21} for each element over the entire RF signal path from the source to the RF port of the harmonic converter.

The source used for the S_{21} measurement should ideally

Fig. 1d. A water-immersed lens antenna for receiver calibrations is shown. This derived the measured data for phase and amplitude conjugations to accomplish three-dimensional focusing.

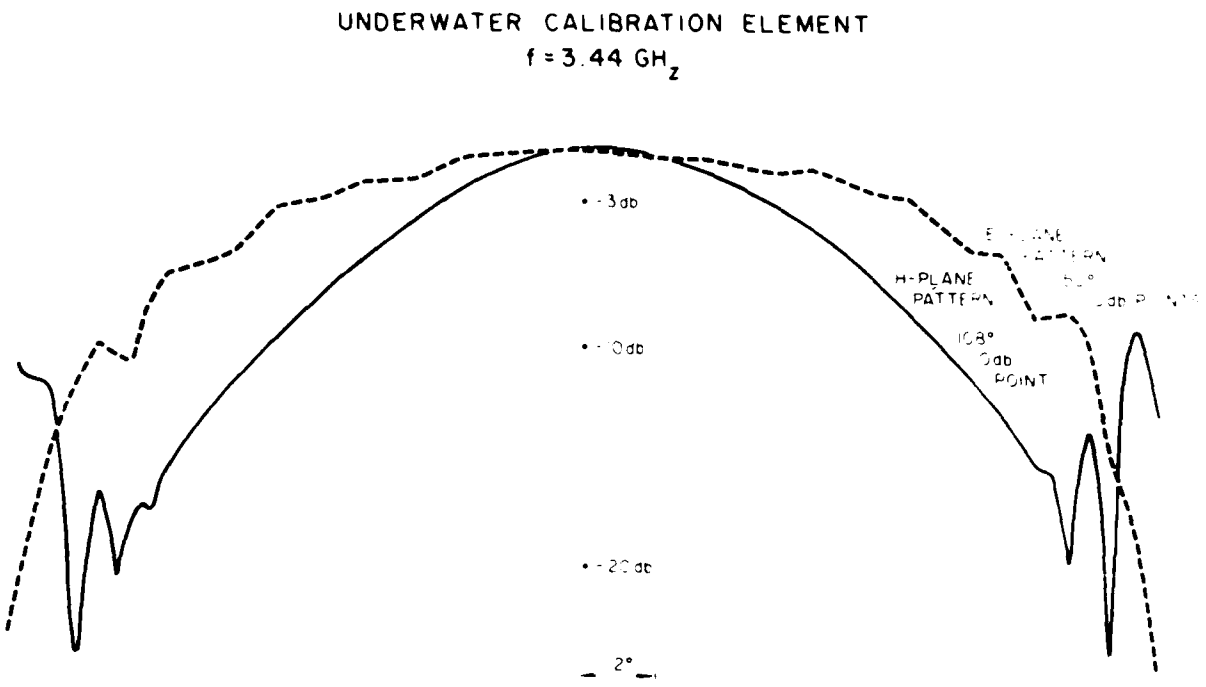

Fig. 1e. Pattern cuts from the dielectric lens calibration antenna.

consist of a 2π steradian omnidirectional radiator. One realization of such a calibration source is shown in. Fig. 1d. This design is based upon a dielectric lens. It provides a 3-dB beamwidth of 130° in azimuth and in elevation as shown in Fig. 1e. The measured amplitude for each element, inclusive of its path to the harmonic converter, for a given position of the calibration source provides the amplitude taper needed to compensate for path losses through the coupling medium and insertion losses in the switch matrix. That is, the needed amplitude taper is the inverse of the measured amplitude taper for that position of the calibration source. The needed phase taper to insure coherent addition at each position of the calibration source is the conjugate of the measured phase taper. All focal spot positions are provided by translation of the calibration source.

The calibration data set derived as described above is then applied to the S_{21} measurements in the presence of a target for each element for each focal point. In this way, the forward scattered fields are scanned by a sensitive volume element. The receiver array focusing takes place off-line. The array is focused only in the coupling medium, not in the target. The forward scattered fields from the target are differenced from the beam pattern of the illuminator recorded at the same plane in the absence of the target.

3. THE LOCAL FIELD ANALYSIS

In this section, the formula for the electromagnetic field in the neighborhood of a lattice radiation source is derived. The formula will be used to calculate the field pattern of the antenna array and the beam characteristics. The antenna array is treated as a localized distribution of charge and current in a lattice structure. The following three assumptions are made:

Assumption 1: If d_ℓ and d_t represent, respectively, the longitudinal and transverse dimensions of each array element with respect to the direction of the point of observation, and r_n the distance from the nth element to the observation point, it is assumed that, for every element, the following magnitude comparisons are valid:

$$r_n \gg d_\ell \text{ and } d_t,\ \lambda \gg d_\ell,\ \lambda \gg d_t^2/r_n \qquad (1)$$

where λ is the wave length of the microwave signal in water. Under this assumption, the field due to each radiating element may be approached by the dipole approximation.

Assumption 2: Mutual couplings between the radiating elements are included in the local field formula to the extent that the effect of all coupling is assumed to be identical in every element. In other words, the difference between the peripheral elements and the interior elements with regard to the effect of mutual coupling is assumed to be negligible.

Assumption 3: Mutual coupling between the radiating elements is linear with respect to the phase and amplitude of the power input to the elements. Measured mutual coupling using a Hewlett Packard 8542C Automated Network Ana

lyzer proved this assumption to be true and demonstrated that mutual coupling is less than −30 dB.

It is remarked that Assumption 1 is of a quantitative nature, in the sense that its degree of satisfaction depends on the degree of quantitative precision needed for the field pattern. Although the broad dimension of each array element is about half a wavelength in the coupling medium, it is the actual current distribution that determines the size of the source. Since the dominant mode (TE_{10}) of the electric field in the aperture with respect to boresight angle is known to be sinusoidal, the effective size of the current distribution is shorter than the broad dimension of the guide due to center weighting. Our calibration measurement shows that the field of each individual array element resembles that of a dipole, indicating that this assumption is valid for the system. It will be made clear where this assumption, as well as the other two assumptions, enter into the derivation, so that the percentage error of the derived quantities may be determined.

To derive the local field formula, consider a localized charge density, ρ, and current density, $\vec{J}$, distributed in a space region V. For an antenna in a free space, V indicates the space occupied by the antenna array, as well as its accessories. Without losing any generality, monochromatic time-variation is assumed, so that

$$\rho(\vec{x},t) = \rho(\vec{x})e^{-i\omega t}$$

and (2)

$$\vec{J}(\vec{x},t) = \vec{J}(\vec{x})e^{-i\omega t}.$$

Accordingly, all other field quantities resulting from ρ and $\vec{J}$ also vary with time monochromatically. Any other time-variation can always be obtained by superposition of monochromatic waves. From Maxwell's equation, the vector potential at any point outside of V is given by, in the Gaussian system of units [18],

$$\vec{A}(\vec{x}) = \int_V \frac{1}{c}\vec{J}(\vec{x}')\frac{\exp(ik|\vec{x}-\vec{x}'|)}{|\vec{x}-\vec{x}'|}\,d\vec{x}', \tag{3}$$

from which one obtains the magnetic induction $\vec{B}$ and electric field strength $\vec{E}$:

$$\vec{B}(\vec{x}) = \nabla \times \vec{A}(\vec{x}) \tag{4}$$

and

$$\vec{E}(\vec{x}) = \frac{1}{k}\nabla \times \vec{B}(\vec{x}), \tag{5}$$

where k is the magnitude of the wave vector in the medium. For water, k is a complex quantity $k_1 + ik_2$ where k_1 is equal to 2π times the inverse of the wave length and k_2 is the inverse of the distance over which the field is attenuated by a factor of e = 2.72 (equivalent to a power loss of 8.7 dB). At an operating frequency of 3 GHz in water, the values of k_1 and k_2 are

$$k_1 = 5.5\ \text{cm}^{-1} \text{ and } k_2 = 0.44\ \text{cm}^{-1}. \tag{6}$$

The current-charge volume, V, is divided into a number of subvolumes, each denoted by V_n, which represents the space occupied by the nth radiating element. Let $\vec{x}_n$ be the center of V_n and denote by $\vec{J}_n$ and ρ_n, respectively, the current density and the charge density in V_n with respect to its center, then

$$\vec{J}_n(\vec{x}) = \vec{J}(\vec{x} + \vec{x}_n) \text{ and } \rho_n(\vec{x}) = \rho(\vec{x} + \vec{x}_n). \tag{7}$$

Clearly, Equation 3 may also be written as:

$$\vec{A}(\vec{x}) = \sum_{n=1}^{N} \int_{V_n} \frac{1}{c}\vec{J}(\vec{x})\frac{\exp(ik|\vec{x}-\vec{x}'|)}{|\vec{x}-\vec{x}'|}\,d\vec{x}'. \tag{8}$$

Making the change of variable $\vec{x}' \to \vec{x}_n + \vec{x}'$, where the new $\vec{x}'$ is a vector from the center of each element to the volume $d\vec{x}'$, which is identical for every n and thus may simply be regarded as a vector in V_1, using Eq. 7, Eq. 8 becomes

$$\vec{A}(\vec{x}) = \sum_{n=1}^{N} \int_{V_1} \frac{1}{c}\vec{J}_n(\vec{x}')\frac{\exp ik|(\vec{x}-\vec{x}_n)-\vec{x}'|}{|(\vec{x}-\vec{x}_n)-\vec{x}'|}\,d\vec{x}'. \tag{9}$$

Note that each integral in the right hand side of Eq. 9 is the same as that in Eq. 3, except that $\vec{x}$ is replaced by $\vec{x} - \vec{x}_n$ and the space of integration is over only the center element, V_1, instead of the entire array, V. Therefore, even though the observation point is in the neighborhood of the array, as long as $|\vec{x} - \vec{x}_n| = r_n$ is much greater than the size of each array element, d, one may expand the integrand in Eq. 9 in powers of $\vec{x}'/r_n$ (note that $|\vec{x}'| \leq d$).

So, denote by $\vec{x}_\ell'$ and $\vec{x}_t'$, respectively, the longitudinal and transverse components of $\vec{x}'$, i.e., the projections of $\vec{x}'$ in the directions parallel and perpendicular to $\vec{x} - \vec{x}_n$, then

$$\vec{x}_\ell' = \frac{1}{r_n^2}[\vec{x}' \cdot (\vec{x} - \vec{x}_n)](\vec{x} - \vec{x}_n) \tag{10}$$

and

$$\vec{x}_t' = -\frac{1}{r_n^2}[\vec{x}' \times (\vec{x} - \vec{x}_n)] \times (\vec{x} - \vec{x}_n). \tag{11}$$

Define

$$x_\ell' = |\vec{x}_\ell'|,\ x_t' = |\vec{x}_t'|. \tag{12}$$

Then one has the identity

$$|\vec{x} - \vec{x}_n - \vec{x}'| = [(r_n - x_\ell')^2 + x_t'^2]^{1/2}$$

or (13)

$$|\vec{x} - \vec{x}_n - \vec{x}'| = r_n\left(1 - \frac{x_\ell'}{r_n}\right)\left[1 + \frac{(x_t'/r_n)^2}{(1 - x_\ell'/r_n)^2}\right]^{1/2}.$$

Under Assumption 1, x_t'/r_n and x_ℓ'/r_n are both small quantities. So expand $|\vec{x} - \vec{x}_n - \vec{x}'|$ and other functions of it in powers of x_ℓ'/r_n and x_t'/r_n, then the following series result:

$$k|\vec{x} - \vec{x}_n - \vec{x}'| = kr_n\left\{1 - \frac{x_\ell'}{r_n} + \frac{1}{2}\left(\frac{x_t'}{r_n}\right)^2 - \frac{1}{2}\left(\frac{x_\ell'}{r_n}\right)\left(\frac{x_t'}{r_n}\right)^2 + \left(\frac{x_t'}{r_n}\right)^2 \cdot O\left[\left(\frac{x_\ell'}{r_n}\right)^2, \left(\frac{x_t'}{r_n}\right)^2\right]\right\} \tag{14}$$

and

$$\frac{1}{|\vec{x} - \vec{x}_n - \vec{x}'|} = \frac{1}{r_n}\left\{1 + \frac{x_\ell'}{r_n} + \left(\frac{x_\ell'}{r_n}\right)^2 - \frac{1}{2}\left(\frac{x_t'}{r_n}\right)^2 + \left(\frac{x_\ell'}{r_n}\right) \cdot O\left[\left(\frac{x_\ell'}{r_n}\right)^2 \cdot \left(\frac{x_t'}{r_n}\right)^2\right] + O\left[\left(\frac{x_t'}{r_n}\right)^4\right]\right\}. \quad (15)$$

As to the factor $\exp(ik|\vec{x} - \vec{x}_n - \vec{x}'|)$, its expansion depends not only on the relative magnitude of r_n and d, but also on the magnitudes of kr_n and kd. If the real part of kd is small, which is valid under Assumption 1, then, except for the first term, every term on the right hand side of Eq. 14 is much smaller than 1. The exponential of the series then gives

$$\exp(ik|\vec{x} - \vec{x}_n - \vec{x}'|) = \exp(ikr_n)(1 - ikx_\ell' + \ldots). \quad (16)$$

Combining this expansion with Eq. 15, the integrand of Eq. 9 becomes

$$\frac{1}{c} J_n(\vec{x}') \frac{\exp(ik|\vec{x} - \vec{x}_n - \vec{x}'|)}{|\vec{x} - \vec{x}_n - \vec{x}'|} = \frac{1}{c}\frac{\exp(ikr_n)}{r_n} J_n(\vec{x}')\left\{1 + \frac{x_\ell'}{r_n} - ikx_\ell' + \ldots\right\}. \quad (17)$$

Substituting the leading term on the right hand side of Eq. 17 into Eq. 9, an approximation for the vector potential is obtained as

$$\vec{A}(\vec{x}) = \sum_{n=1}^{N} \frac{1}{c}\frac{\exp(ikr_n)}{r_n} \int_{V_1} \vec{J}_n(\vec{x}')d\vec{x}'. \quad (18)$$

It can be shown that the integral in the right hand side is proportional to the total dipole moment, $\vec{p}_n$, of the array element v_n:

$$\vec{p}_n = \frac{i}{ck}\int_{V_1} \vec{J}_n(\vec{x}')d\vec{x}' = \frac{i}{ck}\int_{V_n} J(\vec{x}')d\vec{x}', \quad (19)$$

where the dipole, $\vec{p}_n$, is defined as the moment of the charge distribution of the nth radiating element with respect to its center:

$$\vec{p}_n = \int_{V_1} \vec{x}'\rho(\vec{x}')d\vec{x}'. \quad (20)$$

Therefore, the vector potential may also be written as

$$\vec{A}(\vec{x}) = -ik \sum_{n=1}^{N} \vec{p}_n \frac{\exp(-ik|\vec{x} - \vec{x}_n|)}{|\vec{x} - \vec{x}_n|}. \quad (21)$$

which is the field due to N radiating dipoles.

Assumptions 2 and 3 are now applied to Eq. 21. Noting that all elements have the same geometry, the only factors that could contribute to different values of $\vec{p}_n$ for different elements are the input power and phase and the differences in the current-charge distributions due to mutual coupling. Under Assumption 2, the last factor is assumed to be negligible, and, under Assumption 3, $\vec{p}_n$ must be proportional to the input phase and amplitude factor. Therefore $\vec{p}I_nC_n$ may be substituted for $\vec{p}_n$ in Eq. 21, where $\vec{p}$ is the dipole moment for each radiating element at a certain standard input, I_n is the illumination factor for the nth element, and C_n is a complex factor representing the phase and amplitude conjugations. I_n is used as a controlling factor to modify the mainbeam shape. Equation 21 then becomes

$$\vec{A}(\vec{x}) = -ik\vec{p} \sum_{n=1}^{N} I_nC_n \frac{e^{ik|\vec{x} - \vec{x}_n|}}{|\vec{x} - \vec{x}_n|}. \quad (22)$$

The electric and magnetic fields may be obtained from the above equation by applying Eqs. 4 and 5 on $\vec{A}(\vec{x})$. Again applying Assumption 1, the results are

$$\vec{B}(\vec{x}) = -k^2\vec{p} \times \sum_{n=1}^{N} I_nC_n \frac{\vec{x} - \vec{x}_n}{|\vec{x} - \vec{x}_n|}\frac{\exp(ik|\vec{x} - \vec{x}_n|)}{|\vec{x} - \vec{x}_n|} \quad (23)$$

and

$$\vec{E}(\vec{x}) = -k^2 \sum_{n=1}^{N} I_nC_n \left(\vec{p} \times \frac{\vec{x} - \vec{x}_n}{|\vec{x} - \vec{x}_n|}\right) \times \frac{\vec{x} - \vec{x}_n}{|\vec{x} - \vec{x}_n|}\frac{\exp(ik|\vec{x} - \vec{x}_n|)}{|\vec{x} - \vec{x}_n|}. \quad (24)$$

The definition of the quantities in Equations 22 through 24 are summarized below:

- $\vec{A}$ = the vector potential, in the Gaussian system of units
- $\vec{B}$ = the magnetic induction, in the Gaussian system of units
- C_n = the complex number representing the phase and amplitude conjugation for the nth radiating element (see next section)
- $\vec{E}$ = the electric field intensity, in the Gaussian system of units
- I_n = the illumination factor for the nth element; this factor is used to control the beam shape (see next section)
- k = the complex number representing the magnitude of the wave vector of the radiation in water; the values of its real and imaginary parts for a 3 GHz radiation are given in Equation 6
- n = a subscript denoting the nth radiating element
- N = the total number of radiating elements in the array
- $\vec{p}$ = the dipole moment of each radiating element at a standard phase and amplitude input (i.e., for I_n and C_n being unity), in the Gaussian system of units
- $\vec{x}$ = the vector representing the observation point with respect to the center of the array
- $\vec{x}_n$ = the vector representing the center of the nth radiating element with respect to the center of the array.

4. PHASE AND AMPLITUDE CONJUGATIONS AND THREE-DIMENSIONAL FOCUSING

The field patterns presented in Eqs. (22–25) depend on the set of factors $\{I_nC_n\}$. In this section we introduce a formula for assigning the values of C_n to provide a maximum relative field at a desirable focal point. The idea is that, if one wishes to focus the field of the array at a point, say, $\vec{x}_f$, one can maximize the field at that point by applying a phase and amplitude taper which compensates the propagation loss

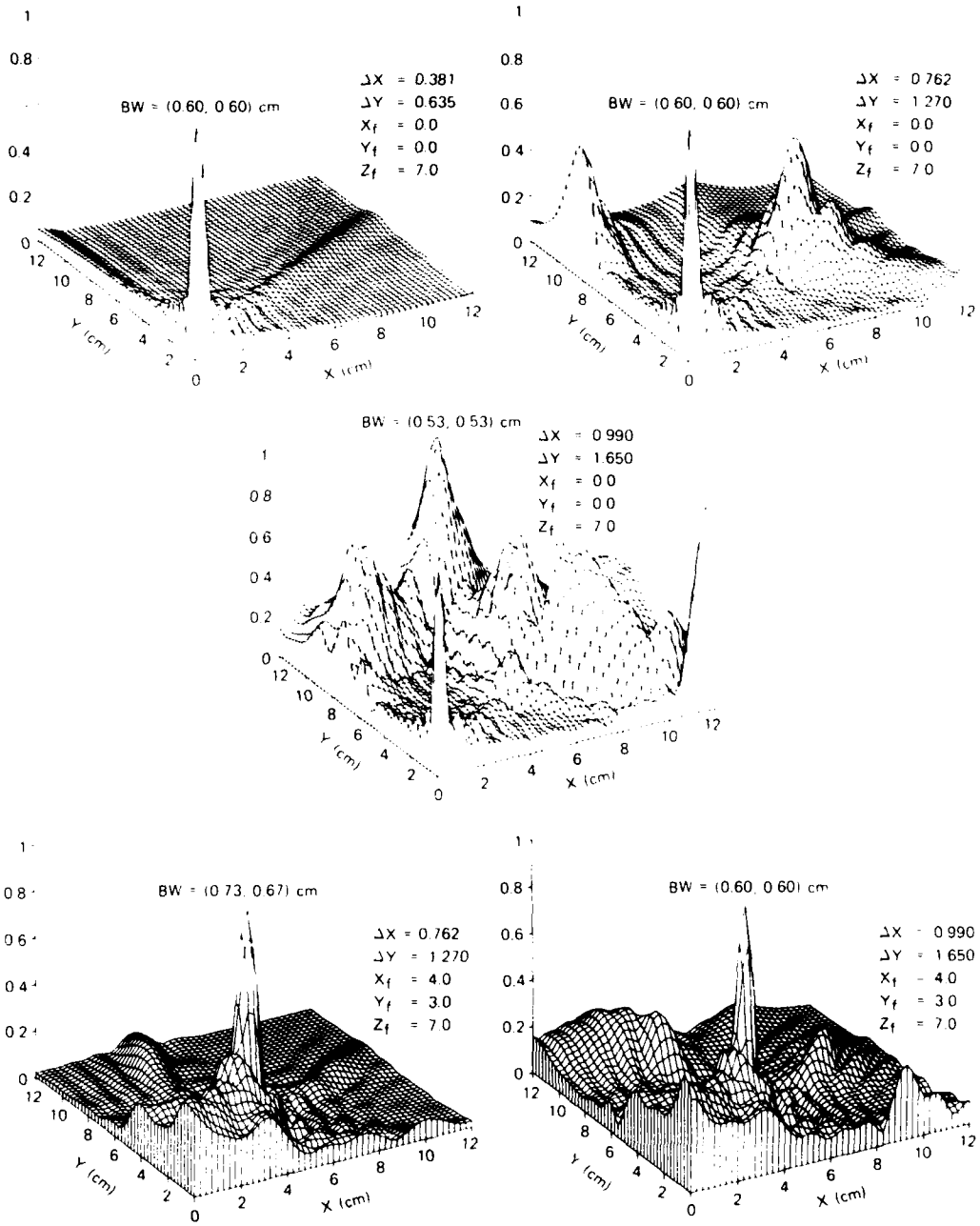

Fig. 2a–2c. Relative amplitude of the vector field in the surface z = 7 cm with phase and amplitude conjugations focused at $\vec{x}_f$ = (0, 0, 7) cm. The element spacings are (a) ΔX = 0.381 cm and ΔY = 0.635 cm, (b) ΔX = 0.762 cm and ΔY = 1.270 cm, (c) ΔX = 0.990 cm and ΔY = 1.650 cm. The 3 dB widths of the main-beam in both x- and y-directions are as indicated.

Figs. 2d–2e. Relative amplitude of the vector field in the surface z = 7 cm with phase and amplitude conjugations focused at $\vec{x}_f$ = (4, 3, 7) cm. The element spacings are (d) ΔX = 0.762 cm and ΔY = 1.270 cm, (e) ΔX = 0.990 cm and ΔY = 1.650 cm. The 3 dB widths of the main-beam in both x- and y-directions are as indicated.

and phase differential from each array element to the focal point. Thus, to focus the main beam at the point $\vec{x}_f$, the factor C_n is assigned as

$$C_n = |\vec{x}_f - \vec{x}_n| \exp(-ik|\vec{x}_f - \vec{x}_n|). \quad (25)$$

Noting that k is a complex number, the exponential factor in the above equation includes a phase factor and an amplitude factor to compensate for the absorption by the coupling medium. For this reason, we call C_n the phase-ampli-

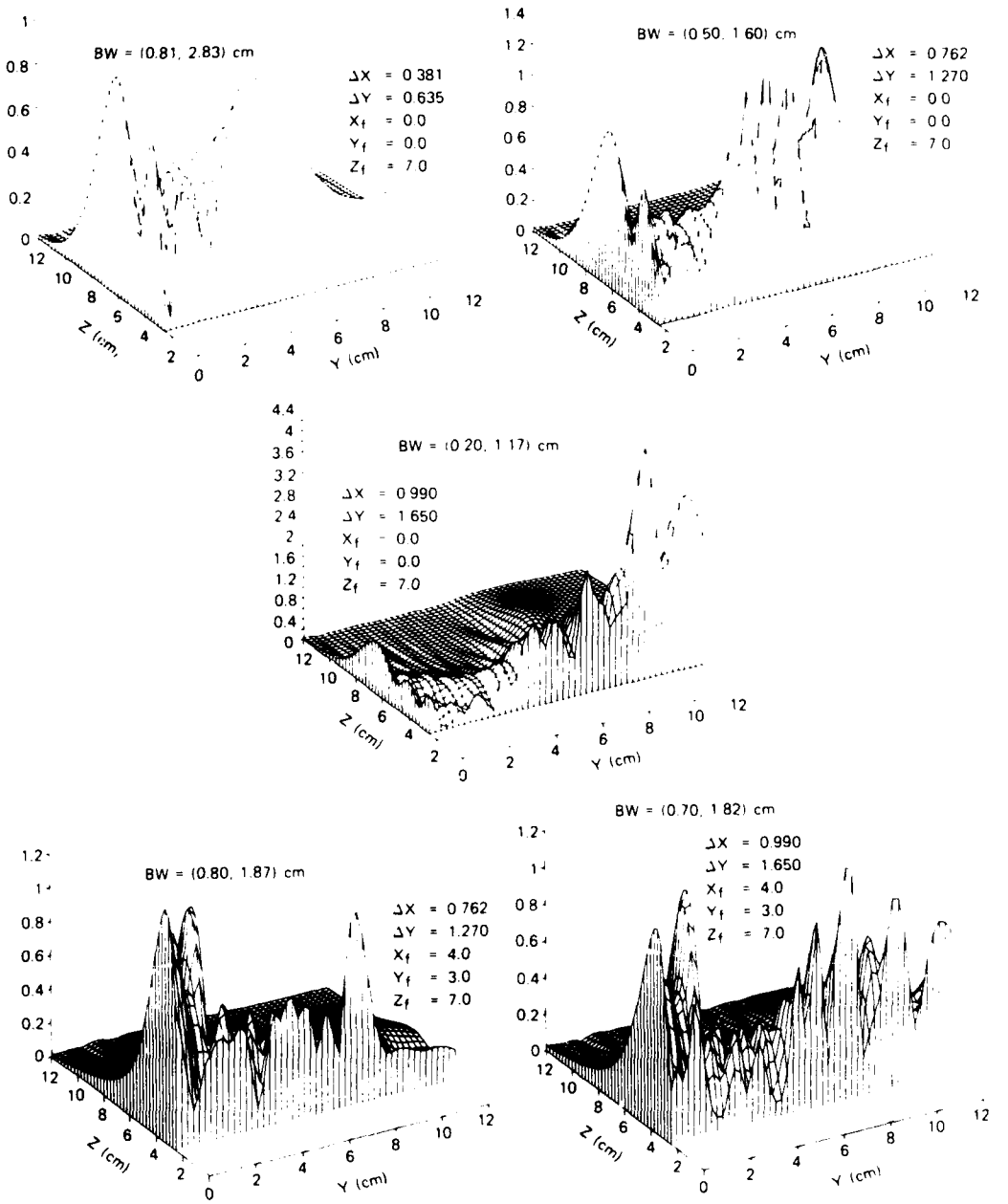

Figs. 3a–3e. Relative amplitude of the vector field in the yz-plane at x = 0, with focusing and element spacings corresponding to those in Figs. 2a–2e, respectively. The 3 dB widths of the main-beam in both cm y- and z-directions are as indicated.

tude conjugation factor. The factor I_n in Eqs. (22–24), which is called the illumination factor, may be used as additional leverage to provide optimal resolution and minimize the side lobes.

For a planar array of N × M radiating dipole elements, Eqs. 22 and 23 may be written as

$$\vec{A}(\vec{x}) = -ik\hat{p}\sum_{n=1}^{N}\sum_{m=1}^{M} I_{nm}C_{nm}\frac{e^{ik|\vec{x}-\vec{x}_{nm}|}}{|\vec{x}-\vec{x}_{nm}|} \qquad (26)$$

and

$$C_{nm} = |\vec{x}_f - \vec{x}_{nm}|\exp(-ik|\vec{x}_f - \vec{x}_{nm}|), \qquad (27)$$

As we shall see below, the phase-amplitude conjugation as presented in Eq. (25) does not make the field peak at exactly the point $\vec{x}_f$. This is simply due to the fact that we are in the local field region. For the array structure described in

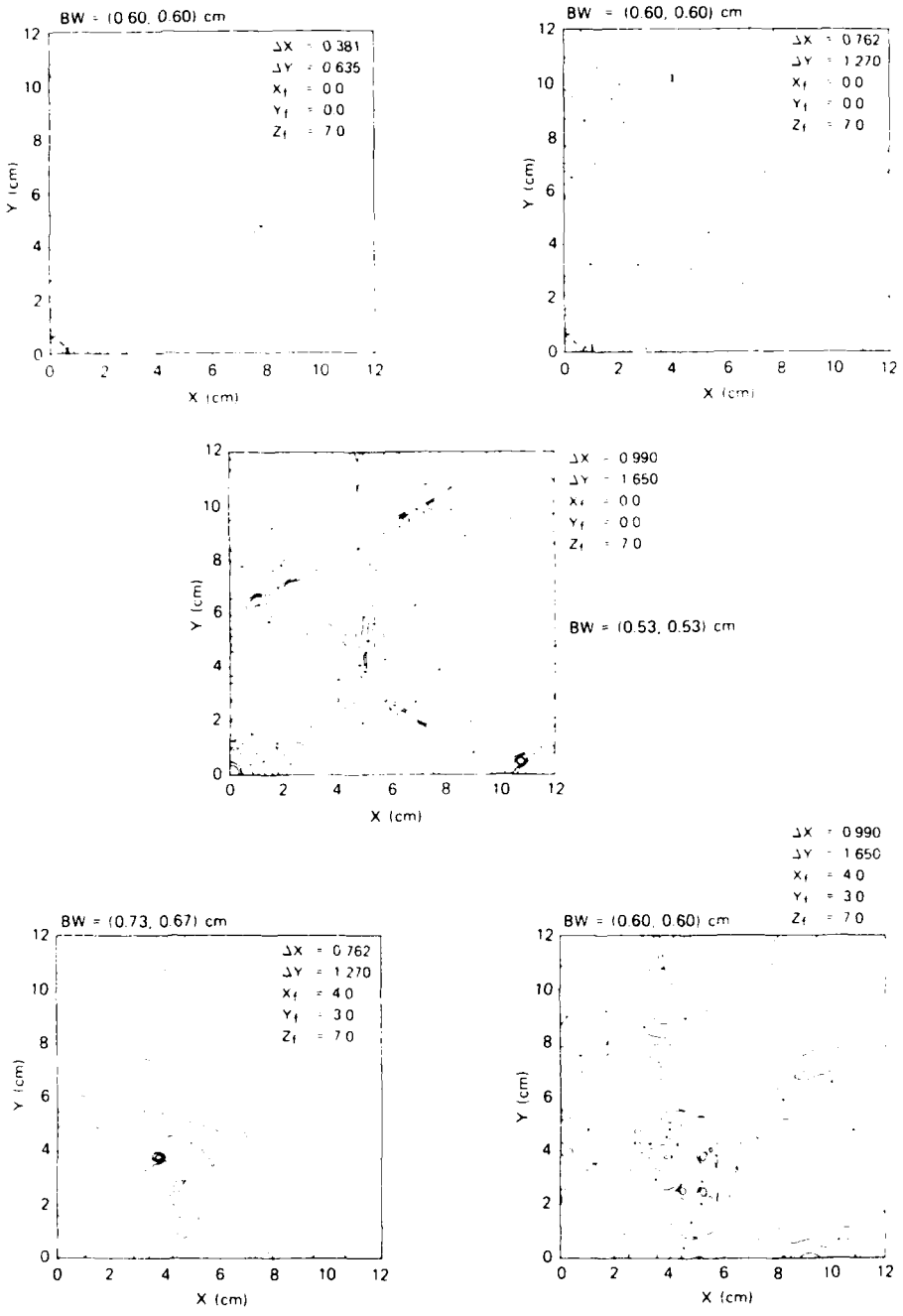

Figs. 4a–4e. Amplitude contours of the vector field in isodecibels corresponding to the cases indicated in Figs. 2a–2e respectively.

Section 2, the main lobe beamwidth is minimized when I_{nm} is taken to be a uniform illumination.

Now we present some result of the field patterns using the phase and amplitude conjugations. Only the absolute value of vector potential and the corresponding field characteristics are presented here. The structure of the array lattice is illustrated in Fig. 1a, and the equations used are (26), (27) and (6), with illumination factor $I_{nm} = 1$, and polarization taken to be in y-direction. In all the figures, the plane of the array is taken to be the xy-plane and the z-axis is perpendicular to the array plane and pointing to the forward direction. In the following discussion and in all figures, the phrase "mainbeam" is used in reference to field characteristics of the 3-dimensional focal region. Figures 2(a) through

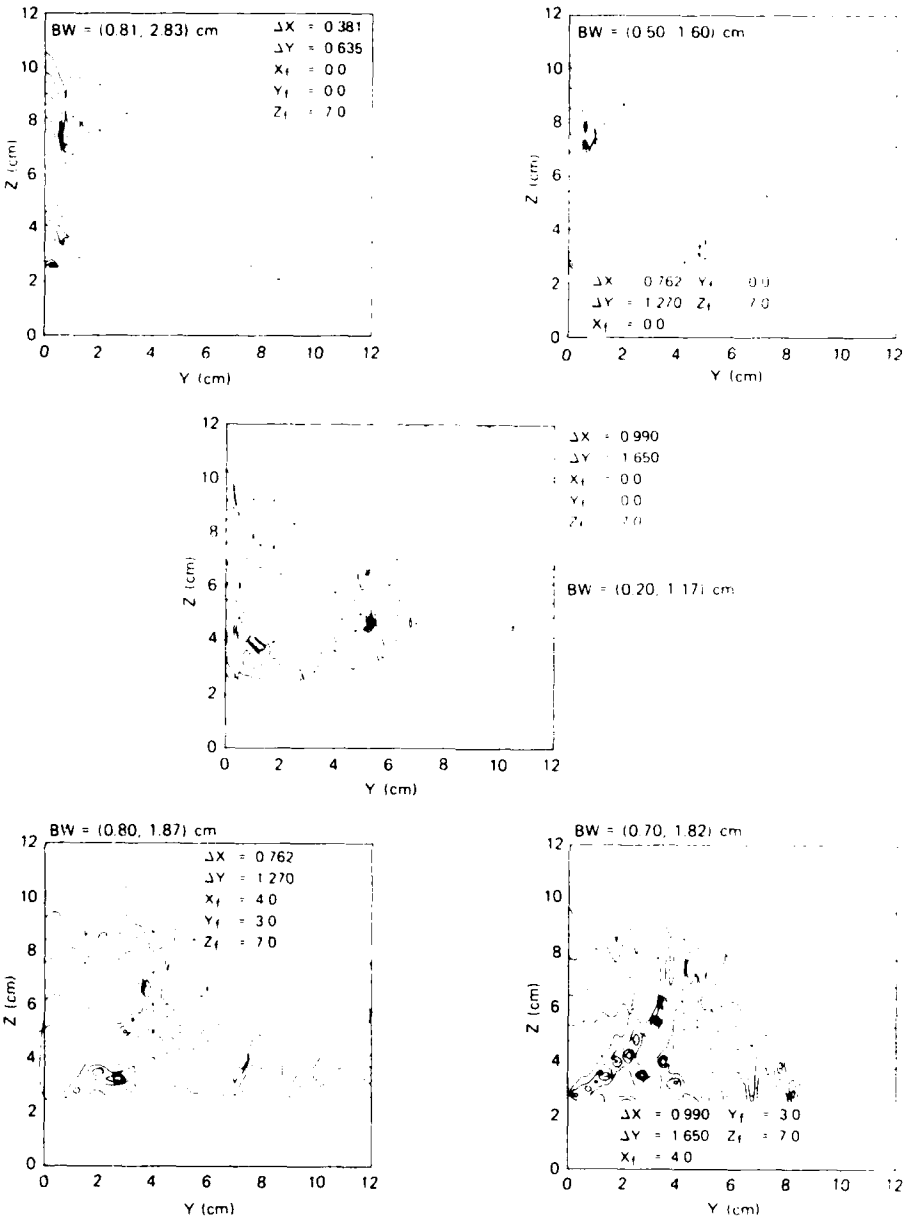

Figs. 5a–5e. Amplitude contours of the vector field in isodecibels corresponding to the cases indicated in Figs. 3a–3e respectively.

2(e) show various field patterns with different interelement spacings in the transverse plane at an axial distance of 7 cm, which is also the axial distance of the desired focal point. Similarly, Figs. 3(a) through 3(e) are the longitudinal field patterns at different interelement spacings and focal points. The corresponding 3-dB full mainbeam width is given on each figure. Note that Figs. 2(b),2(c) and 3(b),3(c) are for the array with lattice structure shown in Fig. 1a. Figures 2(d)-,2(e) are for arrays that are similar to the one shown in Fig. 1a, except with different lattice spacings. Figures 2(a) and 3(a) are for the same size array as shown in Fig. 1a but with 419 instead of 127 elements. Figures 4 and 5 are the corresponding pictures of Figs. 2 and 3, and plotted in isodecibel field contours. For easy comparison, the beam characteristics of these figures are tabulated in Table I. These data show that larger interelement spacings result in narrower 3-dB beamwidths and more accurate focusing; however, larger interelement spacings also bring grating lobes closer to the mainbeam. This result demonstrates that, with respect to beamwidth reduction, the array size plays a more important

Table 1

ARRAY BEAM CHARACTERISTICS OF THE FIELD PATTERNS AT 3 GHz

FOCAL POINT (x y z) cm	ELEMENT SPACING (dx dy) cm	PEAK AT Z=7 (x y z) cm	PEAK AT X=X_f (x y z) cm	BEAMWIDTH AT Z=7 (dx dy) cm	BEAMWIDTH AT X=X_f (dy dz) cm
0 0 7	.381 .635	0 0 7	0 0 6	.60 .60	.81 2.83
0 0 7	.762 1.27	0 0 7	0 0 6	.60 .60	.50 1.60
0 0 7	.990 1.65	0 0 7	0 0 6.5	.53 .53	.20 1.17
4 3 7	.762 1.27	4 3 7	4 2.75 6.25	.74 .67	.80 1.87
4 3 7	.900 1.65	4 3 7	4 3 6.5	.60 .60	.70 1.82

role than the number of elements. The resolutions of $\frac{1}{2}\lambda$ in transverse direction and 1λ in longitudinal direction can be achieved with the use of phase and amplitude conjugation. Note also that the peaks along z = 2.5 cm shown in Figs. 3(a)–3(e) and Figs. 5(a)–5(e) are due to the single element that is closest to each of these peaks. As the distance becomes so close to an individual element, the coherent addition from other elements is negligible in comparison. As long as the target is not closer than 3 cm from the array, these peaks will not cause any problem for actual applications in microwave imagery.

5. THE INVERSE SCATTERING THEOREM AND ITS APPLICATION TO IMAGE RECONSTRUCTION

The objective of all inverse scattering problems is to reconstruct the target from the scattered field. From Maxwell's electromagnetic theory, if one knows the field everywhere in space, the polarization charge-current distribution of the scattering source can be derived completely. However, in practice, one can only measure the scattered field at a limited number of points in space which are often confined in a small region. The question is then how much information on the scattering target one can infer based on a limited knowledge of the scattered field. Here we present a theorem [8], which is indeed a generalization of the Lorentz reciprocity theorem [19]–[21], and show that it can provide a good facility in answering the above question.

In this section we shall state the theorem and describe its application to microwave biological imaging, and leave the details of the proof to the next section. Consider a dielectric target immerged in a homogeneous and dissipative medium of dielectric constant ϵ_m and dielectric susceptibility χ_m (both are complex numbers). Let $\chi(\vec{x})$ describe the dielectric susceptibility of the entire system, including the homogeneous medium and the target, so that $\chi - \chi_m$ is null outside the target. It is assumed that there is no free charge or current distribution (including ionic charge and current) in the target or the medium, and that both have the same homogeneous magnetic permeability μ_m; however, we remark that the theorem may be generalized to include free charge-current and magnetization. Let the target be illuminated by a plane wave $\vec{E}_{inc}$ of frequency $\omega/2\pi$, which induces electric polarization $\vec{P}$ in the target and produces a scattered field $\vec{E}_{scatt}$. Let $\vec{J}_w$ be some weighing function and $\vec{A}_w$ be the corresponding field derivable from $\vec{J}_w$ in the same way as the vector potential is derivable from a current density. More precisely,

$$(\nabla^2 + k_m^2)\vec{A}_w = -\frac{4\pi\mu_m}{c}\vec{J}_w, \tag{28}$$

or its reverse equivalence,

$$\vec{A}_w(\vec{x}) = \frac{\mu_m}{c}\int \frac{e^{ik_m|\vec{x}-\vec{x}'|}}{|\vec{x}-\vec{x}'|}\vec{J}_w(\vec{x}')d\vec{x}'. \tag{29}$$

Then the inverse scattering theorem may be stated as below:

$$-\frac{1}{c}\int\int\int \vec{A}_w(\vec{x})\cdot\left[\frac{c^2}{\mu_m\epsilon_m}\nabla\rho_s + \frac{\partial}{\partial t}\vec{J}_s\right]d\vec{x} = \int\int\int \vec{J}_w\cdot\vec{E}_{scatt}d\vec{x} \tag{30}$$

where k_m, defined as $\sqrt{\mu_m\epsilon_m}\omega/c$, is the complex wave number in the homogeneous medium, and ρ_s and $\vec{J}_s$ represent the equivalent charge density and its time derivative, the current density, due to the polarization of the target in excess of the homogeneous background polarization:

$$\rho_s = -\nabla\cdot\frac{\chi-\chi_m}{\chi}\vec{P},\ \vec{J}_s = \frac{\chi-\chi_m}{\chi}\frac{\partial\vec{P}}{\partial t} \tag{31}$$

As we shall see in the next section, ρ_s and $\dot{J}_s$ are indeed the source of the scattered field.

This theorem is more general than the Lorentz reciprocity theorem [19]-[21] since $\dot{J}_w$, as well as the associated vector field $\dot{A}_w$, is only a weighing function. They need not be physical quantities; for example, $\dot{J}_w$ needs not satisfy the equation of continuity and $\dot{A}_w$ needs not satisfy the Lorentz gauge condition (or any alternative gauge). The proof of this theorem is based on the fact that the medium is dissipative and therefore a Hilbert space may be defined in which all the differential operators involved may have their Hermitian conjugations defined. The great facility of this theorem in applications to image reconstuction lies on the flexibility of choosing the weighing function $\dot{J}_w$. If the scattered field $\dot{E}_{scatt}$ is measured at a set of spatial points $\{\hat{x}_n\}$, which are the lattice points of our receiving array, and if, say, only the y-polarization is measured, then the weighing function $\dot{J}_w(\hat{x})$ may be chosen to be only in the y-direction and to be a discrete distribution over the points $\{\hat{x}_n\}$. It then follows from Eq. (29) that the resulting weighing vector potential $\dot{A}_w(\hat{x})$ will also be in the y-direction. One may further adjust the phases and amplitudes of $\dot{J}_w(\hat{x}_n)$ to optimize the weighing potential $\dot{A}_w(\hat{x})$ at any desired point of the target. It was shown in the previous section that applying the phase and amplitude conjugations to a transmitting array could provide a 3-dimensionally focused radiation in the neighborhood of the array. For imagery application with an incident plane wave, this technique may be applied to the receiving array to "focus" the weighing potential. Thus, by setting $\dot{J}_w(\hat{x}_n)$ to be the phase and amplitude conjugation factor, one may make $\dot{A}_w(\hat{x})$ negligibly small inside the target organ, except for a sharp peak near any desired point, say $\hat{x}_f$, which we shall call the focal point. Note that, since ρ_s vanishes outside the target region and so the integration in the left hand side of Eq. (30) is limited to only the target region, $\dot{A}_w(\hat{x})$ may assume any value, however large, outside the target region. Then the right hand side of Eq. (30) is obtainable from the measured data, whereas the integration on the left hand side is dominated by the integrand at the focal point.

It is emphasized that the "focusing" described above does not involve active focusing of the transmitted microwave energy on any point of the target. Rather, it is simply a mathematical management of the measured scattering data so that the retrieved information of the dielectric property may be "focused" on a desired point inside the target. In this sense, it may be considered as a focusing of the receiving array. Since one microwave exposure of the target will provide N samples of the complex scattered field, where N is the number of receiving elements, it is then theoretically possible to retrieve N estimates of the spatial distribution of the complex dielectric properties of the target by optimal management of the measured data. The inverse scattering theorem described above is to provide a basis for such purpose. We shall discuss in Section 7 the maximum limit of retrievable information from a single exposure of microwave radiation.

To express this imagery application more clearly, we set $\dot{J}_w(\hat{x}) = \Sigma_n \delta(\hat{x} - \hat{x}_n)\hat{y}J_n$ and substitute Eq. (31) for ρ_s and $\dot{J}_s$ in Eq. (30), then replace $\partial^2\dot{P}/\partial t^2$ by $-\omega^2\dot{P}$ and perform partial integration on the first term on the left hand side. Noting that $\dot{A}_w$ vanishes at infinity, one then gets

$$\frac{c}{\epsilon_m\mu_m}\int\int\int\left[-(\nabla\cdot\dot{A}_w)\left(\nabla\cdot\frac{\chi-\chi_m}{\chi}\dot{P}\right)+k_m^2\dot{A}_w\cdot\frac{\chi-\chi_m}{\chi}\dot{P}\right]d\hat{x}=\sum_n J_n E_{scatt}(\hat{x}_n) \quad (32)$$

With the discrete distribution of $\dot{J}_w(\hat{x})$, Eq. (29) reduces to

$$\dot{A}_w(x)=\sum_n\frac{\hat{y}\cdot J_n}{|\hat{x}-\hat{x}_n|}\exp(ik_m|\hat{x}-\hat{x}_n|) \quad (33)$$

which is similar to the vector potential produced by a set of dipoles as given by Eq. (22). To obtain the dielectric information at any given point $\hat{x}_f$ inside the target from the measured scattered field at the points $\{\hat{x}_n\}$, one sets J_n in the right hand side of Eq. (32) to be the phase-amplitude conjugation factor:

$$J_n(\hat{x}_f)=(c/\mu_m)|\hat{x}_n-\hat{x}_f|\cdot\exp(-ik|\hat{x}_n-\hat{x}_f|) \quad (34)$$

Based on the phase-amplitude conjugation discussed in the previous section, the resulting $A_w(\hat{x})$ has a sharp peak at $\hat{x}_f$ and is otherwise negligible in the target region. Owing to the factor $\chi - \chi_m$ which vanishes outside the target region, all sidelobes of $A_w(\hat{x})$, however large, which lie outside the target region will not contribute to the integral on the left hand side of Eq. (32). The main contribution of the integral is the dielectric characteristics of the target at the point $\hat{x}_f$, which is then equal to the weighted version of the measured values $\Sigma_n J_n E_{scatt}(\hat{x}_n)$. For this reason we refer to the point $\hat{x}_f$ as a focal point since, by Eq. (32), the sum of the products of the conjugation factors and the measured scattered fields, $\Sigma_n J_n E_{scatt}(\hat{x}_n)$, "focuses" the result to the dielectric polarization at the point $\hat{x}_f$ inside the target. By scanning the vector $\hat{x}_f$ in Eq. (34) through the target region, one then reconstructs an image of the target. The response peak in $\dot{A}_w(\hat{x})$ at the "focal point" determines the spatial resolution, and the flat response of $\dot{A}_w(\hat{x})$ within the target elsewhere contributes to ana'ytical interpretation of the imagery [7]. The size of the target is limited by the locations of the grating lobes, since these grating lobes will not contribute to the integral on the left hand side of Eq. (32) as long as they are outside of the target region. Another method to reduce the grating lobe interference is to limit the illumination region so that the local field is negligible in the grating lobe region. For a larger target, this will require dividing the target into smaller illumination regions.

6. PROOF OF THE INVERSE SCATTERING THEOREM

Our first approach in proving the theorem is to separate the target from the surrounding homogeneous medium so that the scattered field may be considered as due to a localized charge-current source. We shall consider the entire system to be a superposition of a distribution of dielectric suscep

tibility $\chi(\vec{x}) - \chi_m$ and a homogeneous medium of dielectric susceptibility χ_m; thus $\chi - \chi_m$ may be considered as the excess susceptibility of the system over the homogeneous background. Since the medium is homogeneous, the propagation of the scattered field is then governed by a set of Maxwell equations similar to that in free space except that the free space permitivity and permeability are replaced by that of the homogeneous medium. Using the notations and assumptions that were described at the beginning of the previous section, the Maxwell's equations for the total field $(\vec{E}, \vec{B})$ may be written as

$$\begin{aligned} &\nabla \cdot (1 + 4\pi\chi)\vec{E} = 0 \\ &\frac{1}{\mu_m} \nabla \times \vec{B} - \frac{(1 + 4\pi\chi)}{c} \frac{\partial \vec{E}}{\partial t} = 0 \\ &\nabla \cdot \vec{B} = 0 \\ &\nabla \times \vec{E} + \frac{1}{c} \frac{\partial \vec{B}}{\partial t} = 0 \end{aligned} \tag{35}$$

In order to separate the source of the scattered field from the homogeneous background, we transport all quantities involving excess dielectric susceptibility to the right hand sides of the above equations, so that the left hand sides resemble that of the Maxwell equations in free space. The results are, with the definition of ρ_s and $\vec{J}_s$ given by Eq. (31).

$$\begin{aligned} &\epsilon_m \nabla \cdot \vec{E} = 4\pi\rho_s \\ &\frac{1}{\mu_m} \nabla \times \vec{B} - \frac{\epsilon_m}{c} \frac{\partial \vec{E}}{\partial t} = \frac{4\pi}{c} \vec{J}_s \\ &\nabla \cdot \vec{B} = 0 \\ &\nabla \times \vec{E} + \frac{1}{c} \frac{\partial \vec{B}}{\partial t} = 0 \end{aligned} \tag{36}$$

where $\epsilon_m = 1 + 4\pi\chi_m$ is the dielectric permitivity of the homogeneous medium, and $\vec{P} = \chi\vec{E}$ is the electric polarization in the target. Replacing the total field $(\vec{E}, \vec{B})$ in Eq. (36) by the sum of the incident wave and the scattered field, since the incident wave satisfies the homogeneous (viz. sourceless) version of Eq. (36), one finds that the scattered field satisfies exactly Eq. (36). Denote the scattered field by a subscript s, one then has

$$\begin{aligned} &\epsilon_m \nabla \cdot \vec{E}_s = 4\pi\rho_s \\ &\frac{1}{\mu_m} \nabla \times \vec{B}_s - \frac{\epsilon_m}{c} \frac{\partial \vec{E}_s}{\partial t} = \frac{4\pi}{c} \vec{J}_s \\ &\nabla \cdot \vec{B}_s = 0 \\ &\nabla \times \vec{E}_s + \frac{1}{c} \frac{\partial \vec{B}_s}{\partial t} = 0 \end{aligned} \tag{37}$$

Thus the scattered field alone may be considered as that produced by the localized charge-current density $(\rho_s, \vec{J}_s)$.

Due to the dissipation of the medium, the electromagnetic field vanishes exponentially as $|\vec{x}| \to \infty$. Thus it is possible to define a Hilbert space in which the electromagnetic fields and charge densities are vectors. We define the scalar product between any pair of vectors (f, g) as the integral over the entire space:

$$\iiint f^*(\vec{x})g(\vec{x})d\vec{x},$$

which exists owing to the fact that f and g diminish exponentially as $|\vec{x}| \to \infty$. With this definition, all differential operators involved in the Maxwell equations as well as all derivative equations may have their Hermitian conjugations defined. It is based on this fact that the inverse scattering theorem can be proved. For mathematical simplicity, we shall prove the theorem using the Hilbert space notations. Noting that the Hilbert space product combined with the hermiticity of linear operators is equivalent to integration by parts involving differential operators, the proof may also be made equivalently in conventional differential equation form.

We shall now derive the inverse scattering theorem from Eq. (37). First note that the third and fourth equations of Eq. (37) show that the scattered electric field and magnetic induction are derivable from a pair of scalar and vector potentials $(\phi_s, \vec{A}_s)$, which shall be called the scattered potentials:

$$\begin{aligned} &\vec{B}_s = \nabla \times \vec{A}_s \\ &\vec{E}_s = -\nabla\phi_s - \frac{1}{c} \partial\vec{A}_s/\partial t \end{aligned} \tag{38}$$

The relationships of Eq. (38) still leave another degree of freedom on the choice of the potentials. We shall use the conventional choice of Lorentz gauge condition

$$\nabla \cdot \vec{A}_s + \frac{\epsilon_m\mu_m}{c} \frac{\partial\phi_s}{\partial t} = 0. \tag{39}$$

Then, from the first two equations of Eq. (37), the scattered potentials satisfy the wave equation with ρ_s and $\vec{J}_s$ respectively as the source:

$$\begin{aligned} &(\nabla^2 + k_m^2)\phi_s = -4\pi\rho_s/\epsilon_m \\ &(\nabla^2 + k_m^2)\vec{A}_s = -\frac{4\pi}{c} \mu_m\vec{J}_s \end{aligned} \tag{40}$$

where $k_m^2 = (\omega^2/c^2)\mu_m\epsilon_m$ and we have replaced $\partial/\partial t$ by $-i\omega$.

To facilitate our proof of the theorem, we shall denote by $|A_s\rangle$ and $|J_s\rangle$ respectively the 4-dimensional potential and the 4-dimensional current density:

$$|A_s\rangle = \begin{pmatrix} \phi_s \\ \vec{A}_s \end{pmatrix}, \quad |J_s\rangle = \begin{pmatrix} \frac{c}{\epsilon_m}\rho_s \\ \mu_m\vec{J}_s \end{pmatrix}.$$

Also denote by K_m the 4-dimensional Helmholtz operator associated with k_m:

$$K_m = (\nabla^2 + k_m^2) \begin{pmatrix} 1 & 0 \\ 0 & \bar{1} \end{pmatrix} \tag{41}$$

Then Eq. (40) may be expressed as

$$K_m|A_s\rangle = -\frac{4\pi}{c} |J_s\rangle \tag{42}$$

To express the relationship between the electric field and the vector potential, we define the 4-dimensional E-vector,

$$|E_s\rangle = \begin{pmatrix} 0 \\ \vec{E} \end{pmatrix} \tag{43}$$

and the 4-dimensional S-operator and its hermitian conjugate,

$$S_m = \begin{pmatrix} \frac{ic}{\omega} k_m^2 - \nabla \\ -\nabla \quad \frac{i\omega}{c} \bar{1} \end{pmatrix}, \quad S_m^\dagger = - \begin{pmatrix} \frac{ic}{\omega} (k_m^2)^* - \nabla \\ -\nabla \quad \frac{i\omega}{c} \bar{1} \end{pmatrix} \tag{44}$$

Then the second equation of Eq. (38) may be expressed as

$$|F_s\rangle = S_m|A_s\rangle \tag{45}$$

Note that the above equation actually represents two relationships: the scalar component is equivalent to the gauge condition Eq. (39), and the vector condition gives the electric field in terms of the potentials. Since the operators K_m and S_m commute with each other, operating both sides of Eq. (42) by S_m yields the wave equation for $|E_s\rangle$:

$$K_m|E_s\rangle = -\frac{4\pi}{c} S_m|J_s\rangle = -\frac{4\pi}{c}|F_s\rangle \tag{46}$$

which shows that $S_m|J_s\rangle$ may be considered as the source of $|E_s\rangle$ as much as the current density $|J_s\rangle$ is the source of the potential $|A_s\rangle$, therefore we denote it by $|F_s\rangle$. By the equation of continuity $\nabla\cdot\vec{J}_s - i\omega\rho_s = 0$, we then have

$$|F_s\rangle \equiv S_m|J_s\rangle = \begin{pmatrix} 0 \\ -\frac{c}{\epsilon_m}\nabla\rho_s - \frac{\mu_m}{c}\frac{\partial \vec{J}_s}{\partial t} \end{pmatrix} \tag{47}$$

So far we have rewritten all electrodynamic equations for a dissipative medium in their Hilbert space representations. To complete our description of the Hilbert space, we define, for any vector $|F\rangle$, a complex conjugate vector $|\bar{F}\rangle$ which corresponds to the complex conjugate in the $\hat{x}$-representation,

$$\langle \hat{x}|\bar{F}\rangle = (\langle \hat{x}|F\rangle)^*$$

Also, given any pair of 4-dimensional vectors $|F\rangle = (f, \vec{F})$ and $|G\rangle = (g, \vec{G})$, their Hilbert space scalar product is defined as

$$\langle F|G\rangle = \int\int\int (f^* g + \vec{F}^* \cdot \vec{G}) d\hat{x}$$

With these Hilbert space representations, the proof of the inverse scattering theorem becomes rather straightforward. Let $|J_w\rangle$ be any 4-dimensional vector, and $|A_w\rangle$ be the 4-dimensional vector derivable from $|J_w\rangle$ in the same way as $|A_s\rangle$ is derivable from $|J_s\rangle$. That is,

$$K_m|A_w\rangle = -\frac{4\pi}{c}|J_w\rangle \tag{48}$$

$|J_w\rangle$ and $|A_w\rangle$ are weighing vectors which satisfy only the wave equations, but not the equation of continuity nor the gauge condition. So they are not physical quantities. For instance, the weighing current $|J_w\rangle$ may be a point function with only the vector component, viz., a delta-function current in space without charge density. From Eq. (41), the complex conjugate of K_m is equal to its hermitian conjugate, therefore the complex conjugate of Eq. (48) gives $(K_m)^\dagger|\bar{A}_w\rangle = -4\pi/c|\bar{J}_w\rangle$, where † denotes the hermitian conjugation. The hermitian conjugate of this equation then gives $\langle \bar{A}_w|K_m = \langle \bar{J}_w|(-4\pi/c)$. Taking the scalar product of both sides with $|E_s\rangle$ and utilizing Eq. (46), it then gives

$$-\frac{4\pi}{c}\langle \bar{J}_w|E_s\rangle = \langle \bar{A}_w|K_m|E_s\rangle = -\frac{4\pi}{c}\langle \bar{A}_w|F_s\rangle$$

Therefore

$$\langle \bar{A}_w|F_s\rangle = \langle \bar{J}_w|E_s\rangle \tag{49}$$

which is the Hilbert space form of the inverse scattering theorem. Take $|J_w\rangle$ to be $(0, \vec{J}_w(\hat{x}))$, so that the scalar component of $|A_w\rangle$ also vanishes, then, with the aid of Eq. (47), the above equation gives the inverse scattering theorem stated in the previous section, viz., Eq. (30).

One may wish to express Eq. (49) in a more symmetric form, such as one involves $|J\rangle$ and $|E\rangle$ in both sides of the equality. To do this, we first replace $|F_s\rangle$ in the left hand side of Eq. (49) by $S_m|J_s\rangle$, as defined in Eq. (47), then Eq. (49) becomes

$$\langle \bar{A}_w|S_m|J_s\rangle = \langle \bar{J}_w|E_s\rangle \tag{50}$$

If we also define a weighing electric field $|E_w\rangle$ in the same way as a physical electric field is related to the vector potential through Eq. (45), then $|F_w\rangle = S_m|A_w\rangle$. Taken its complex conjugation followed by hermitian conjugation, this relationship gives $\langle \bar{A}_w|(S_m)^{*\dagger} = \langle \bar{E}_w|$. From Eq. (44) one sees that $(S_m)^{*\dagger}$ differs from S_m by having opposite signs in all off-diagonal elements while being equal to S_m in all diagonal elements, therefore the left hand side of Eq. (50) is not equal to $\langle \bar{E}_w|J_s\rangle$, as what would have been expected from a symmetric expression. Therefore we define another field $|\tilde{E}_w\rangle = (S_m)^{*\dagger}|A_w\rangle$, so that its hermitian conjugation followed by complex conjugation is $\langle \tilde{E}_w| = \langle \bar{A}_w|S_m$. Then Eq. (50) may also be stated in the following form:

$$\langle \tilde{E}_w|J_s\rangle = \langle J_w|E_s\rangle \tag{51}$$

It is remarked that, while $|A_w\rangle$ may be considered as the potential due to the source current density $|J_w\rangle$, neither $|\tilde{E}_w\rangle$ nor $|E_w\rangle$ defined above has a parallel analogy. From Eq. (43), a parallel analogy would require that the scalar components of $|\tilde{E}_w\rangle$ and $|E_w\rangle$ vanish. But, since $|A_w\rangle$ may not satisfy the Lorentz gauge condition, the scalar components of $S_m|A_w\rangle$ and $(S_m)^{*\dagger}|A_w\rangle$ do not vanish.

Equation (51) appears to be similar to the Lorentz reciprocity theorem as expressed by Carson [19]-[21]. The difference here is that $|J_w\rangle$ and $|\tilde{E}_w\rangle$ are only weighing functions and they need not be physical quantities. Therefore this theorem may be considered as a generalization of the reciprocity theorem. The theorem is valid only if a Hilbert

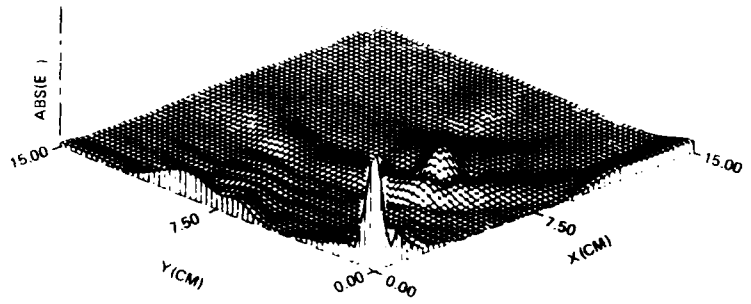

Figure 6a

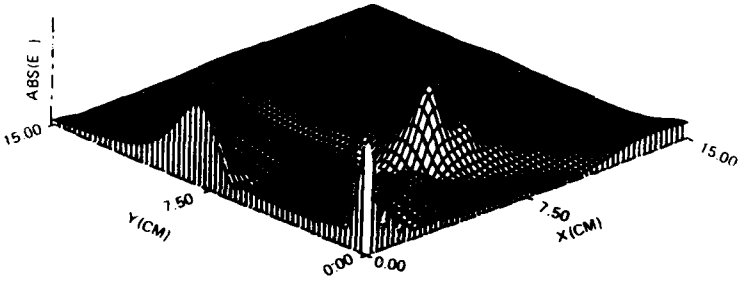

Figs. 6a–6b. Comparison of the electric fields in the $z = 7$ cm surface generated by a planar array and a volumetric array, with the phase and amplitude conjugation focusing on the axis at 7 cm from the center of the array. (a) For a system of 5 parallel arrays spaced at 1 cm from each other, the 3 dB main-beam width and the mainbeam to first sidelobe ratio in the (x, y) directions are respectively, (0.56, 0.82)cm and (24, 18)dB. (b) For a planar array, the 3 dB main-beam width and the mainbeam to first sidelobe ratio in the (x, y) directions are respectively, (0.64, 0.82)cm and (10, 16)dB.

space may be defined in which the fields, the sources, and the weighing functions are Hilbert space vectors, which is the case when the propagation medium is dissipative.

7. REMARKS AND CONCLUSIONS

Three main topics have been presented in this article: (1) an instrumental and hardware description of a microwave array system being developed for medical application, (2) the phase and amplitude conjugation technique which may be used to actively focus a transmitting microwave array or, with the help of the inverse scattering theorem, to passively focus a receiving array; in either case, it may achieve a 3-dimensional focusing in the neighborhood of the array, and (3) an inverse scattering theorem on retrieving information of a scattering target from limited data of the scattered field, which, if applied in conjunction with the phase and amplitude conjugations, may provide an optimal 3-dimensional imaging from one sampling of the scattering field measured by a receiving array.

On the quality of 3-dimensional focusing using the phase and amplitude conjugations, we have presented several results graphically. Summarizing these results, the following conclusions may be drawn:

1. Using the method of phase and amplitude conjugations, one may achieve a satisfactory degree of 3-dimensional focusing in the neighborhood of radiation sources in a lattice structure. There is a slight shift of the peak point of the field from the intended focal point as defined in the phase-amplitude conjugation factor. The shift, as outlined in Table I, generally points toward the center of the array. This should not pose any problem for practical applications since it can be calibrated.

2. Upon applying the phase and amplitude conjugations, the field patterns and the beam characteristics in the transverse direction appear to have similar dependency upon the lattice structure and the array size as that of a Fraunhofer field. Thus, the transverse beamwidth becomes narrower as the element spacing increases, at the expense of more grating lobes. Interestingly, this behavior also applies to the longitudinal beamwidth. Therefore, for a smaller target, it is possible to improve the resolution further by increasing the element spacing, as long as the target does not extend to the region covered by grating lobes. Alternatively, the regions covered by the grating lobes may be excluded from illumination by active control on the transmitting array.

3. Along the longitudinal direction, the field patterns and the beam characteristics using the phase and amplitude conjugations differ considerably from that of a Fraunhofer field. A Fraunhofer field is invariant in the longitudinal direction except for the inverse-square dependence, whereas a local field under phase and amplitude conjugations has a diffraction structure in the longitudinal direction, as well as

in the transverse direction. Therefore some degree of focusing of the local field along the longitudinal direction may be achieved using the phase and amplitude conjugation technique. It must be remarked that, as the axial distance increases, the sensitivity of longitudinal focusing to the phase-amplitude conjugation decreases. Our analysis of the field pattern for focusing at 30 cm axial distance indicates that the conjugation factor is totally overcome by the exponential attenuation. However, the transverse focusing remains good even at this axial distance.

4. If all array elements may be represented by parallel dipoles, then clearly the vector potential everywhere must be polarized in the dipole direction. However, in the local region, the electric field will still have strong polarization dependency. This polarization dependency is reduced as the axial distance increases, and, at an axial distance of 30 cm and beyond, the electric field is highly polarized in the direction of the source dipoles [13].

The 3-dimensional resolution and the allowable target volume may further be optimized by varying the lattice structure and the element spacing of the receiving array. However, based on information theory, there is a theoretical limit on the ratio of the target volume and the resolution. If the total number of the array elements is N, then each sampling of the scattered field provides an information equivalent to 2N real numbers, where the factor 2 accounts for the measurements of both phase and amplitude. The value 2N is the maximum information one may expect from the image reconstruction. The theoretical limit of the 3-dimensional resolution from each sampling of the scattered field may then be described by the equation:

$$\frac{\text{volume of the target}}{\text{volume of the focal region}} \lesssim 2N. \tag{52}$$

Therefore, if the target is smaller, the resolution may be further improved without increasing the number of elements. For example, for the enlarged interelement spacings corresponding to Figs. 2c and 3c, the resolution is improved to about half-wavelength transversely and one-wavelength longitudinally.

It is possible to acquire more target information, and thereby improve the three-dimensional resolution, by making multiple views from different angles with respect to the direction of the incident wave as suggested by the models of diffraction tomography. Multiple views at different ranges from the target for a fixed transmitter position are also possible; however, analysis of such a volumetric synthesis due to the superposition of parallel planar arrays discloses that such an approach may be of limited value, because much of the information contained in parallel samples of the scattered field are redundant. Figure 6(a) shows the field pattern of five parallel arrays separated at 1 cm from one another. Comparing to the field pattern of a single array as shown in Fig. 6(b), the five-array system provides slightly narrower main-beam width and smaller grating lobes. However, the difference may not repay the minimum of five times the data acquisition and data processing time.

ACKNOWLEDGMENT: This work was supported in part by the Walter Reed Army Institute of Research through the U.S. Army Medical R&D Command under the U.S. Naval Sea Systems Command Contract N00024-83-C-5301 to the Johns Hopkins University Applied Physics Laboratory.

References

1. A. S. Pressman, *Electromagnetic Fields and Life*, Plenum Press, New York, 1970.
2. L. E. Larsen and J. H. Jacobi, "Microwave scattering parameter imagery of an isolated canine kidney," *Med. Phys.*, Vol. 6, pp. 394–402, 1979.
3. J. H. Jacobi, L. E. Larsen, and C. T. Hast, "Water-immersed microwave antennas and their application to microwave interrogation of biological targets," *IEEE Trans. Microwave Theory Tech.*, Vol. MTT-27, pp. 70–78, 1979.
4. J. H. Bolomey, A. Izadnegahdar, L. Jofre, Ch. Pichot, G. Peronnet, and M. Solaimani, "Microwave diffraction tomography for biomedical applications," *IEEE Trans. Microwave Theory Tech.*, Vol. MTT-30, pp. 1998–2000, 1982.
5. N. H. Farhat, D. L. Jaggard, T. H. Chu, D. B. Ge, and S. Mankoff, presented at the 3rd Annual Benjamin Franklin Symposium on Advances in Antennas and Microwave Technology, Philadelphia, Pennsylvania, 1983.
6. L. E. Larsen and J. H. Jacobi, "Methods of microwave imagery for diagnostic application," *Diagnostic Imaging in Medicine*, NATO Advanced Science Institute Series E, No. 61, C. R. Reba, ed., Nijhoff Publishers, The Hague, pp. 68–123, 1983.
7. T. C. Guo, W. W. Guo, and L. E Larsen, "Comment on 'Microwave diffraction tomography for biomedical applications'," *IEEE Trans. Microwave Theory Tech.*, Vol. 32, p. 473, 1984.
8. T. C. Guo, W. W. Guo, and L. E. Larsen, Proc. IEEE 8th International Conference on Infrared and Millimeter Waves, Miami Beach, Florida, December 12–17, 1983.
9. M. Melek and A. P. Anderson, "Theoretical studies of localized tumour heating using focused microwave arrays," *IEE Proc.*, Vol. 127, Pt. F, No. 4, pp. 319–321, 1980.
10. J. Mendecki, E. Friedenthal, and C. Botstein, "Microwave-induced hyperthermia in cancer treatment: apparatus and preliminary results," *Int. J. Radiat. Oncol. Biol. Phys.*, Vol. 4, No. 11, pp. 1095–1103, 1978.
11. D. A. Christensen and C. H. Durney, "Hyperthermia production for cancer therapy: a review of fundamentals and methods," *J. of Microwave Power*, Vol. 16, No. 2, June, 1981.
12. T. C. Guo, W. W. Guo, and L. E. Larsen, "A local field study of a water-immersed microwave antenna array for medical imagery and therapy," *IEEE Trans. Microwave Theory Tech.*, Vol. MTT-32, pp. 844–854, 1984.
13. L. E. Larsen, J. H. Jacobi, W. W. Guo, T. C. Guo, and A. C. Kak, "Microwave imaging systems for medical diagnostic applications," Proceedings—Sixth Annual Conference of IEEE Engineering in Medicine and Biology Society—Frontiers Eng. Computing in Health Care, pp. 532–539, ed. John L. Semmlow and Walter Welkowitz, Los Angeles, CA., September, 1984.

14. I. Yamaura, "Measurements of 1.8–2.7 GHz microwave attenuation in the human torso," *IEEE Trans. Microwave Theory Tech.*, Vol. MTT-25, pp. 707–710, 1977.
15. J. H. Jacobi and L. E. Larsen, "Microwave time delay spectroscopic imagery of isolated canine kidney," *Med. Phys.*, Vol. 7, No. 1, pp. 1–7, 1980.
16. H. P. Schwan, "Radiation biology, medical applications, and radiation hazards," *Microwave Power Engineering*, Vol. 2, E. C. Okress, ed., Academic Press, New York, pp. 215–232, 1968.
17. K. Kurokawa, "Electromagnetic wave and waveguides with wall impedance," *IEEE Trans. Microwave Theory Tech.*, Vol. MTT-13, pp. 314–320, 1962.
18. J. Jackson, *Classical Electrodynamics*, John Wiley and Sons, New York, 1962, Ch. 9.
19. J. R. Carson, "Reciprocal theorems in radio communication," *Proc. IRE*, Vol. 17, pp. 952–956, 1929.
20. J. H. Richmond, "A reaction theorem and its application to antenna impedance calculations," *IRE Trans. Antennas Propag.*, Vol. AP-9, pp. 515–520, 1961.
21. L. D. Landau and E. M. Lifshitz, *Electrodynamics of Continuous Media*, Pergamon Press, Oxford, 1960.